INVESTIGATION OF THE TRANSIENT BEHAVIORS OF PHOTOCATALYTIC NO OXIDATION OVER TiO_2

A THESIS SUBMITTED TO
THE GRADUATE SCHOOL OF NATURAL AND APPLIED SCIENCES
OF
MIDDLE EAST TECHNICAL UNIVERSITY

BY

SELIN ERNAM

IN PARTIAL FULFILLMENT OF THE REQUIREMENTS
FOR
THE DEGREE OF MASTER OF SCIENCE
IN
CHEMICAL ENGINEERING

JANUARY 2022

Approval of the thesis:

INVESTIGATION OF THE TRANSIENT BEHAVIORS OF PHOTOCATALYTIC NO OXIDATION OVER TiO_2

submitted by **SELIN ERNAM** in partial fulfillment of the requirements for the degree of **Master of Science in Chemical Engineering Department, Middle East Technical University** by,

Prof. Dr. Halil Kalıpçılar
Dean, Graduate School of **Natural and Applied Sciences** _____

Prof. Dr. Pınar Çalık
Head of Department, **Chemical Engineering** _____

Prof. Dr. Deniz Üner
Supervisor, **Chemical Engineering, METU** _____

Examining Committee Members:

Prof. Dr. Gürkan Karakaş
Chemical Engineering, METU _____

Prof. Dr. Deniz Üner
Chemical Engineering, METU _____

Prof. Dr. Ramazan Yıldırım
Chemical Engineering, Boğaziçi University _____

Assist. Prof. Dr. Gökhan Çelik
Chemical Engineering, METU _____

Assist. Prof. Dr. Necip Berker Üner
Chemical Engineering, METU _____

Date: 12.01.2022

I hereby declare that all information in this document has been obtained and presented in accordance with academic rules and ethical conduct. I also declare that, as required by these rules and conduct, I have fully cited and referenced all material and results that are not original to this work.

Name, Surname: Selin Ernam

Signature :

ABSTRACT

INVESTIGATION OF THE TRANSIENT BEHAVIORS OF PHOTOCATALYTIC NO OXIDATION OVER TiO_2

Ernam, Selin
M.S., Department of Chemical Engineering
Supervisor: Prof. Dr. Deniz Üner

January 2022, 108 pages

The objective of this thesis is to investigate the bottlenecks of photocatalytic NO oxidation reaction. This reaction is used as a standard diagnostic tool for photocatalytic activity according to the well defined protocols described by the ISO Standard (22197-1-2007). One of the problems with photocatalytic NO oxidation is the transient period of NO conversion between the beginning of illumination and the time the conversions reach a steady state. The nature of this behavior depends strongly on parameters such as the illumination intensity and the concentration of the reactants, in particular the moisture content. In order to reveal the effect of the illumination intensity and the moisture content, devices with sensors and microcontroller boards were built. Controlled experiments revealed that at higher light intensities, the reaction starts with a very high conversion and need longer times to reach steady state, at a lower conversion value. In contrast, experiments with low light intensities reach this steady conversion level almost immediately after the reaction starts. Using the light intensity measurement device built for this purpose, a relationship was obtained between the steady state reactant conversion and illumination intensity (at 365 nm) as follows: $X = \frac{aI^b}{c + aI^b}$ where a = 0.1809, b = 0.3733, c = 0.7265.

Furthermore, the effect of water injections to the system was also investigated using a relative humidity measurement device specifically built for this purpose. The water injection transient data collected in this study revealed the qualitative nature of the interactions. The system can be effective at collecting data and can be used to determine a reaction model.

Keywords: TiO_2, Photocatalysis, Illumination Intensity, NO Oxidation, Water Injection

ÖZ

TiO_2 ÜZERİNDE FOTOKATALİTİK NO OKSİDASYONUNUN DEĞİŞKEN DAVRANIŞININ İNCELENMESİ

Ernam, Selin
Yüksek Lisans, Kimya Mühendisliği Bölümü
Tez Yöneticisi: Prof. Dr. Deniz Üner

Ocak 2022 , 108 sayfa

Bu tezin amacı, fotokatalitik NO oksidasyon reaksiyonunun darboğazlarını araştırmaktır. ISO Standardı (22197-1-2007) ile standartlaştırılmış protokollere sahip olan bu reaksiyon, fotokatalitik aktivite için bir ölçüm aracı olarak kullanılır. Fotokatalitik NO oksidasyonu ile ilgili sorunlardan biri, aydınlatmanın başlangıcı ile dönüşümlerin yatışkın hale ulaştığı zaman arasındaki değişken NO dönüşüm periyodudur. Bu davranış aydınlatma yoğunluğu ve tepkenlerin konsantrasyonu, özellikle nem içeriği gibi parametrelere bağlıdır. Aydınlatma şiddeti ve nem içeriğinin etkisini ortaya çıkarmak için sensörler ve mikrodenetleyici kartlar ile cihazlar yapılmıştır. Kontrollü deneyler, daha yüksek ışık yoğunluklarında, reaksiyonun çok yüksek bir dönüşümle başladığını ve daha düşük bir dönüşüm değerinde yatışkın duruma ulaşmak için daha uzun sürelere ihtiyaç duyduğunu ortaya koydu. Buna karşılık, düşük ışık yoğunluklu deneyler, reaksiyon başladıktan hemen sonra bu yatışkın dönüşüm seviyesine ulaştı. Bu amaçla oluşturulmuş ışık şiddeti ölçüm cihazı kullanılarak, kararlı hal tepken dönüşümü ile 365 nm'de aydınlatma yoğunluğunun $X = \frac{aI^b}{c + aI^b}$ denklemiyle ilişkili olduğu bulundu. Bu denklemde a = 0.1809'a, b = 0.3733'e ve c = 0.7265 olarak bulundu.

Ayrıca, bu amaç için özel olarak yapılmış bir bağıl nem ölçüm cihazı kullanılarak su enjeksiyonlarının sisteme etkisi de araştırılmıştır. Bu çalışmada toplanan su enjeksiyonu verileri, etkileşimlerin nitel doğasını ortaya çıkarmıştır. Bu sistem veri toplamak ve reaksiyonu modellemek kullanılabilir.

Anahtar Kelimeler: TiO_2, Fotokataliz, Aydınlatma Şiddeti, NO Oksidasyonu, Su Enjeksiyonu

To my family

ACKNOWLEDGMENTS

Firstly, I am sincerely grateful to my supervisor Prof. Dr. Deniz Üner. Her support, patience and guidance were invaluable. Her insight and way of thinking inspired me in every step of the way. A great mentor, she also granted me freedom in my work which allowed me to develop and learn diverse subjects. It has been an honor working with her.

Secondly, I would like to thank Hakan Ernam for providing the electronic components including the microcontroller board used in this study and his guidance in electronics.

Thirdly, I thank all the Cactus Research Group members. Especially Orhun Kahraman, who introduced me to the lab and taught me the very first things I learned, with patience and diligence. I am grateful to Melis Yarar for her help with ESR measurements. I also thank my lab and roommate Begüm Yılmaz for her help and company. We had many fun adventures together.

We had pleasant times together with my friends in the department Beste Avcı, my roommate Salih Ermiş, Toprak Çağlar, Ezgi Altıntaş, Ahmet Fırat Taşkın and Öznur Kavak.

I had the best of times during my time in university with my crew Ayça Sema Arısoy, Duygu Keser, Cansu Şendil and Yağmur Başkaya. Neverending training sessions and rowing races with them taught me how to get through difficult times later on. I am also thankful to rowing masters of "older and older, faster and faster", I wish I had met them sooner. Not to forget my long time friend Bilge Özkan whom I met in high school. She was a great friend. I would also like to thank Burhan Acarsoy, my chemistry teacher in high school, who introduced me to chemistry subjects beyond high school level. His influence played an important role in my choice to study chemical engineering.

My cat buddies brought me immense joy. Even though they couldn't talk, their com-

pany is appreciated.

Last but not least, I would like to thank my mom and dad who not only supported me during my research, but helped me in every way possible since I can remember. Their love, support, patience and guidance were invaluable. My mother Feyza, selflessly helped me whenever I needed her. Her love is truly unconditional. My father Hakan, who is also an engineer, was my mentor at home. He began teaching me mathematics, logic and engineering methods at a young age. Even though I was sometimes grumpy about it, he was patient, to which I am grateful now. My small family also includes my only and dear uncle Ferdi Hacışerifoğlu who supported me and was always by my side. I enjoy our conversations about various topics very much. He was also very interested in my research topic and gave me motivation. Finally, I am thankful to my dear grandparents Hüsnü and Ayşe.

TABLE OF CONTENTS

LIST OF TABLES

TABLES

LIST OF FIGURES

FIGURES

NOMENCLATURE

ABBREVIATIONS

BET	Brunauer Emmett Teller
CH	Channel
DFT	Density Functional Theory
DHT	Digital Humidity and Temperature
GND	Ground
LCD	Liquid Crystal Display
MFC	Mass Flow Controller
RH	Relative Humidity
SCCM	Standard Cubic Centimetres per Minute
SiG	Signal
TPD	Temperature Programmed Desorption

SYMBOLS

I	Light Intensity
X	Conversion

CHAPTER 1

INTRODUCTION

1.1 Photocatalysis in the Scope of Chemical Engineering

A catalyst, by definition, is a substance that accelerates a chemical reaction by participating in the reaction mechanism, but remains unchanged at the end. Catalytic reactions are at the heart of chemical processes. A catalyst functions by lowering the activation barrier of a reaction and/or altering its mechanism. 90% of industrial reactive processes are carried out with a catalyst [1]. Even with the use of catalysts, many of these reactions are still not easy to carry out and the processes are very energy intensive. 33% of the total energy produced in the U.S. is used by the industrial sector [2]. Of that, 37% goes to chemical processes [2].

Photocatalysis is catalysis driven by light. Among many exciting properties of semiconductors, when illuminated with photons carrying sufficient energy, they can exhibit photocatalytic activity. A photon striking the semiconductor can generate charge carriers. These charge carriers are electron and hole pairs in the conduction and the valence energy bands of the solid. The electron/hole pairs can later migrate to the surface of the semiconductor where they can initiate chemical reactions with adsorbed molecules.

1.2 Photocatalytic NO Oxidation

Photocatalytic NO oxidation is a means of measuring photocatalytic activity of a semiconductor photocatalyst. The process is standardized by the ISO-22197 standard [3]. This document explains how the instruments should be set up, how to prepare

a test piece and describes the experimental procedures. The measurement procedure is divided into three time dependent key steps to ensure an accurate measurement of catalytic activity. The first of these time dependent processes is for the preparation of the gases and calibration of the measurement. The second is for establishing adsorption desorption equilibrium with the gas phase and the test piece. The third transient is for the photocatalytic reaction.

Thorough investigation of a semiconductor catalyst in this way can therefore reveal much about photocatalytic reactions and the shortcomings of these reactions can be identified. Many photocatalytic processes have bottlenecks in steps that are not specific to reactants but rather in common photocatalytic processes such as charge carrier dynamics. Therefore investigation of an arbitrary but easily measurable photocatalytic process such as NO oxidation can reveal much about the fundamental steps. This would lead to uncovering key unknowns about photocatalytic processes.

1.3 The Outline of the Thesis

This thesis investigates photocatalytic NO oxidation over TiO_2 and focuses on the bottlenecks of the reaction. TiO_2 exhibits great photoactivity towards oxidation of NO. However, the process is transient and conversion declines throughout the reaction. This thesis will focus on problems about the transient behavior of the reaction and how experimental parameters have an effect on it. A systematic study was conducted to unravel the effects of illumination intensity and water vapor pressure on the rates and transient behaviors of photocatalytic NO oxidation over TiO_2.

CHAPTER 2

LITERATURE REVIEW

2.1 Photocatalysis

As discussed in Chapter 1, semiconductors are essential to photocatalysis. In this section, the fundamentals behind semiconductors and photocatalysis will be briefly discussed.

2.1.1 Band Theory of Solids

When many atoms are close together, their wave functions start to overlap. In bulk solids, a large number of atoms are in close proximity to each other, therefore continuous energy bands are formed [4]. In some solids, however, the bands may not overlap. In such cases, there are gaps between the allowed energy bands which correspond to forbidden energy states the electrons cannot have [4]. These regions are called band gaps [4]. The lower energy band is the valence band and the higher energy band is the conduction band. The band gap corresponds to the the difference in energy between the conduction band and the valence band [5].

Solids are classified as insulators, conductors and semiconductors according to their band structures. Conductors do not have an apparent band gap between the conduction and the valence bands. In contrast, insulators have large band gaps separating these bands. Semiconductors have a relatively smaller band gap [6]. Figure 2.1 represents the band structure of metals, semiconductors and insulators.

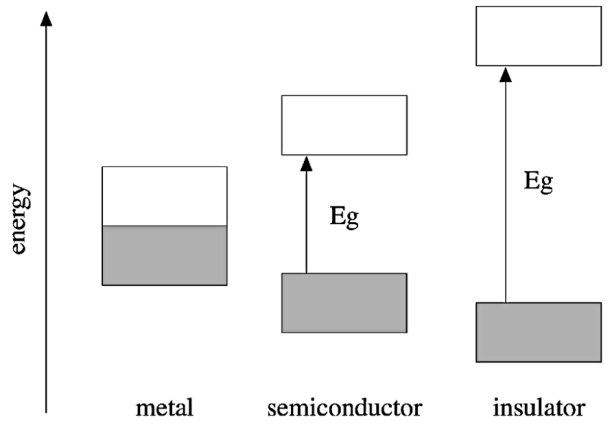

Figure 2.1: Band structure of metals, insulators and semiconductors. Adapted from [7].

2.1.2 Semiconductors and Their Optical Properties

For band gaps below 4 eV, solids are classified semiconductors. This band gap is small enough that at room temperature, some electrons can be thermally excited into the conduction band [8]. The interaction of light can create similar effects. Solids cannot absorb photons if their energy is less than the band gap; the photon cannot excite an electron from the valence band to the conduction band [8]. Photons that do not get absorbed pass through the solid. However, if the photons have an energy greater than the band gap of the semiconductor, light will get absorbed. As a result of this process, an electron will be excited to the conduction band [8].

2.1.2.1 Charge Carrier Generation

Free carriers in semiconductors can be generated optically by external electromagnetic fields, thermally by phonon fields, or by electric fields [9]. When an electron is excited to the conduction band, it leaves a hole in the valence band [10]. These electron-hole pairs are called charge carriers.

One more factor which has a role in charge carrier generation is the band gap structure of the semiconductor. If the k value, the wave vector of the conduction band minimum is the same as the valence band maximum, then the band gap is called a direct band

gap. If there is a difference in the k values, the band gap is called an indirect band gap [8],[11]. With indirect transition, momentum transfer is also necessary [8]. Figure 2.2 depicts indirect and direct transitions.

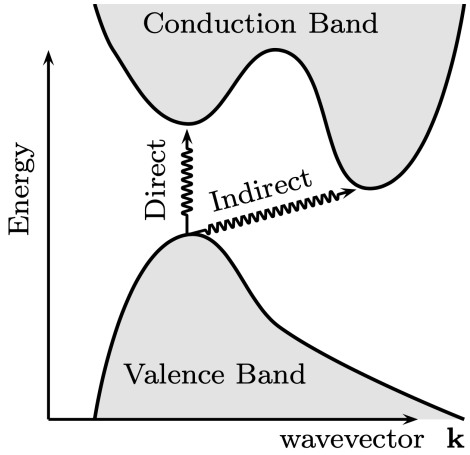

Figure 2.2: Direct and indirect band structure and transition. For indirect transition, momentum transfer is necessary. Adapted from [8].

2.1.2.2 Recombination

Charge carriers can be generated by externally applied fields but to reach a steady state, for every carrier generated, there must be an inverse process, which is called recombination [9]. Charge carrier recombination occurs in two paths. First is non-radiative recombination where thermal energy is released. Second is radiative recombination via luminescence [9].

In non-radiative recombination, the absorbed energy of the photon is redistributed among the lattice vibrations (phonons) [12]. Non-radiative recombination essentially converts an energy supplied to the system to heat, increasing the entropy [9]. Therefore, for most applications it is undesired since it decreases the efficiency [9].

TiO_2 is an indirect band gap semiconductor; the valence band maximum and the conduction band minimum are not aligned in the momentum space. In order for radiative recombination to take place in titania, phonon assistance is required, which makes the process less likely to happen [13]. However, through non-radiative recombination, momentum can be conserved easily via emitted phonons, increasing the probability

of non-radiative recombination [13].

2.1.3 Semiconductor Photocatalysis

The photocatalytic processes happening on a semiconductor surface can be summarized as [14]:

- Charge carrier generation
- Migration and trapping of charge carriers
- Charge transfer
- Adsorption of reactants
- Reaction
- Charge recombination

Figure 2.3 depicts the processes occurring on a semiconductor particle. Upon illumination with light having greater energy than the band gap of the photocatalyst, charge carriers are generated. The charge carriers are in fact an electron in the conduction band and a hole in the valence band of the semiconductor.

Chemically, holes can be characterized as a bound lattice oxygen or an OH radical [15]. The holes can further engage in interfacial charge transfers, oxidation reactions [15],[16] or undergo charge recombination.

If migration of the charge carriers carriers to the surface occurs, redox processes can occur with electron donors (D) or acceptors (A) adsorbed on the surface [15]:

$$\text{semiconductor} \longrightarrow \mathrm{e^-} + \mathrm{h^+}$$
$$\mathrm{h^+} + \mathrm{D} \longrightarrow \mathrm{D^{\bullet +}}$$
$$\mathrm{e^-} + \mathrm{A} \longrightarrow \mathrm{A^{\bullet -}}$$

Interaction of holes with water present on the surface can produce OH radicals [16]. OH radicals are thought to have a major role in photocatalytic processes. Importance of OH radicals and their role in photocatalytic NO oxidation will be discussed in the following sections.

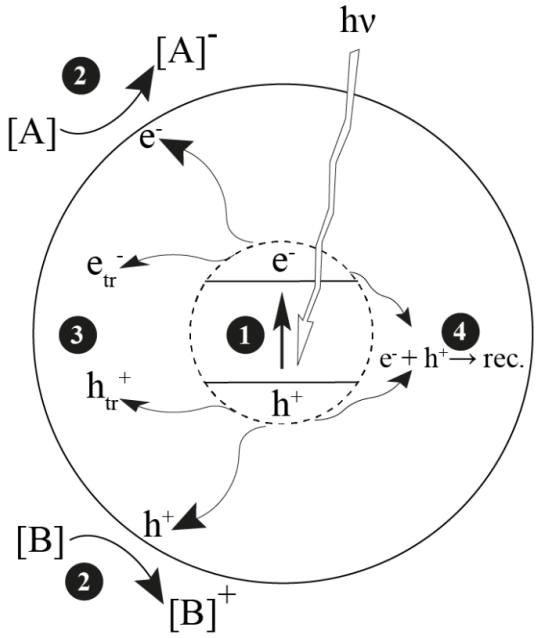

Figure 2.3: Photocatalytic processes on a semiconductor particle [17]. (1) is charge carrier generation. (2) is reaction with adsorbed species. (3) is charge carrier trapping. (4) is recombination.

2.2 OH Radicals and Photocatalysis

In 1990, Turchi and Ollis published an article on the role of hydroxyl radicals in photocatalytic reaction mechanisms. Kinetic data acquired from many photocatalytic oxidation reactions involving different species were similar, yet these species would have different adsorption characteristics. A common rate determining step would explain this similarity. Meanwhile, studies were showing that photocatalytic surface hydroxilation was necessary for oxidation reactions and reaction intermediates were mainly hydroxilated species. Due to evidence pointing towards OH radicals, authors sought the answer there and analyzed four different cases regarding the reacting species and OH radicals. These cases are as follows:

1. The reacting species and the hydroxyl radical are both adsorbed on the surface.
2. The radical is adsorbed on the surface, but the reacting species is not.
3. The reacting species is adsorbed but the OH radical is not.
4. Neither of the species are adsorbed.

These cases were modeled and evaluated. Case 1 and 2 are rather straightforward in terms of catalysis. Investigation and an order of magnitude analysis of case 3 and 4 showed that diffused OH radicals can certainly start reactions, although their diffusion length would be small. None of the cases were identified as the true representation, but the findings revealed that the possibilities were plausible [18].

Minero et al. published a series of articles on TiO_2/F systems in 2000. Fluoride ions displace most of the hydroxyl groups on titania surface. The authors observed an increase in the rate of photocatalytic degradation of phenol on TiO_2/F catalysts compared to bare TiO_2 as seen in Figure 2.4. This was attributed to the decreased hole trapping abilities of the fluorinated surface since there was no hydroxyl groups to capture the hole and form $OH\cdot$. This in turn led to more holes lingering and forced the reaction to proceed in different paths [19].

The authors later used alcohols as free OH radical scavengers to further investigate the possible pathways with TiO_2/F catalysts. Although they were skeptical of the

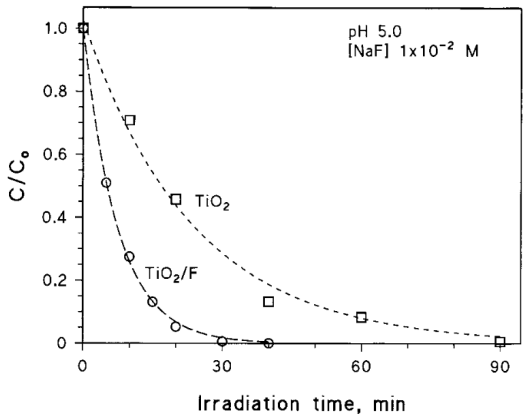

Figure 2.4: Photocatalytic degradation of phenol on TiO_2/F catalysts [19].

technique, it was concluded that with fluorinated surfaces the reaction proceeds homogeneously with $OH\cdot$, not with surface bound $OH\cdot$ species [20].

Choi et al. investigated photocatalytic tetramethylammonium (TMA) degradation in an aqueous medium. pH of the solution affects how TMA interacts with the catalyst. FTIR spectroscopy analysis showed that in acidic mediums TMA is repelled by the catalyst but adsorbs at high pH. To investigate the role of OH radicals on the reaction, t-BuOH, a free OH radical scavenger was used. The reaction was completely inhibited in the acidic medium, implying that possible free OH radicals which can degrade the non-adsorbed TMA was captured by the scavenger. At higher pH, however, the reaction was only partially inhibited, suggesting that the surface bound radicals were still reacting with the adsorbed TMA [21].

In 2004, Salvador et al. analyzed the kinetics of photooxidation reactions in aqueous media with electrodes, utilizing external potentials. The authors constructed kinetic models involving reactions of direct and indirect hole transfers. The direct hole transfer mechanism involves the photo generated hole reacting directly with the adsorbed molecule. In indirect hole transfer, the photo generated hole reacts with an hydroxyl group on the surface and yields an OH radical on the surface. The radical then oxidizes the reacting species, which is not adsorbed in this case. They claimed that the two mechanisms could be distinguished by analyzing the behavior of photocurrent with respect to photon flux density. With direct hole transfer, the photocurrent depends linearly on the illumination intensity, but with indirect hole transfer mech-

anism, the rate of change of photocurrent with respect to flux decreases. In cases where both pathways exist, distinguishing between them becomes more difficult. The authors later backed their claims up with experimental evidence, testing two different molecules known to be involved with either of the mechanisms, direct or indirect [22],[23]. Three years later, Salvador group published another paper presenting their advances on the topic. They disregarded the possibility of desorption of photo generated OH radicals from the surface into an aqueous solution, calling it a misconception [24].

In 2006, Murakami et al. claimed to have detected free OH radicals in the gas phase, diffused from TiO_2 surface under UV illumination for the first time. The study was done in situ using laser induced fluorescence technique [25], [26]. When non-photocatalytic powders were tested, this effect was not observed [26]. This also eliminates the possibility of free moisture as a source of OH radicals. In 2010, Murakami et al. also detected diffused gas phase OH radicals from Pt/TiO_2 and WO_3/TiO_2 proving that the phenomena is not limited to bare TiO_2 [27]. Laser induced fluorescence was also used by other studies to find OH radicals in the gas phase near TiO_2 confirming the possibility of gas phase oxidation of molecules by photocatalysis [28],[29].

In a recent interesting study by Ding et al. it was suggested that the presence of Brönsted acid/base sites on TiO_2 was responsible for free OH radicals. For comparison, BiOCl was analyzed. BiOCl lacks Brönsted acid/base sites, and was found to be an unfavorable catalyst for free OH radical formation. However, when modified to contain more acid/base sites, the generation of free OH radicals was enhanced [30].

In addition to the ones already discussed, several more authors have studied the importance of OH radicals in photocatalytic reactions but no definite answer on how exactly the mechanisms occur was reached [31],[32],[33],[34].

2.3 Photocatalytic NO Oxidation over TiO_2

2.3.1 Mechanisms

Many researchers have proposed mechanisms regarding photocatalytic NO oxidaiton over TiO_2. All of the proposed steps start with photogeneration of charge carriers, electron and hole pairs. These charge carriers later start photocatalytic reactions where disagreements occur. Several of the mechanisms are proposed are described below.

In 2002, Dalton et al. [35] proposed the following mechanism:

$$\mathrm{TiO_2 + hv \longrightarrow e^-_{CB} + h^+_{VB}}$$
$$\mathrm{OH^-_{(ads)} + h^+_{VB} \longrightarrow OH^\bullet_{(ads)}}$$
$$\mathrm{O_{2(ads)} + e^-_{CB} \longrightarrow {O_2}^-{}_{(ads)}}$$

Oxidation with hydroxyl radicals:

$$\mathrm{NO + 2\,OH^\bullet_{(ads)} \longrightarrow NO_{2ads} + H_2O_{(ads)}}$$
$$\mathrm{NO_{2(ads)} + OH^\bullet_{(ads)} \longrightarrow {NO_3}^-{}_{(ads)} + H^+_{(ads)}}$$

Oxidation with ${O_2}^-$:

$$\mathrm{NO_{(ads)} \xrightarrow{{O_2}^-{}_{ads}} {NO_3}^-{}_{(ads)}}$$

Reaction with Ti-OH via disproportionation:

$$\mathrm{3\,NO_2 + 2\,OH^- \longrightarrow 2\,{NO_3}^- + NO + H_2O}$$

In 2009, Ohko et al. [36] proposed a reaction mechanism where the oxidizing species

were lattice oxygen species instead of OH radicals:

$$
\begin{aligned}
\mathrm{TiO_2 + hv} &\longrightarrow \mathrm{e^-_{CB} + h^+_{VB}} \\
\mathrm{NO + h^+_{VB} + H_2O_{(ads)}} &\longrightarrow \mathrm{HNO_2 + H^+} \\
\mathrm{NO + O^-_{surface} + H_2O_{(ads)}} &\longrightarrow \mathrm{HNO_2 + V[O^{2-}_{surface}] + OH^-_{ads}} \\
&\longrightarrow \mathrm{HNO_2 + O^{2-}_{surface} + H^+} \\
\mathrm{HNO_2 + h^+_{VB}} &\longrightarrow \mathrm{NO_2 + H^+} \\
\mathrm{HNO_2 + O^-_{surface}} &\longrightarrow \mathrm{NO_2 + O^{2-}_{surface} + H^+} \\
\mathrm{HNO_2 + O^-_{surface}} &\longrightarrow \mathrm{HNO_3{}^- + V[O^{2-}_{surface}]} \\
\mathrm{V[O^{2-}_{surface}] + OH^-_{ads}} &\longrightarrow \mathrm{O^{2-}_{surface} + H^+} \\
\mathrm{HNO_3{}^- + O^-_{surface}} &\longrightarrow \mathrm{HNO_3 + O^{2-}_{surface}}
\end{aligned}
$$

where $\mathrm{V[O^{2-}_{surface}]}$ represent bridging oxygen vacancies and $\mathrm{O^{2-}_{surface}}$ represent terminal oxygen species [36].

In 2010, Yu et al. [37] proposed:

$$
\begin{aligned}
\mathrm{TiO_2 + H_2O} &\longleftrightarrow \mathrm{H_2O_{(ads)}} \\
\mathrm{TiO_2 + O_2} &\longleftrightarrow \mathrm{O_{2(ads)}} \\
\mathrm{TiO_2 + NO} &\longleftrightarrow \mathrm{NO_{(ads)}} \\
\mathrm{TiO_2 + hv} &\longrightarrow \mathrm{e^-_{CB} + h^+_{VB}} \\
\mathrm{h^+_{VB} + H_2O_{(ads)}} &\longrightarrow \mathrm{OH^\bullet + H^+} \\
\mathrm{e^-_{CB} + O_{2(ads)}} &\longrightarrow \mathrm{O_2{}^{\bullet -}} \\
\mathrm{NO_{(ads)} + OH^\bullet} &\longrightarrow \mathrm{HNO_{2(ads)}} \\
\mathrm{HNO_{2(ads)} + OH^\bullet} &\longrightarrow \mathrm{NO_{2(ads)} + H_2O} \\
\mathrm{NO_{2(ads)} + OH^\bullet} &\longrightarrow \mathrm{NO_3{}^- + H^+}
\end{aligned}
$$

In 2015, Uner et al. [38] proposed:

$$\begin{aligned}
\mathrm{TiO_2 + hv} &\longrightarrow \mathrm{TiO_2{}^* + h^+_{VB} + e^-_{CB}} \\
\mathrm{e^-_{CB} + Ti^{4+}} &\longrightarrow \mathrm{Ti^{3+}} \\
\mathrm{h^+_{VB} + O^{2-}_{(surface)}} &\longrightarrow \mathrm{O^-_{(surface)}} \\
\mathrm{O_2 + Ti^{3+}} &\longrightarrow \mathrm{O_2{}^-{}_{(ads)} + Ti^{4+}} \\
\mathrm{H_2O + O^-_{(surface)}} &\longrightarrow \mathrm{H_2OO^-_{(surface)}} \\
\mathrm{H_2OO^-_{(surface)}} &\longrightarrow \mathrm{2\,OH^-_{(surface)}} \\
\mathrm{2\,OH^-_{(surface)} + O^-} &\longrightarrow \mathrm{2\,OH^\bullet_{(surface)} + O^{2-}}
\end{aligned}$$

Presence of OH radicals on the surface, adsorbed NO can oxidize effectively as:

$$\begin{aligned}
\mathrm{NO + OH^\bullet_{(surface)}} &\longrightarrow \mathrm{HNO_{2(surface)}} \\
\mathrm{HNO_{2(surface)} + OH^\bullet_{(surface)}} &\longrightarrow \mathrm{NO_2 + H_2O} \\
\mathrm{NO + HO^\bullet} &\longrightarrow \mathrm{HNO} \\
\mathrm{NO + O_2{}^{\bullet-}} &\longrightarrow \mathrm{NO_3{}^-}
\end{aligned}$$

2.4 Effect of Light Intensity

2.4.1 Case on Illumination Intensity

Illumination is the beginning of photocatalysis; photons generate charge carriers and the rest follows this step. Photon flux is therefore one of the main parameters affecting a photocatalytic process.

Studies on illumination intensity show that the rate of a photocatalytic reaction depends on irradiance, with higher photon fluxes reaction rates usually increase. A general relation between reaction rates and illumination intensity is the following. At low illumination intensities, the reaction rate is first order with respect to light intensity, the rates increase linearly with increasing light intensity. Above 1 sun equivalent illumination, this relation becomes a square root relation, meaning that photocatalytic reaction rates increase with illumination intensity raised to the power of 0.5. At even higher intensities, the reaction rate is not a function of intensity, and the system becomes saturated [39].

The transition between the linear region and the square root region depends on the catalyst, gas flow and mass transfer behavior of the system. It is also worth noting that addition of some charge carrier acceptors may extend the first order region to higher illumination intensities [39].

2.4.2 Photocatalytic NO Oxidation: Effect of Light Intensity

One of the earlier publications studying several experimental parameters of photocatalytic NO oxidation is by Lim et al. in 2000 [40]. The authors used TiO_2 P25 for the catalyst, however their reactor was an annular flow type reactor where the catalyst is coated on the inner surface of the tubes and the UV light is supplied from exterior. UV light intensity was among the experimental parameters they tested. Two different wavelengths were used for different light intensities, the reason for this is not explained. For low intensities a 365 nm lamp, and for high intensities a 254 nm lamp was used. The authors argue that their results are in good agreement with the literature where for low irradiance reaction rate increases almost linearly and at higher

irradiances the rate increases with a square root relation. The power law relation was given as:

$$Rate = (Rate_0) * (Intensity)^n$$

Where n is 0.47 at high intensities and 0.87 at lower intensities. However, the two regimes correspond to different wavelengths and the effect is not thoroughly discussed. One information mentioned is the following: at shorter wavelengths, light is absorbed more strongly by the catalyst resulting in a shorter penetration depth of photons. The charge carriers are therefore generated closer to the surface, their migration to the surface becomes easier. This possibly increases the efficiency of the process by reducing the time available for charge recombination [40].

Hüsken et al. studied the effect of illumination intensity on photocatalytic NO oxidation over various concrete pavement blocks mixed with TiO_2. Their experimental results was fitted as $Conversion = 8.58 * (Intensity)^{0.43}$. The authors explain that their results are not in agreement with previous studies where a linear dependency is shown for low light intensities and at high intensities the relations become a square-root relation [41].

In 2010, Ballari et al. studied kinetic modelling of photocatalytic NO oxidation over TiO_2 in addition to their experimental studies. The study also focused on light intensity as a parameter. They argued that according to widely accepted reaction mechanisms, illumination only has an effect on the reaction steps where NO and NO_2 are involved since these are the steps that are initiated via hydroxyl radicals. This is because photogenerated holes are trapped by the water molecules forming hydroxyl radicals [42].

When the catalyst is illuminated, photogenerated holes are trapped by the water molecules forming hydroxyl radicals. According to reaction mechanisms proposed, NO and NO_2 molecules react with these hydroxyl radicals. This means that illumination intensity only has an effect on the NO and NO_2 degradation steps. The authors propose the following rate constant relations for irradiance and NO/NO_2 reaction with hydroxyl radicals:

$$k_{NOx} = k'_{NOx}(-1 + \sqrt{1 + \alpha I})$$

where k is the rate constant, α and k' are numerical factors for the model.

The authors models are in very good agreement with their experimental results [42]. They also claim that their model equations agree with other studies that show linear dependency for low irradiance and a square root dependency for high irradiance.

Hunger et al. later argued in 2010 that an equilibrium constant related to NO adsorption in their mathematical model discussed in their previous study [42], is not affected by illumination intensity. This means that light intensity has no effect on the adsorption behavior. However, in making this decision, they omitted the first 3 data points of their 11 measurements. These 3 data correspond to low irradiance and show some dependency on illumination. The authors justify this decision by arguing that their light set up is not stable at these low illumination intensities. It is worth noting that light adjustment was made using a light dimmer rather than utilizing distance as intensity control[43].

In 2009, Yu et al. published an extensive study on NO oxidation over carbon doped TiO_2, testing various experimental parameters including flow rate, humidity, inlet NO concentration and light intensity. Their light intensity tests revealed logarithmic relations between illumination intensity and conversion as seen in Figure 2.5. However, carbon doped titania is photocatalytically active in the visible light region and blue visible light was used in this study [44].

Dillert et al. conducted experiments at different inlet NO concentrations with varying light intensities, adding another dimension to the topic. One interesting observation they made was at higher light intensities, NO conversion increased with increasing inlet concentrations. However, at lower intensities, increasing the inlet NO concentration does not have an effect after a certain concentration. The authors fitted their experimental data into Langmuir-Hinshelwood type kinetics.

$$rate = \frac{k(I)K(I)c_{NO}^{m}}{1 + K(I)c_{NO}^{m}}$$

$$k(I) \propto I$$

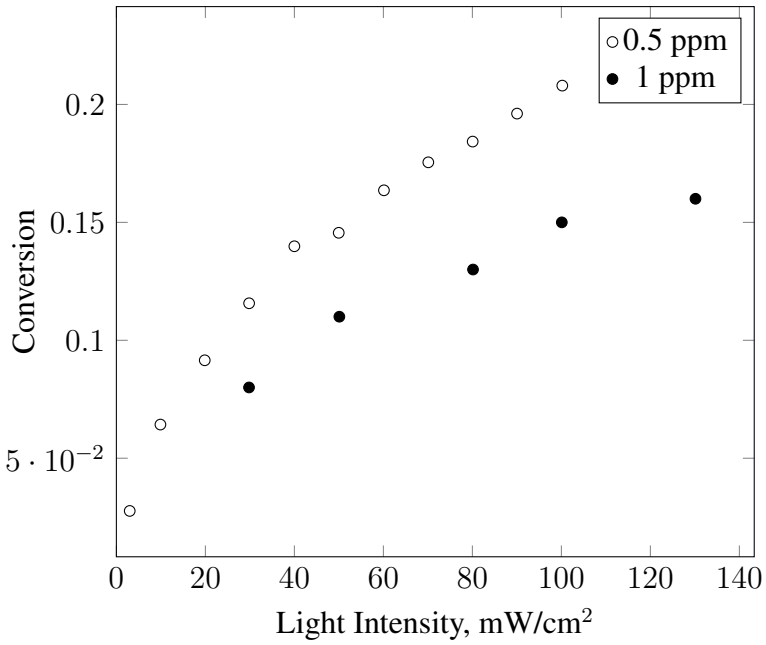

Figure 2.5: Effect of UV light intensity on NO conversion over carbon doped TiO_2 [44].

$$K(I) = \frac{k_{ads}}{k_{des} + k(I)}$$

Numerical values for k_{ads}, k_{des} were obtained by non-linear regression analysis [45]. Their model agrees with the experimental data as seen in Figure 2.6. However, they do not find a power relation between UV intensity and conversion. In addition, one of the most important assumptions they make is that nitric oxide is the only nitrogen containing species adsorbed on the surface [45],[46].

In 2015, Sikkema et al. also studied photocatalytic NO oxidation over concrete pavements containing titania. Their investigation of illumination intensity revealed a linear relationship between light intensity and NO oxidation rate [47].

Reported conversions with respect to light intensity are compiled and presented in Figure 2.7. Unless otherwise noted, experiments were done at 50% relative humidity, 1 ppm NO inlet and 3 L/min flowrate. The results are also summarized in Table 2.1.

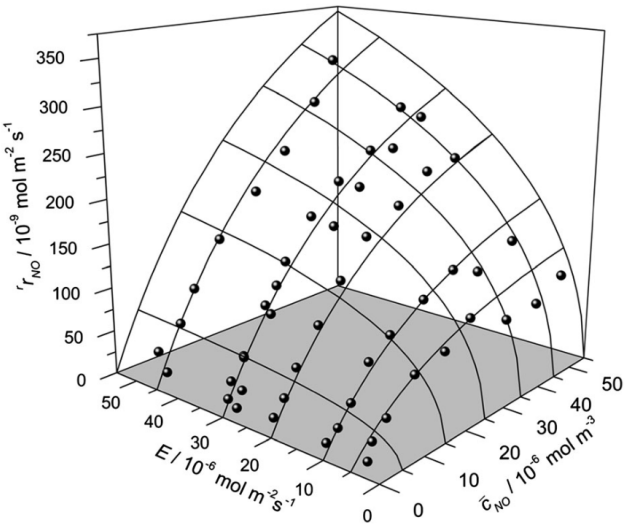

Figure 2.6: NO oxidation rate with respect to light intensity and NO concentration [46]. Points represent experimental data, curves are model predictions.

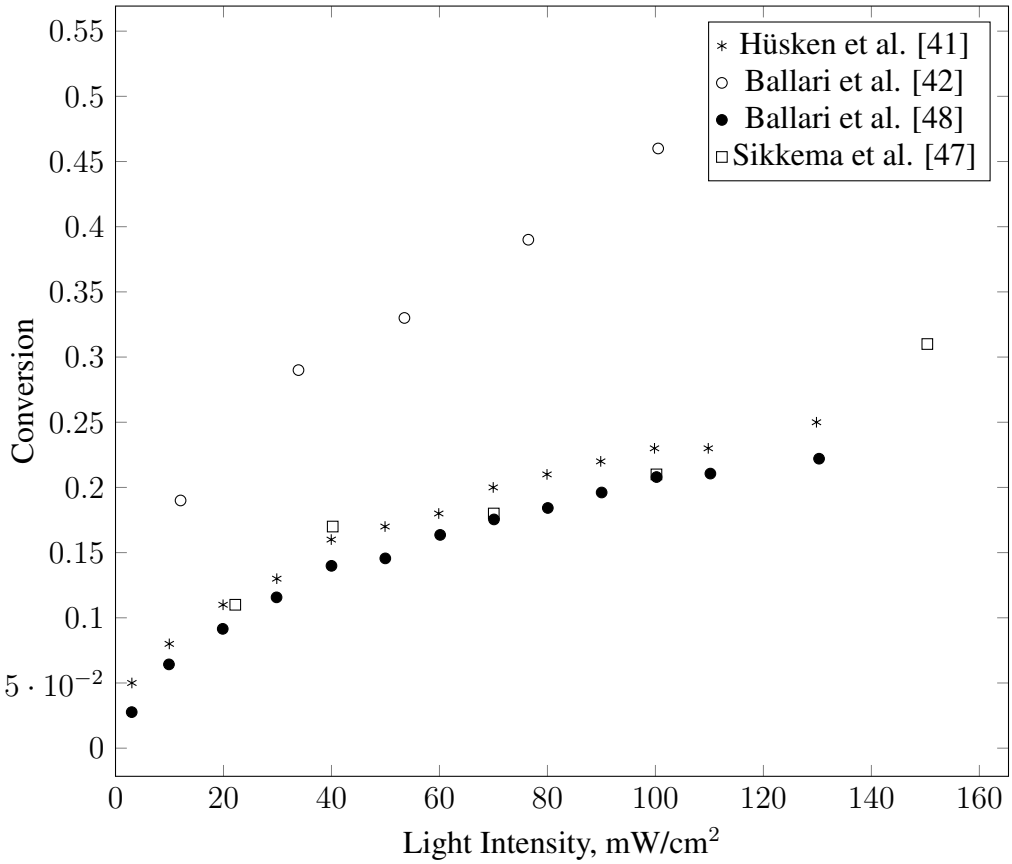

Figure 2.7: Effect of UV light intensity on NO conversion.

Table 2.1: Effect of light intensity on photocatalytic NO oxidation.

Reaction	**Catalyst**	**Light Intensity (mW/cm^2)**	**Relative Humidity**	**Flowrate (L/min)**	**[NO] (ppm)**	**Model Equations**	**Comments**	**Ref.**
NO Oxidation	TiO_2 P25	0-4	-	0.1	50	$rate \propto I^n$	low I: n=0.87 high I: n = 0.47	[40]
	TiO_2/concrete	0-130	50%	3	1	$conversion = 8.58 * I^{0.4}$	No linear behavior was seen.	[41]
	TiO_2/concrete	0-130	50%	3	1	$rate \propto (-1 + \sqrt{1 + \alpha I})$	α is numerical fit parameter.	[42]
	TiO_2/concrete	0-110	50%	3	1	$K_{ads} \neq I$	Adsorption characteristics do not depend on light intensity.	[43]
	C doped TiO_2	0-130	50%	3	0.5	$conversion = 5.43 * ln(I) + 8.41$	Active in visible light region.	[44]
	C doped TiO_2	0-130	50%	3	1	$conversion = 5.99 * ln(I) + 1.67$	Active in visible light region.	[44]
	TiO_2 P25	0-150	50%	3	0.05-1.3	$rate = \frac{k(I)K(I)c_{NO}^m}{1 + K(I)c_{NO}^m}$ $k(I) \propto I$ $K(I) = \frac{k_{ads}}{k_{des} + k(I)}$	No power relation was concluded.	[45],[46]
	TiO_2/concrete	20-150	50%	3	1	-	Linear relationship was found.	[47]
	TiO_2/concrete	20-110	50%	3	1	-	Linear relationship can be interpreted.	[48]
General	-	-	-	-	-	$rate \propto I^n$	low I: n = 1 intermediate I: n = 0.5 high I: n = 0	[39]

2.5 NO_x Adsorption

Many catalytic reaction networks have adsorption of the reacting species on the surface of the catalyst as their initial step. However, photocatalytic systems are complicated and many other species such as water also important roles in the reactions. Regarding this, a literature survey of adsorption of nitric oxide and other NO_x species on to titania is presented below.

2.5.1 FTIR Studies of NO Adsorption

Earlier work done by Hadjiivanov et al. in 1994 investigated NO_2 adsorption on TiO_2 (anatase phase) using FTIR spectroscopy. The authors concluded that the adsorption process leads to three main types of species. The first is TiO_2NOH species where the nitrogen atom is between the lattice oxygens and the OH group, second is mono and bidentate nitrate species with water coordination, and lastly nitrates and NO^+. It is also noted that adsorbed NO_2 species change the surface acidity. Lewis acid sites are blocked when nitrates are formed and Bronsted acidity occurs if an interaction with any existing hydroxyl groups takes place. The authors also investigated O_2 and water co-adsorption. While the introduction of oxygen did not lead to any changes, water presents a different story. Figure 2.8 below shows what happens when water is introduced after NO_2 adsorption and NO_2 is introduced to a water saturated surface. The spectra suggest that there is water adsorbed on the surface if water and NO^+ species does not form with a hydrated surface [49].

A later study of Hadjiivanov et al. in 2000 also used FTIR spectroscopy to investigate NO and NO + O_2 co-adsorption on TiO_2. NO introduction to TiO_2 showed very low intensity signals. However, co-adsorption of NO and O_2 was observed in this study [50]. Figure 2.9 represents a small portion of their results. Upon investigation of the bands and their behavior over time, the authors arrive at the conclusion that after adsorption, NO disproportionates into NO^-, $N_2O_2{}^{2-}$ and surface nitrates [50].

Another study by Sivachandiran et al. in 2013 [51] examined NO and NO_2 adsorption on TiO_2 separately. For nitric oxide, authors claim that there is no significant

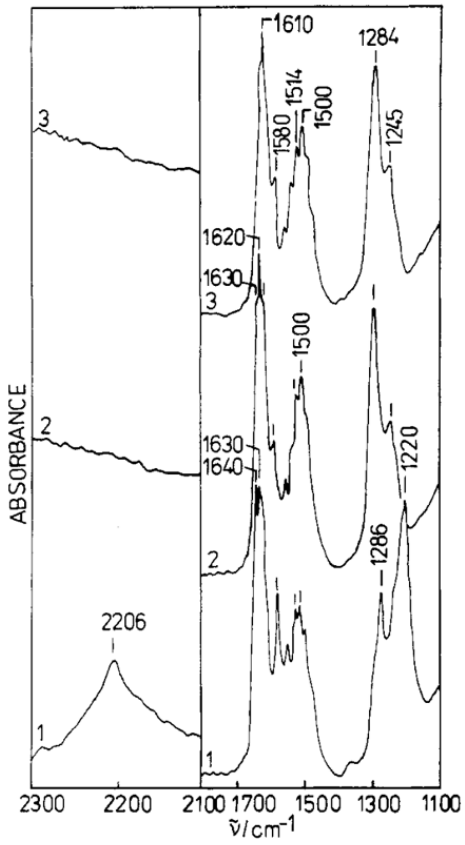

Figure 2.8: (1) NO_2 adsorption alone, (2) NO_2 adsorption followed by water adsorption, (3) Water adsorption followed by NO_2 adsorption [49].

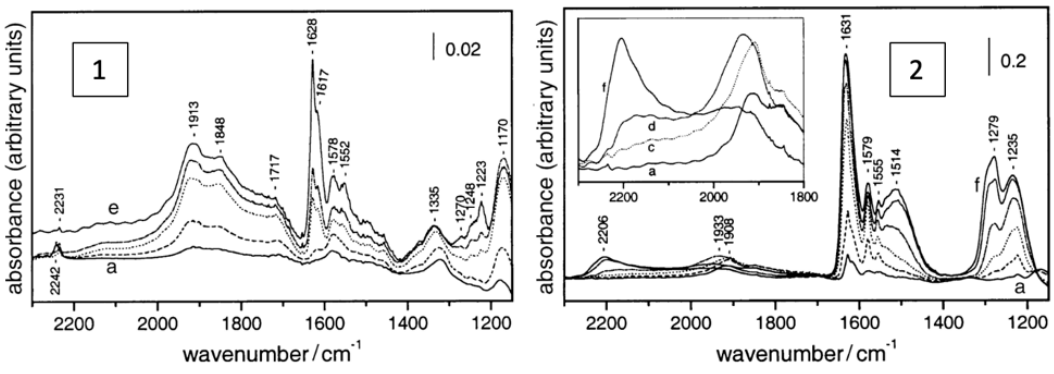

Figure 2.9: (FTIR spectra. (1): NO adsorption on TiO_2 where a is immediately after admission and b-e after time evolution. (2): NO and O_2 co-adsorption where a corresponds to curve e of part (1), c-d are time evolution of co-adsorption and e-f at higher O_2 pressures [50].

adsorption. This conclusion is raised from an experiment where NO is compared with a tracer which does not adsorb (N_2O) on the same reactor simultaneously. They report, however, that NO_2 adsorption is significant and it adsorbs in a reactive way, producing NO in gas phase. Their findings are discussed further under TPD section.

In a later study in 2016, Sivachandiran et al. found that NO_2 produces N_2O_4 instantly on the surface. They also report that if they are in close proximity to each other, NO_2^- and N_2O_4 will react to form NO in the gas phase leaving a strongly adsorbed NO_3^- on the surface [52].

Mikhaylov et al. also reported weak adsorption of NO on TiO_2 [53],[54]. In a 2009 article, the effect of UV irradiation was discussed. The authors claimed that UV-vis irradiation significantly enhanced NO adsorption. With photo-adsorption NO coverage increased. The authors discussed that formation of NO_3^- and NO_2^- followed the photo-adsorption [53].

Mikhaylov et al.'s 2013 article stated that NO adsorption on TiO_2 was weak in the absence of oxygen, as has other authors have claimed until now, but strongly increased in the presence of oxygen. They reported an optimum ratio of NO to O_2 of 3 [54].

A 2020 review article by Pichat references several articles including Ward et al. (who also uses FTIR spectroscopy), and reports that surface nitrato species are very stable that they do not get involved in photocatalytic reactions easily, but the weak adsorption of NO does allow for it. Pichat interestingly points out to the fact that the effect of UV irradiation on these species at room temperature is not yet determined but he does not expect the thermal effect to be high [55],[56].

2.5.2 TPD Studies of NO Adsorption

Yates et al. in 2000 showed with TPD that NO adsorbs weakly on oxidized TiO_2 and desorbs at 127 K. They also reported that for low coverages, NO adsorption occurs nondissociatively and only when coverages surpass 5.5×10^{14} molecules/cm^2 conversion to N_2O starts. This happens because the NO molecules on the surface get very close after a threshold coverage and they start to interact. The authors reported adsorption energies for different species which is given in Table 2.2. These values

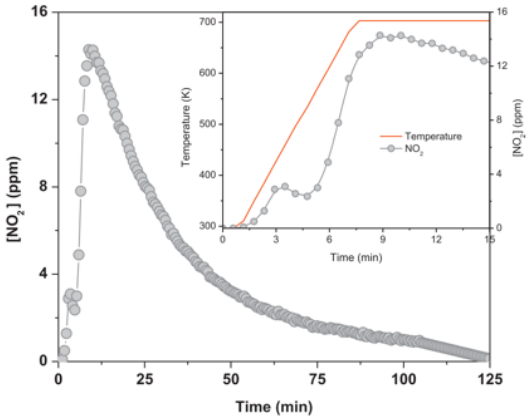

Figure 2.10: TPD curve for NO_2 [51].

are reported to be a combination of calculation and experiment. Adsorption of NO_2 appears to be weaker than NO which is in contradiction with Hadjiivanov's work presented above [57].

Table 2.2: Adsorption energies of NO_x species [57].

Species	Adsorption Energy (kJ/mol)
NO	35.1
N_2O	32.3
NO_2	8.8

Sivachandiran et al. [51] also reported TPD results for NO_2. Their results are shown in Figure 2.10. NO_2 desorption happens with two distinct peaks. The first desorption peak is attributed to the weakly bound NO_2^- or NO_3^-. The second broad peak at 9 minutes was reported to be for strongly adsorbed species. By constructing a material balance, authors claimed that 97% of NO_2 is present as strongly adsorbed NO_3^-. The adsorption mechanism they proposed is presented below.

$$2\,NO_{2(ads)} \rightleftharpoons {NO_2}^- + NO^+_{(ads)}$$

$$NO + O^{2-}_{(TiO2,surfacelattice)} \rightleftharpoons {NO_2}^-{}_{(ads)}$$

$${NO_2}^-{}_{(ads)} + NO_{2(ads)} \rightleftharpoons {NO_3}^-{}_{(ads)} + NO$$

2.5.3 Other Studies

Maiti et al. studied the interaction of NO_2 and TiO_2 using XANES, DFT, and photoemission experiments [58]. It was also concluded here that the main product of the adsorption of NO_2 on TiO_2 is surface nitrate. There is also a small amount of NO_2 chemisorbed. The authors added that adsorbed NO_2 alters the thermochemical stability of the oxygen vacancies, which results in their easier migration from the bulk to the surface.

A conclusion reached by many researchers is that nitric oxide does not adsorb on TiO_2 surface. If, however, NO does not adsorb significantly on TiO_2, questions appear regarding the photocatalytic mechanism. These issues will be discussed later on.

2.6 Transient Behavior of NO Oxidation

In 2003, Devahasdin et al. studied the transient behavior of the photocatalytic NO oxidation over TiO_2 where they found similar results to this thesis. Conversion of NO is high at the beginning of the reaction but later decreases and reaches steady-state in approximately 6 hours. Authors additionally reported that as the amount of catalyst coated increases, this time also increases [59].

The two main products of photocatalytic NO oxidation are NO_2 and HNO_3. A small amount of HNO_2 is also produced. The authors explain that during the transient period, HNO_3 and HNO_2 are both produced. However, in time, equilibrium between the catalyst and the nitrite/nitrate species are established. After equilibrium, NO is only converted to NO_2 [59].

To explain the initial high rates, Devahasdin et al. argued that the OH radicals react with adsorbed NO very quickly to form adsorbed HNO_2. This period lasts between half a minute to 3 minutes. After a few minutes, the reaction between HNO_2 and OH radicals begins to compete with the prior reaction as the amount of HNO_2 generated increases. This reaction produces NO_2 which is adsorbed on the surface. The adsorbed NO_2 can react with another OH radical to produce HNO_3. Eventually, the nitrite/nitrate species on the surface equilibriate and the surface becomes saturated with $NO_3{}^-$ as HNO_3 is very stable and dissociates into H^+ and $NO_3{}^-$. Since the surface is saturated with $NO_3{}^+$, the oxidation only goes as far as converting NO into NO_2 [59].

The proposed reaction regimes for the different stages of the photocatalytic process by Devahasdin et al. are summarized below [59]. This study, in addition to the articles discussed in section NO oxidation mechanisms [36],[37],[38], considers the time dependency of the process. The details of the reactions and the involvements of radical species are also not shown for simplicity by the authors.

Initially, the reactions taking place are the following:

$$\mathrm{NO} \xrightarrow{\text{fast}} \mathrm{HNO_2}$$

$$\mathrm{HNO_2} \xrightarrow{\text{slow}} \mathrm{NO_2}$$

In the transient period:

$$\mathrm{NO} \xrightarrow{\text{slow}} \mathrm{HNO_2}$$
$$\mathrm{HNO_2} \xrightarrow{\text{fast}} \mathrm{NO_2}$$
$$\mathrm{NO_2} \xrightarrow{\text{fast}} \mathrm{HNO_3}$$

The steady-state processes also depend on the space time. At short space times:

$$\mathrm{NO} \xrightarrow{\text{slow}} \mathrm{HNO_2}$$
$$\mathrm{HNO_2} \overset{\text{fast}}{\rightleftharpoons} \mathrm{NO_2}$$
$$\mathrm{NO_2} \overset{\text{fast}}{\rightleftharpoons} \mathrm{HNO_3}$$

At long space times:

$$\mathrm{NO} \rightleftharpoons \mathrm{HNO_2}$$
$$\mathrm{HNO_2} \rightleftharpoons \mathrm{NO_2}$$
$$\mathrm{NO_2} \rightleftharpoons \mathrm{HNO_3}$$

Ohko et al. in 2009 also found that HNO_3 accumulated on the surface of TiO_2 and after the surface was saturated, HNO_3 production stopped. However their results showed that by the time HNO_3 accumulation on the surface reaches a steady state, the NO concentration in the outlet has already reached a constant level. The authors also compared different film thicknesses of TiO_2. As the film thickness increased, more HNO_3 could be retained, therefore more time was required to saturate the surface with HNO_3 [60]. However, time to reach a steady level of outlet NO concentration did not change with increasing film thickness.

The authors later tested the samples where they deposited HNO_3 onto the surface of the catalyst and then tested the sample [60]. The transient behavior of fast to slow NO consumption remained. In conclusion, accumulation of HNO_3 and subsequent discontinuance of HNO_3 production was acknowledged. However, this was not associated with the transient behavior of the system [60].

In 2015, Mills et al. compared photocatalytic NO oxidation activities of TiO_2 coated samples with various coating methodologies [61]. All their samples showed slow

deterioration of photocatalytic activity when ISO standardized tests were conducted. The authors argued that initially NO is oxidized into HNO_3, but as time progresses, the surface becomes saturated with HNO_3. This leads to further HNO_3 produced reacting with NO to produce NO_2. At this moment the net reaction becomes NO to NO_2 conversion [61] which is in agreement with other studies.

The standard photocatalytic oxidation experiments were continued until NO_x removal was effectively stopped. The samples took between 3.5 hours to 74 hours to reach this state [61] which implies the coating methodology also has an effect on the transient behavior. After the samples were used in this manner, the ISO standardize experiments were conducted once more. This time samples showed little to no NO_x removal but acted as NO to NO_2 converters.

The authors then coated new samples and sprayed them with HNO_3. The sprayed samples were tested in the reaction set up. The results revealed an initial rise in the NO_x concentration with the HNO_3 sprayed samples. The authors argued that this is due to the fourth reaction where HNO_3 react with NO to produce NO_2. After sufficiently long time, the samples reached the same level of activity [61].

Krysa et al. also found increased amounts of HNO_3 remaining on the surfaces of TiO_2 and activated carbon/TiO_2 after photocatalytic NO oxidation. The authors, however, do not attribute this to decreased conversion throughout the reaction [62]. One interesting result from this study is the following. When light is turned off at the end of an experiment, NO_x concentration goes back to the inlet level with bare TiO_2, however with TiO_2 mixed with activated carbon, there is excess NO_x species released [62].

Several more authors attributed the transient behavior of the reaction to HNO_3 accumulating on the surface therefore blocking the active sites, resulting in a decreased steady state conversion [63], [64], [65].

Possibility of nitrite/nitrate species affecting the reaction dynamics will be also discussed in this thesis.

CHAPTER 3

MATERIALS AND METHODS

The materials and methods used throughout this study will be explained in this chapter. The materials section will be followed by photocatalytic NO oxidation experiment set up and standardization. Later, use of microcontrollers with sensors will be discussed. These sensors include an analog UV light intensity sensor and a digital temperature and humidity sensor. Finally, light intensity measurements, humidity data acquisition will be explained.

3.1 Materials

Titanium dioxide was coated on a glass substrate for photocatalytic NO oxidation. Degussa P25 TiO_2 by Evonik was used as catalyst. 0.0675 grams of TiO_2 powder was mixed in 1 ml of distilled water. The aqueous mixture was coated on a glass substrate and left to dry.

3.2 Characterization Methods

3.2.1 SEM Imaging

A TESCAN Vega 3 scanning electron microscope (SEM) was used analyze TiO_2 P25 samples. 3 samples were analyzed and compared. These samples were fresh TiO_2, used catalyst from the glass coating and TiO_2 which was mixed with water to form a slurry and then dried.

3.2.2 BET Analysis

BET analysis of two TiO_2 samples were done with a Micromeritics TriStar II surface analyzer. The samples were fresh TiO_2 powder and ceTiO2 which was mixed with water to form a slurry and then dried to simulate the processes occurring when coating glass substrates. The samples were degassed at 120 °C for 6 hours.

3.2.3 XRD Analysis

A Rigaku Miniflex diffractometer (40 kV, 15 mA, Cu K_α radiation) with a one dimensional detector was used analyze TiO_2 P25 samples. Scattering angles were between 10° and 80° with a 1 deg/min scan rate. 2 samples were analyzed and compared. These samples were fresh TiO_2, and TiO_2 which was mixed with water to form a slurry and then dried to simulate the processes occurring when coating glass substrates.

3.2.4 ESR Spectroscopy

Bruker microESR was used for ESR analysis. Fresh and used TiO_2 were compared under ambient conditions and under vacuum. Used TiO_2 was scraped off a NO oxidation test piece glass subjected to reaction conditions and then analyzed with no more then 10 minutes of waiting time.

3.3 Photocatalytic NO Oxidation

Photocatalytic NO oxidation measurements are the main part of this thesis. Experiments reveal performances of catalysts. In order to make meaningful measurements, experiments are conducted according to relevant standards. These standards describe how an experiment set up should be constructed and how experimentation should be carried out.

3.3.1 Measurement Set Up

The NO oxidation measurement set-up consists of the following equipment:

1. An air compressor and a gas cylinder containing a mixture of 100 ppm NO and nitrogen from Linde for the test gas supply.
2. Three mass flow controllers (MFCs) and a TerraLAB control station connected to MFCs.
3. A humidifier for adjusting the humidity content of the test gas by varying the flow rates.
4. A UV light transparent photo-reactor.
5. A 250 W 365 nm UV lamp.
6. A Thermo Scientific Model 42i NOx analyzer.

Figure 3.1 is a schematic of the experiment set-up. The components can be identified in the order given in the list above from left to right on the figure. Note that there are two lines for air, where one goes through a humidifier. By adjusting the flow rates of gases flowing through the humidifier, the humidity of the gas stream can be adjusted. Figure 3.2 shows a technical drawing of the photocatalytic reactor.

3.3.2 Experiment Standardization

Photocatalytic NO oxidation experiments are conducted according to the ISO 22197-1-2007 Standard [3]. A typical experiment is divided into three major steps.

The procedure starts with the air+NO mixture flowing through the by-pass line where the gas is sent directly to the NO_x analyzer. In this by-pass stage, nitric oxide concentration is adjusted from MFC control station. When desired inlet conditions are achieved, the flow is directed to the photo-reactor by turning a valve located before the reactor.

When the flow is directed to the reactor, extra volume due to the reactor causes a sudden volume expansion. This results in a dilution effect; NO concentration drops

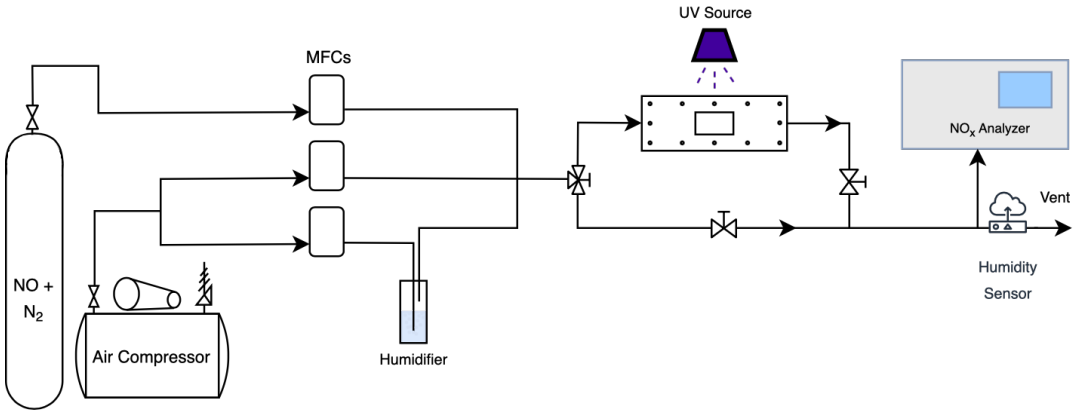

Figure 3.1: NO oxidation experiment set-up.

for a brief period of time and then recovers to its initially adjusted value. This time period also corresponds to the residence time of the reactor.

The test gas is allowed to flow through the reactor for 30 to 40 minutes. There is no UV illumination during this stage hence it is also called the dark stage. Dark stage allows the gases to reach an adsorption/desorption equilibrium with the test piece.

After 40 minutes, illumination is started and the reaction begins immediately. For most of the experiments, the initial conversion is high but it gradually decreases as time progresses and eventually reaches steady-state. The time the system takes to reach steady-state depends on the catalyst usage cycle, type, amount and other various parameters.

The experiment is stopped after steady-state is achieved. UV illumination is stopped. NO flow is shut off and 15 minutes of degassing period is started. After the degas period, the flow is directed back to the by-pass stream from the reactor.

These steps and their effects on a NO concentration versus time graph can be seen in Figure 3.3.

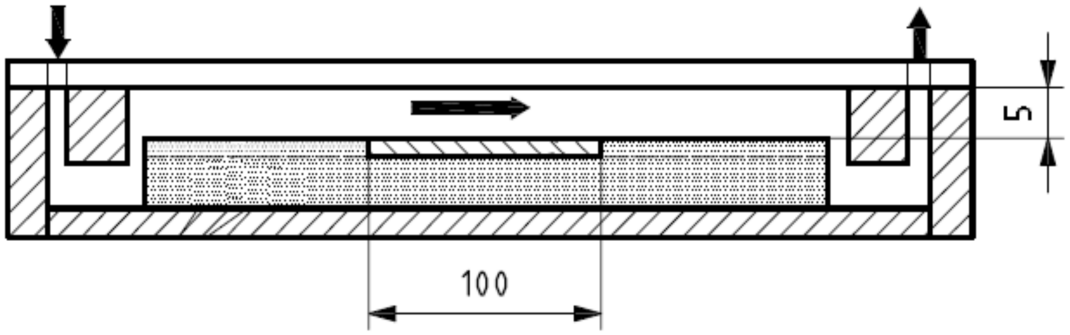

Figure 3.2: Technical drawing of the reactor. Side view [66].

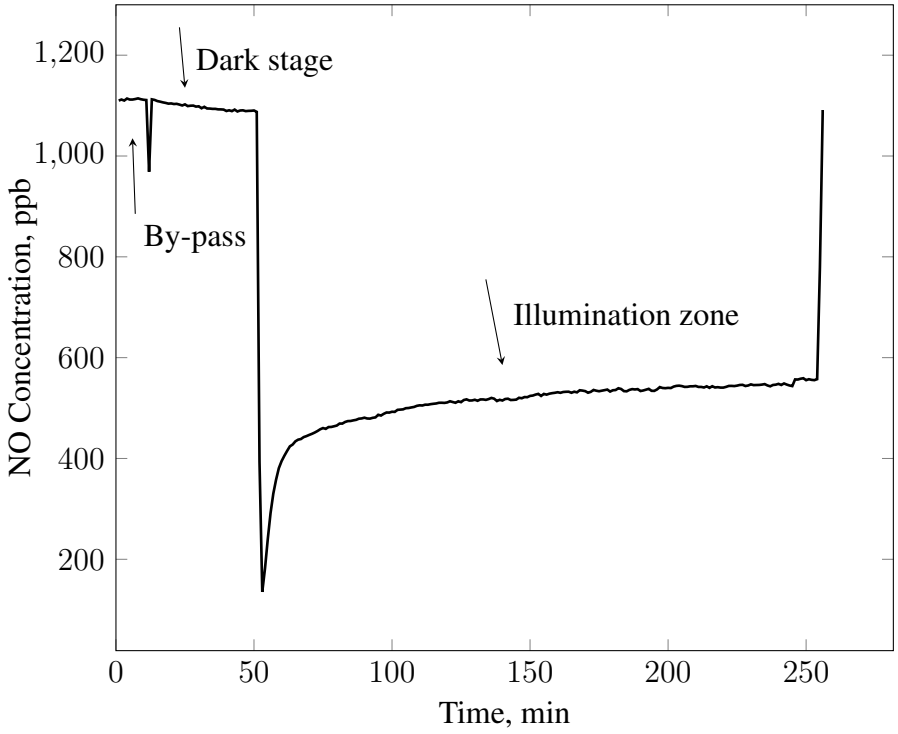

Figure 3.3: A standard photocatalytic NO oxidation experiment. By-pass stage, dark stage and illumination zone can be clearly distinguished.

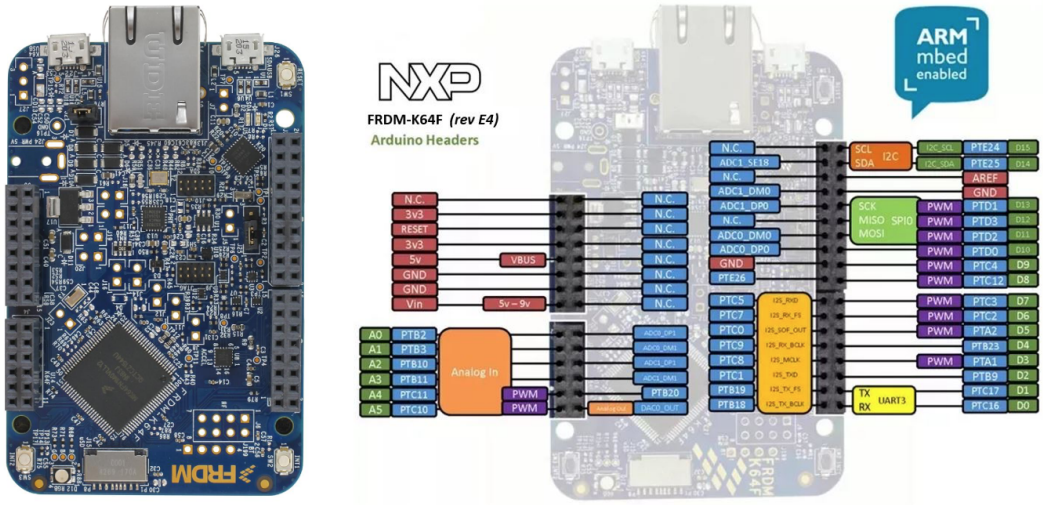

Figure 3.4: FRDM K64F Board and Pinout [68].

3.4 mbed Microcontroller

In order to quantify the experimental parameters in this study, two commercially available sensors were used. Data was acquired from these sensors with a microcontroller board. Embedded systems and how they were used in this study will be discussed in this section.

The essential parts of a computer are the central processing unit (CPU), memory and input/output features. Microcontrollers, in addition to these essential features, have other useful components and peripherals [67]. Microcontroller chips are usually placed on a printed circuit board (PCB) (see Figure 3.4) for easy use and prototyping.

In this study, a Freedom K64F arm mbed microcontroller board was used to log sensor data. The K64F pinout (see Figure 3.4) is similar to an Arduino R3 which is a commonly available microcontroller board. Therefore the K64F is compatible with many shields and other prototyping components designed for the Arduino R3, making it easy to use.

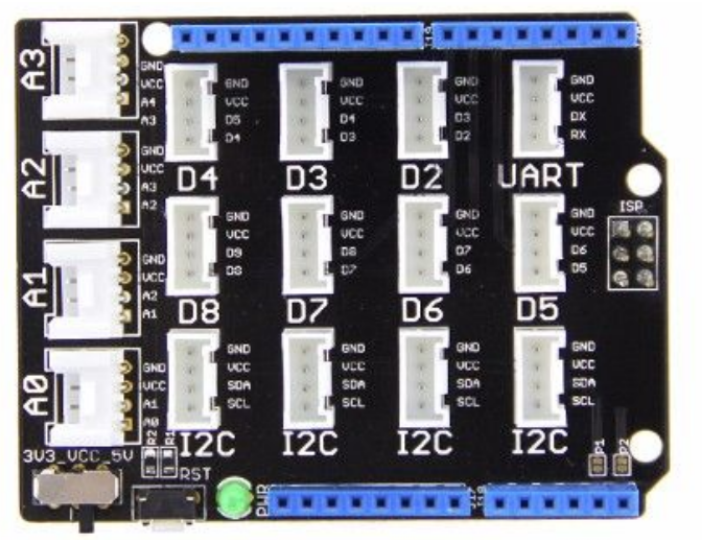

Figure 3.5: Grove Base Shield [69].

3.4.1 Shields

Shields are components that have specific purposes and can be attached on to microcontroller boards without any soldering work required. They are advantageous because they provide easy and quick prototyping. In this study a Grove base shield seen on Figure 3.5 was used. This shield is compatible with many components and sensors. These components can be connected to the microcontroller board via the shield with universal four pin connector cables. In this study the analog, digital and I2C pins for an I2C interfaced LCD were used.

3.4.2 Liquid Crystal Display

The mbed can communicate with a computer serially via a cable. Sensor readings and time can be printed on a terminal emulator. However, a computer may not always be available near the measurement site. Even if a computer is nearby, long cables may be necessary for data transfer. This introduces a difficulty in taking measurements. A portable device where data can also be displayed is convenient for these situations. A small liquid crystal display can be used for such purpose.

A Grove RGB LCD with I2C interfacing was used to display sensor readings and a

clock when necessary. The module is easily attached with a four pin connector to the I2C port on the base shield. I2C is a serial communications protocol where only two interconnect wires are necessary [67]. These are the SDA - serial data, and the SCL - serial clock lines. The clock line is used for synchronization purposes. The data line is for sending and receiving data. Multiple devices can use an I2C port at the same time, with few wires required.

Using a display is very advantageous since the microcontroller board can be powered up with a commonly available 5V USB adapter without the need of a computer. Measurements can be made quickly this way.

3.5 Light Intensity Measurements

Photocatalytic processes are highly dependent on the illumination intensity, as will be discussed later in Chapter 4. Therefore quantitative data on illumination intensity is necessary. In this study, a commercial analog Grove UV light intensity sensor was used to measure UV light intensity. The sensor is used with an mbed microcontroller to acquire serial data.

3.5.1 Light Intensity Sensor

The light intensity sensor and the microcontroller board can be seen in Figure 3.6. In Figure 3.7, a photo of a sample measurement can be seen.

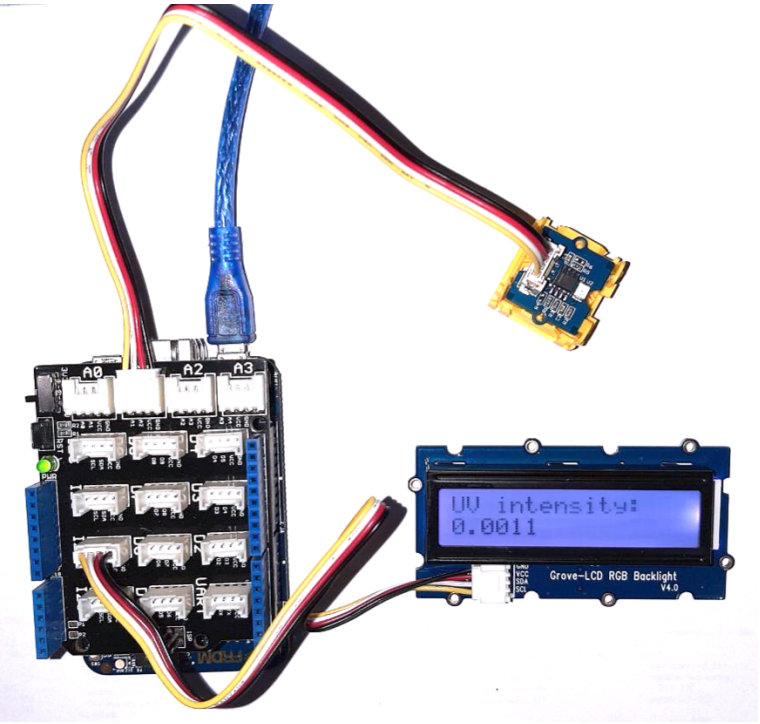

Figure 3.6: UV light intensity sensor with mbed microcontroller board with a base shield.

Figure 3.7: UV light intensity measurement.

3.5.2 Light Intensity Adjustment and Measurement

The main parameter of this study is the effect of light intensity on photocatalysis. The light intensity during experiments were increased or decreased by adjusting the distance between the source and the reactor. For this purpose, an adjustable metal stand where the UV lamp can be placed on was designed and made from steel sigma profiles. To achieve lower illumination intensities, a black carton filter with slits may be used as shown in Figure 3.9.

Illumination intensity of the UV lamp at different heights and positions were measured. The UV lamp was stationed on a height adjustable stand as seen in Figure 3.8. The UV sensor was placed on the bench. Measurements were made at different heights and base distances. The base distance corresponds to the distance from the base of the lamp to the measurement point on the plane it sits. This coordinate is included to account for possible variations in reactor positioning. The photo of the

measurement set up is seen in Figure 3.9.

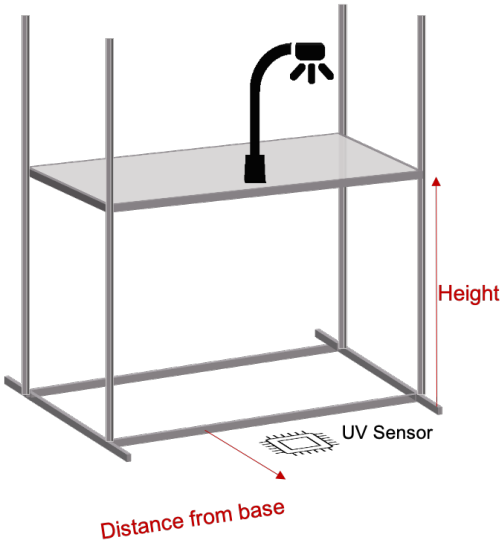

Figure 3.8: UV light intensity measurement set up schematic

3.5.3 UV Light Absorption of Catalyst Coated Glasses Measurement Set-up

Materials absorb a fraction of the UV light incident upon them. Light that is not absorbed gets transmitted. With the UV sensor, how much of the incident light on a test piece gets absorbed and transmitted can be measured. The measurement method is represented in Figure 3.10. First, a blank measurement where nothing is placed between the sensor and the light source is made. This measures the UV light intensity at the point of measurement. Later, absorption measurements can be made by placing the test pieces between the light source and the measuring device. The glass test pieces need to be placed at the same position for accurate measurements. For this purpose, a stand which can hold a glass test piece was made from cartons seen in Figure 3.11. The sensor is also anchored to the bottom to ensure reliable measurements.

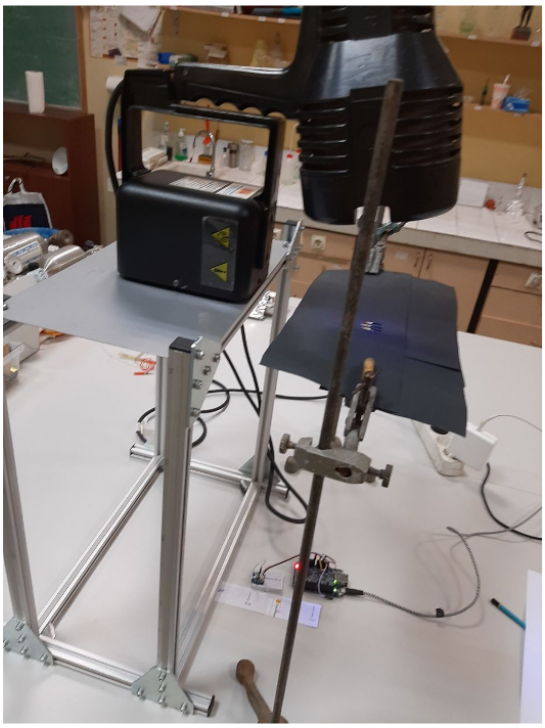

Figure 3.9: UV light intensity measurement set up. UV source is placed on the height adjustable stand. To further decrease illumination, a black carton with slits is used.

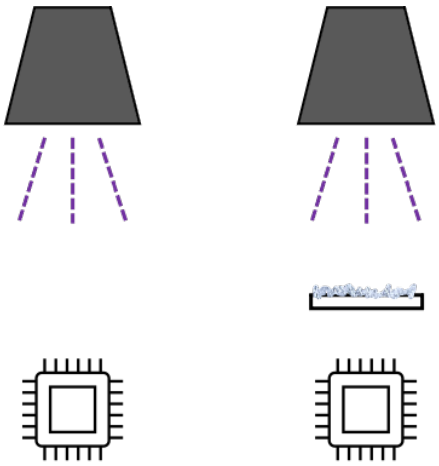

Figure 3.10: UV light absorption measurement. By placing the catalyst coated glass between the light source and the sensor, the amount of incident light that gets absorbed can be measured.

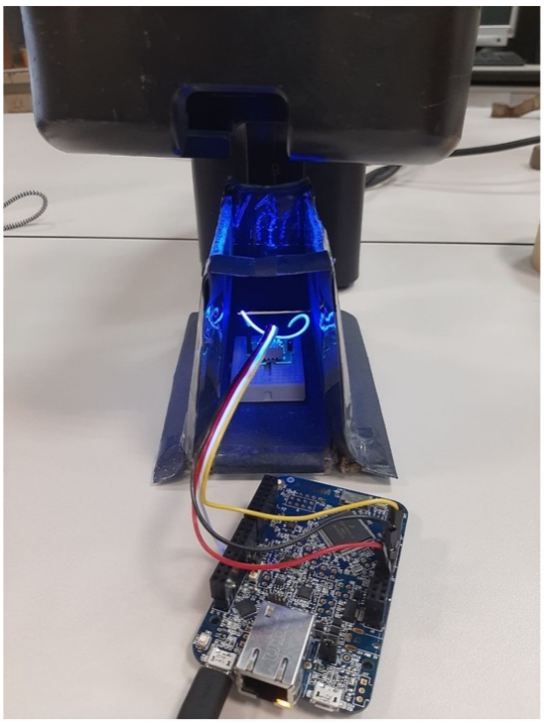

Figure 3.11: UV light absorption measurements of catalyst coated glasses can be done using this home-made stand for catalyst glasses.

3.6 Relative Humidity Measurements

Moisture content of the test gas is another experimental variable in this study. Therefore, quantitative information was required. The relative humidity was measured using a humidity sensor similar to the UV sensor.

3.6.1 Humidity Sensor

A Grove digital temperature and humidity sensor (DHT11) was connected to an mbed microcontroller (see Figure 3.12). The sensor was placed at the outlet of the reactor seen on Figure 3.1.

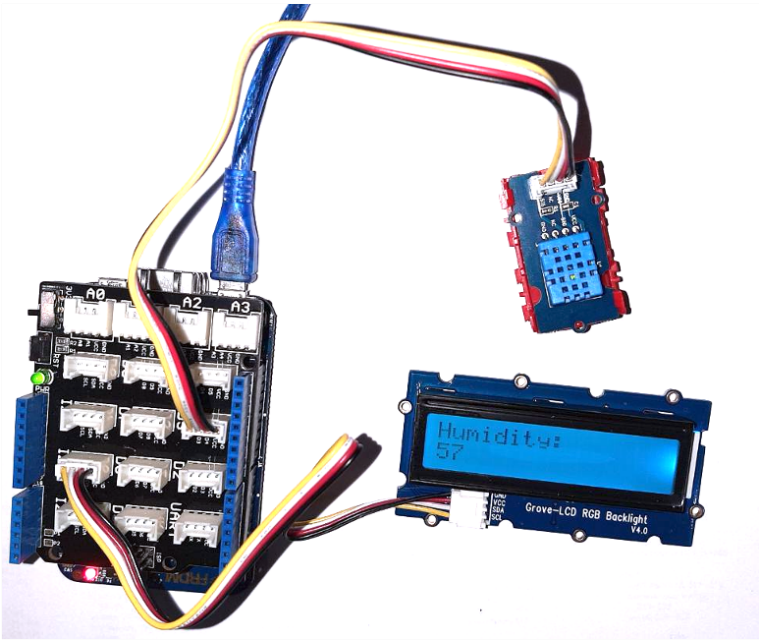

Figure 3.12: Temperature and humidity sensor on the top right corner, mbed with base shield attached on the left and an LCD.

CHAPTER 4

RESULTS AND DISCUSSION

4.1 Characterization

4.1.1 SEM Images

SEM images of 3 different TiO_2 samples are shown in Figure 4.1. Figure 4.1.a is fresh TiO_2 P25 powder, 4.1.b is from the catalyst test piece used for NO oxidation measurements and 4.1.c is an image of TiO_2 P25 powder mixed with water and then dried to simulate the coating process. It can be seen that when fresh TiO_2 P25 powder is mixed with water and later dried, the porous structure changes. Particles are clustered and more chunky in Figures 4.1.b and 4.1.c

4.1.2 BET Analysis

BET analysis results are given in Table 4.1.

Table 4.1: BET surface areas.

Sample	BET Surface Area (m^2/g)
Fresh TiO_2	49.4
Dried TiO_2 Slurry	51.8

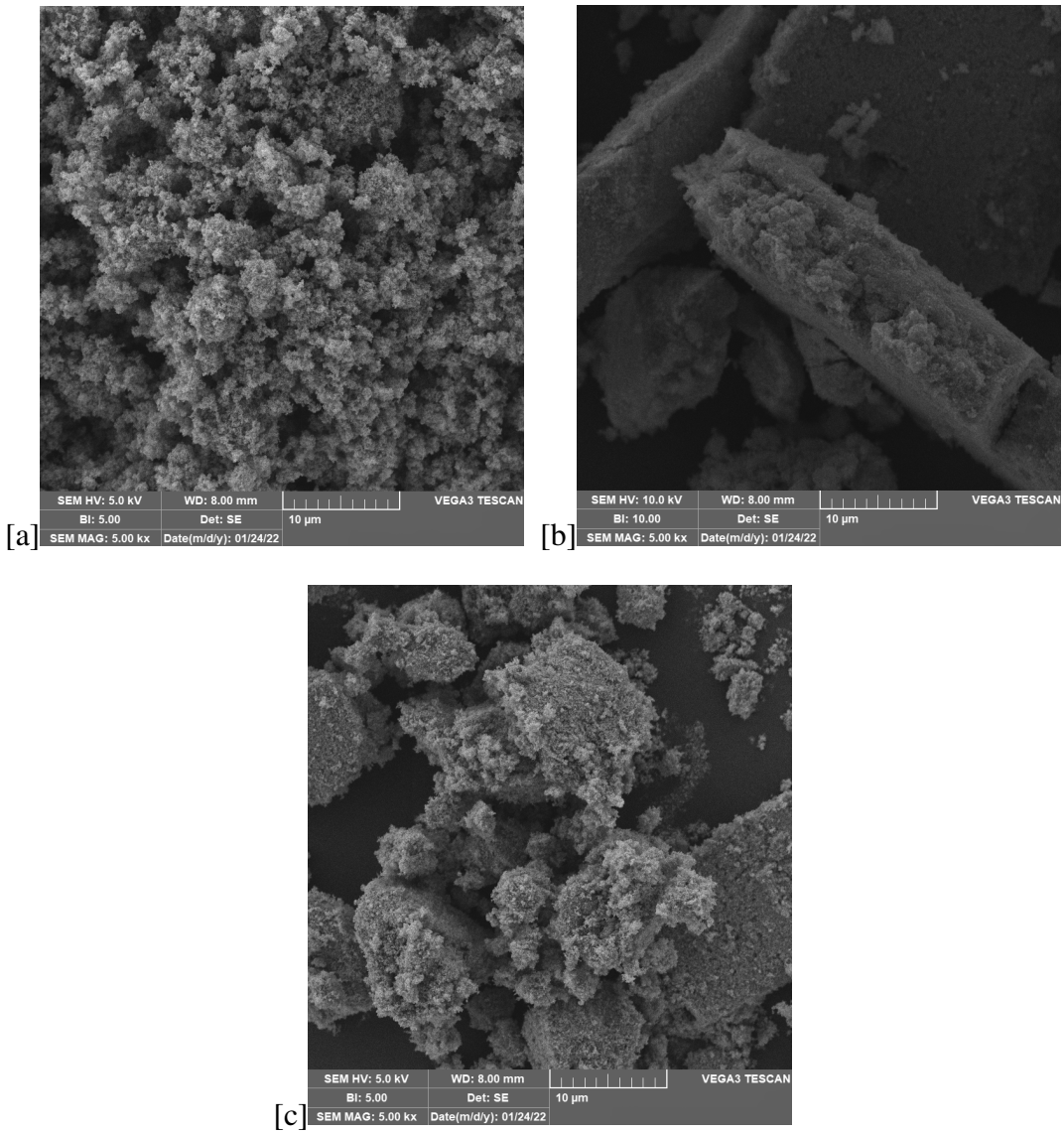

Figure 4.1: SEM images. [a] is fresh TiO_2. [b] is used catalyst obtained from test piece. [c] is dried TiO_2 slurry.

4.1.3 XRD Analysis

XRD analysis of a fresh TiO_2 P25 and dried TiO_2 slurry is shown in Figure 4.2. Anatase to rutile ratio was found to be 81% anatase phase from peak analysis as described in Myers et al. [70].

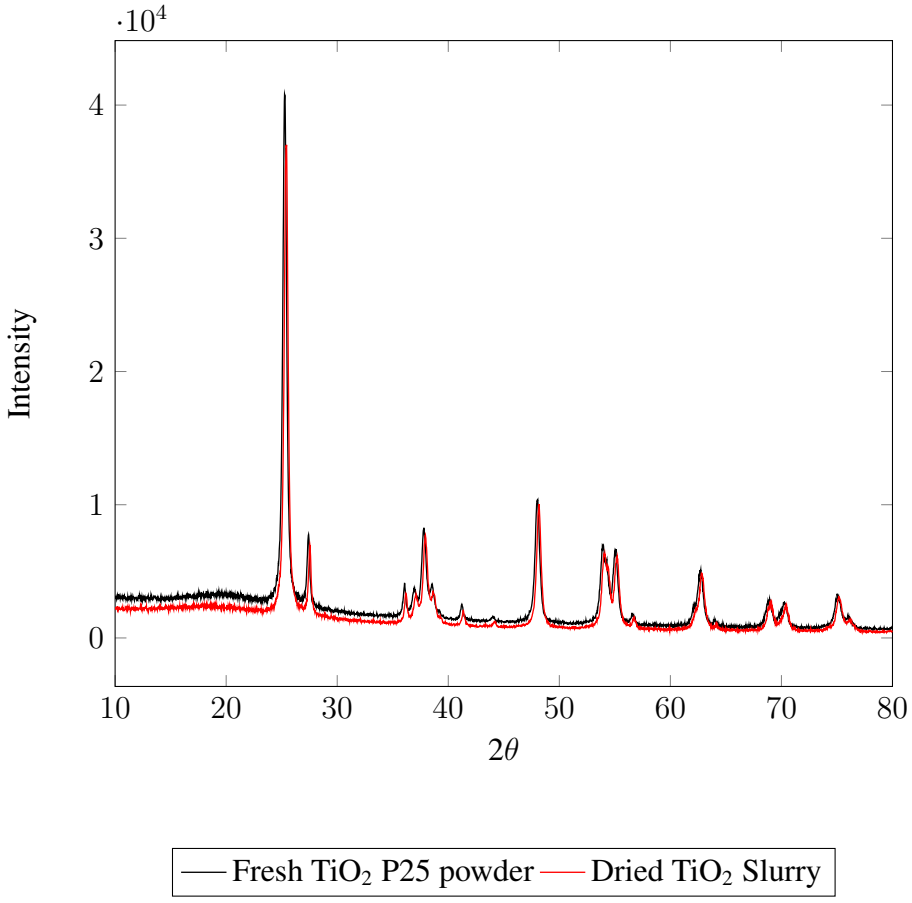

Figure 4.2: XRD patterns of fresh and slurry and then dried TiO_2 P25 powder.

4.1.4 ESR Spectroscopy

ESR spectra of 2 samples are shown in Figure 4.3. The samples are fresh and used TiO_2. The samples were measured both under ambient conditions and under vacuum.

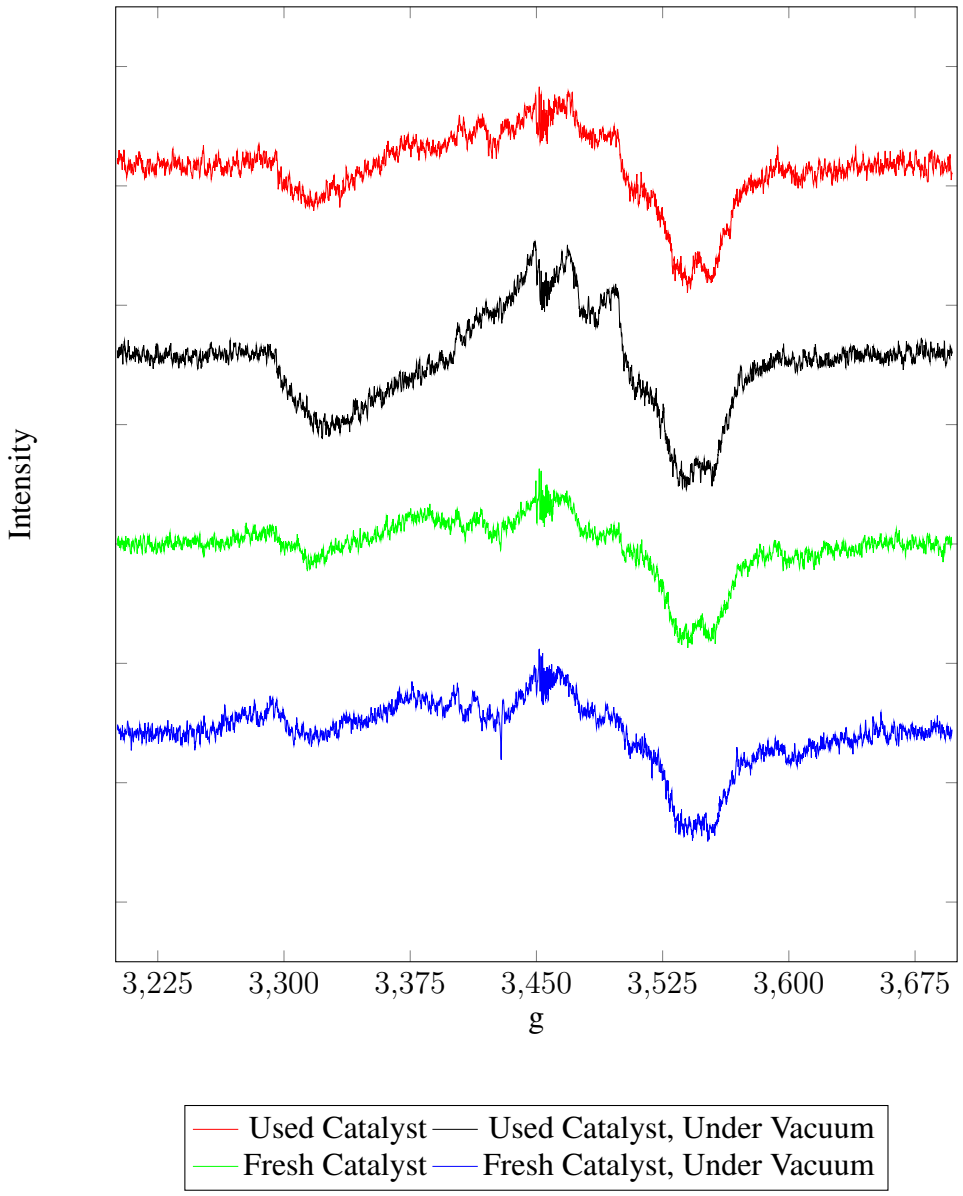

Figure 4.3: ESR Spectroscopy. Comparison of fresh catalyst and used catalyst.

4.2 NO Oxidation Measurements

4.2.1 Effect of Illumination Intensity

Effect of illumination intensity on photocatalytic NO oxidation over TiO_2 was investigated in this study. There is a characteristic decay behavior of the system, discussed in Chapter 3. Conversion is usually higher at the beginning of the reaction, however performance decreases over time and then reaches a steady state value at a much lower conversion. Preliminary experiments showed that this behavior of the reaction depends on light intensity (see Appendix D). At low illumination intensities, this decaying behavior was not observed. To investigate this effect in more detail, further experiments were done in two sets. A set of experiments entails experiments done in consecutive days without allowing the catalyst to rest in ambient conditions for long periods of time.

The first set of these experiments are shown in Figure 4.4. As illumination intensity decreases, the steady-state conversion also decreases. This is what is expected and also seen in other studies [39]. Maximum conversion also decreases with decreasing illumination. As illumination intensity is further decreased, which corresponds to 0.2 mW/cm^2 illumination, the initial NO conversion is lower compared to the initial conversion at higher illumination intensities. However, it is still higher than its steady-state value. At 0.2 mW/cm^2 illumination, conversion also suddenly increases at approximately 340 minutes. This is due to a mechanical failure in the light blocking filter which allowed more light to pass through, leading to an increased reaction rate. The light intensities were not directly measured since the light intensity sensor was not available at the time. Light intensities reported correspond to measurements made later at the same height and position which are available in Table 4.2.

The second set of these measurements are shown in Figure 4.5. Observations similar to the first set of experiments are made. In this set of experiments, illumination intensity was decreased to even lower values than that of the previous measurements. It can be clearly seen that as light intensity is decreased, both the maximum conversion achieved at the beginning and the steady state conversion decrease. At the lowest illumination intensity which corresponds to 0.015 mW/cm^2, initial conversion is very

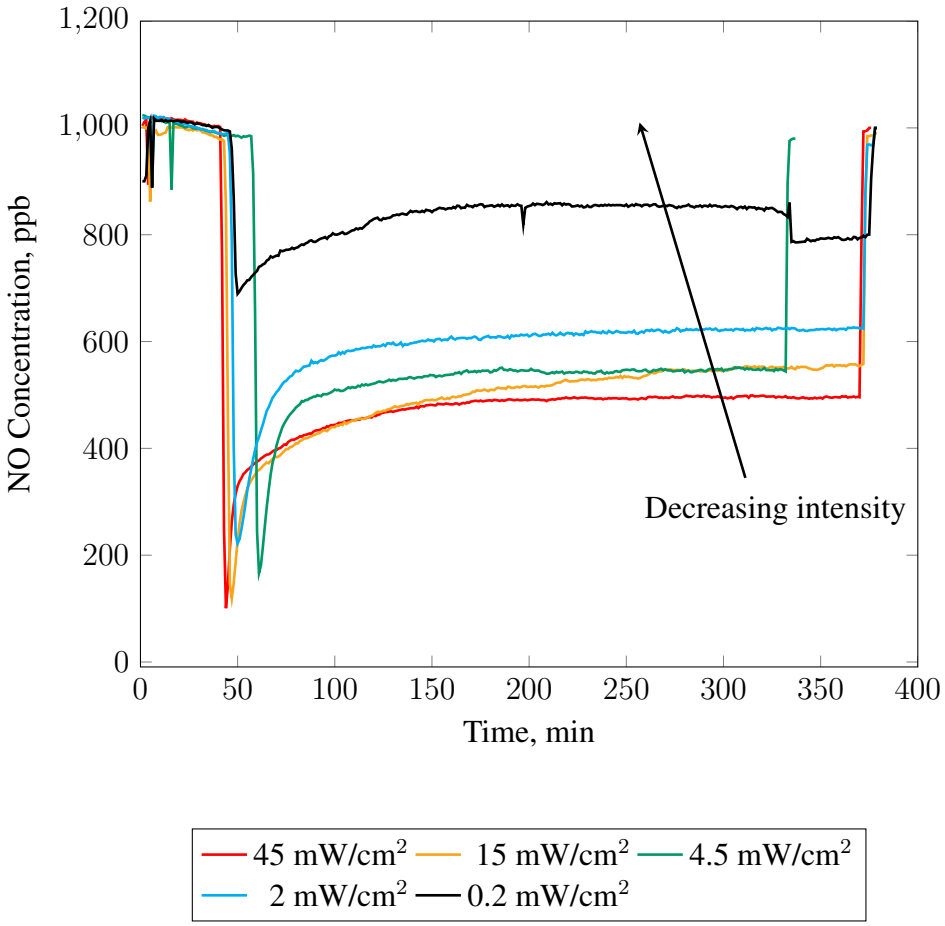

Figure 4.4: Effect of UV light intensity on NO oxidation. First set of experiments.

close to steady-state conversion.

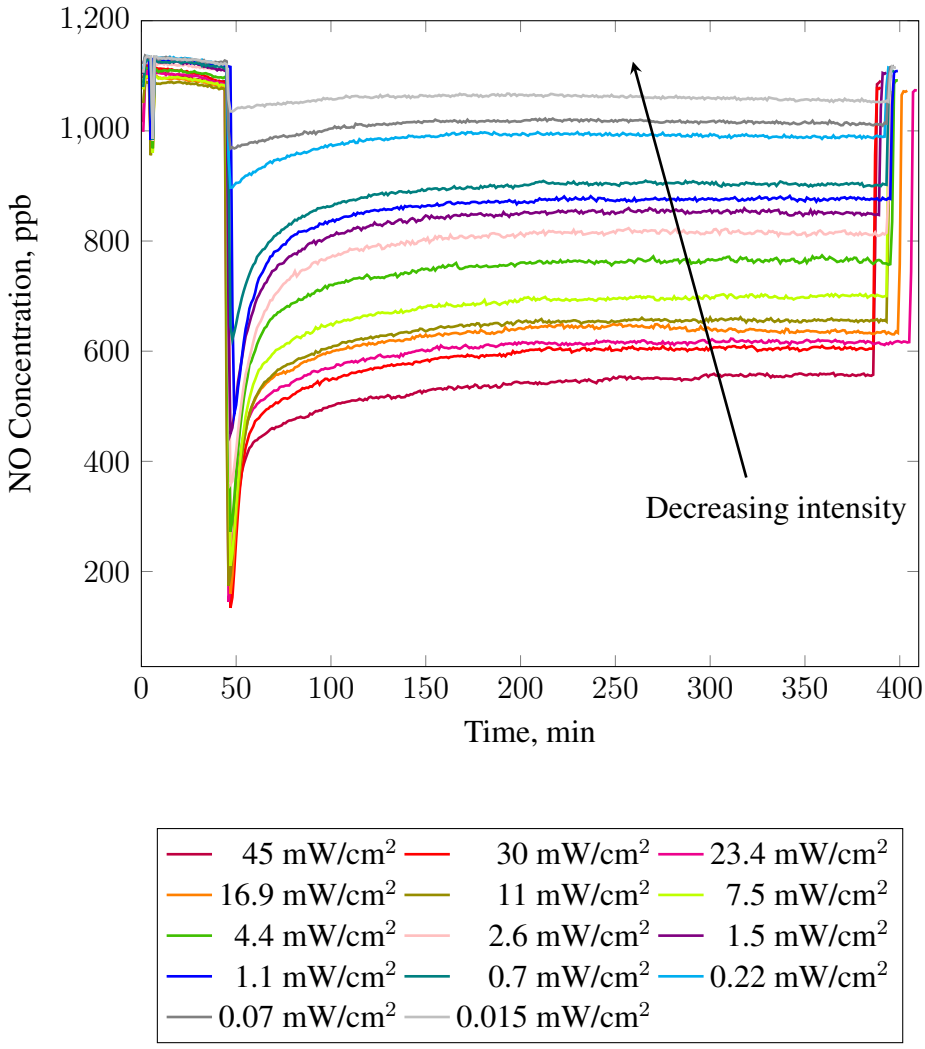

Figure 4.5: Effect of UV light intensity on NO oxidation. Second set of experiments.

4.2.2 Gradually Decreased Illumination

To further analyze the effect of light intensity on the reaction system, light intensity was decreased gradually throughout a single NO oxidation experiment. The experiment was started at a high 45 mW/cm^2 illumination. When steady-state was reached, illumination was ceased by covering the reactor with an opaque sheet for 5 minutes. During this short dark period, the position of the UV light source was adjusted and the light intensity was measured. The cover was then removed. Figure 4.6 shows the results from this experiment. We observe a small initial drop in concentration at the beginning of every cycle, with these drops getting less pronounced as the illumination intensity decreases. This observation is consistent with what is seen with previous experiments. At the last cycle, illumination is increased back to 45 mW/cm^2. The initial concentration does not drop as low as with the first cycle, but steady state conversion is the same. Figure 4.7 shows a close up view of the same experiment starting just before the second cycle.

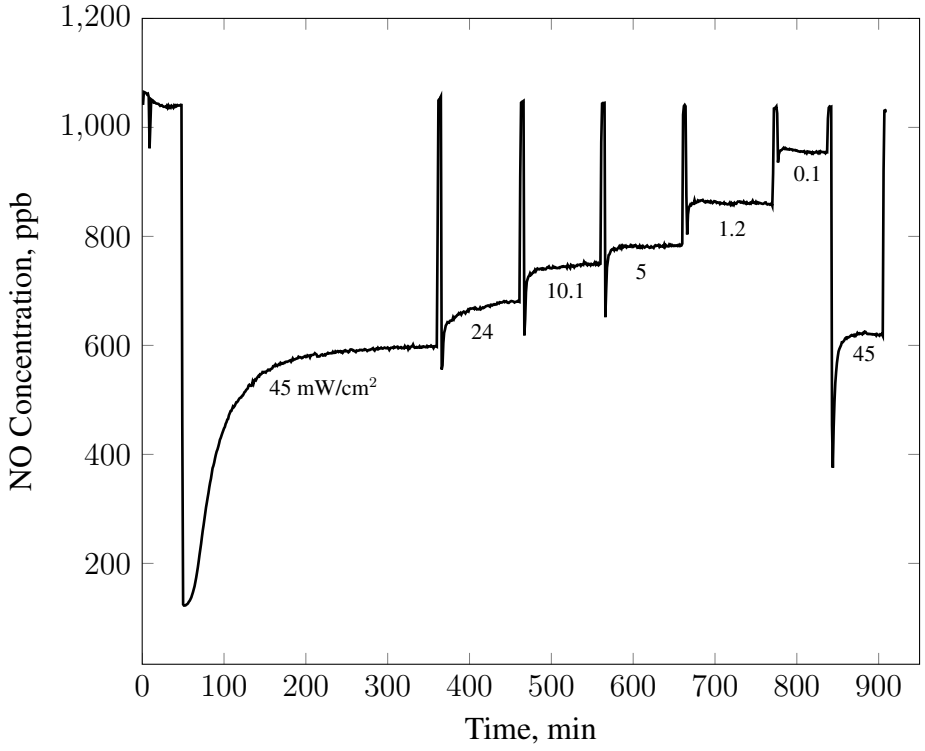

Figure 4.6: Illumination intensity was gradually decreased throughout the experiment. Light intensities are printed on the figure in mW/cm^2.

One interesting observation made in this experiment is that the brief 5 minute dark period between cycles is enough to recreate the decay behavior to some extent. After the cover is removed, the reaction no longer continues at a steady level. The rate is initially fast but decays very quickly.

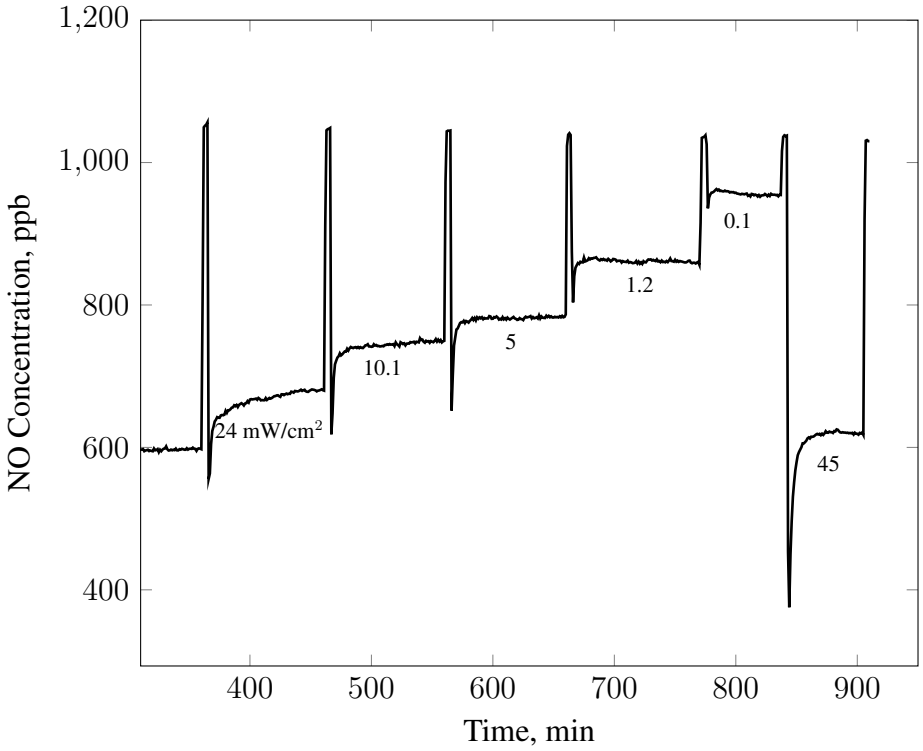

Figure 4.7: Gradually decreased illumination intensity, extended view.

4.2.3 Effect of Catalyst History

Throughout this study, the same test piece was used. In this study, there are two sets of experiments conducted with several months in between as discussed above. As mentioned before, a set of NO oxidation experiments are done in consecutive days without subjecting the test piece to ambient conditions for long periods of time. Therefore, the experiments will be referred to "Day 1", "Day 2", "Day 3" and so forth for the first, second and third day of experimentation of a set. Reasons for conducting experiments in this manner will be explained in this section.

When the test piece was used for the first time after a long period of break, it was observed that the behavior of the catalyst was different and performance was usually increased. One distinct observation made was that steady-state was achieved in a much longer time. However, after a couple of consecutive experiments, the catalyst stabilized.

In Figures 4.8 and 4.9, initial usage effect from the first set of experiments are seen. Day 1 curve from Figure 4.8 and day 2 curve from Figure 4.9 does not have the characteristic fast decay at the beginning of the reaction. The process is slowly decaying, and does not reach steady-state by the end of the experiment. This effect does not last long and the catalyst stabilizes after a couple of days. Effect of this history can be observed in Figures 4.8 and 4.9.

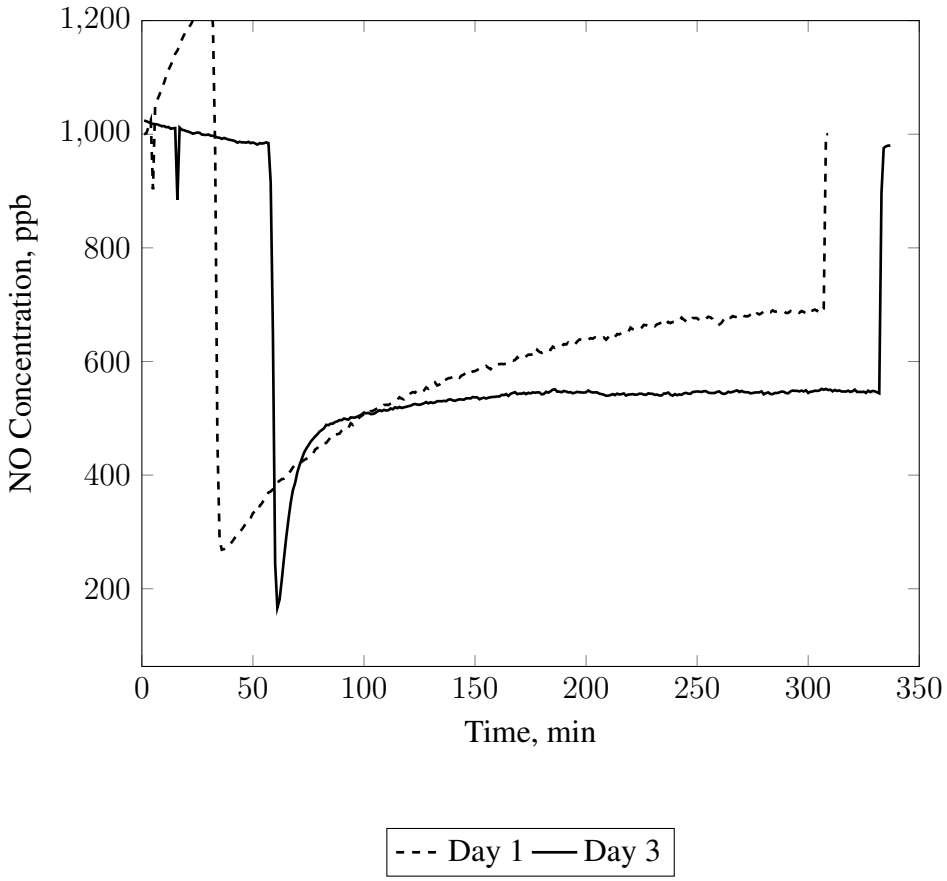

Figure 4.8: Catalyst usage effect at 4.5 mW/cm^2. illumination intensity. Difference between day 1 of usage and day 3 can be seen. The experiments belong to the first set of measurements discussed above. Note that the NOx analyzer may also not be stable in Day 1 experiment.

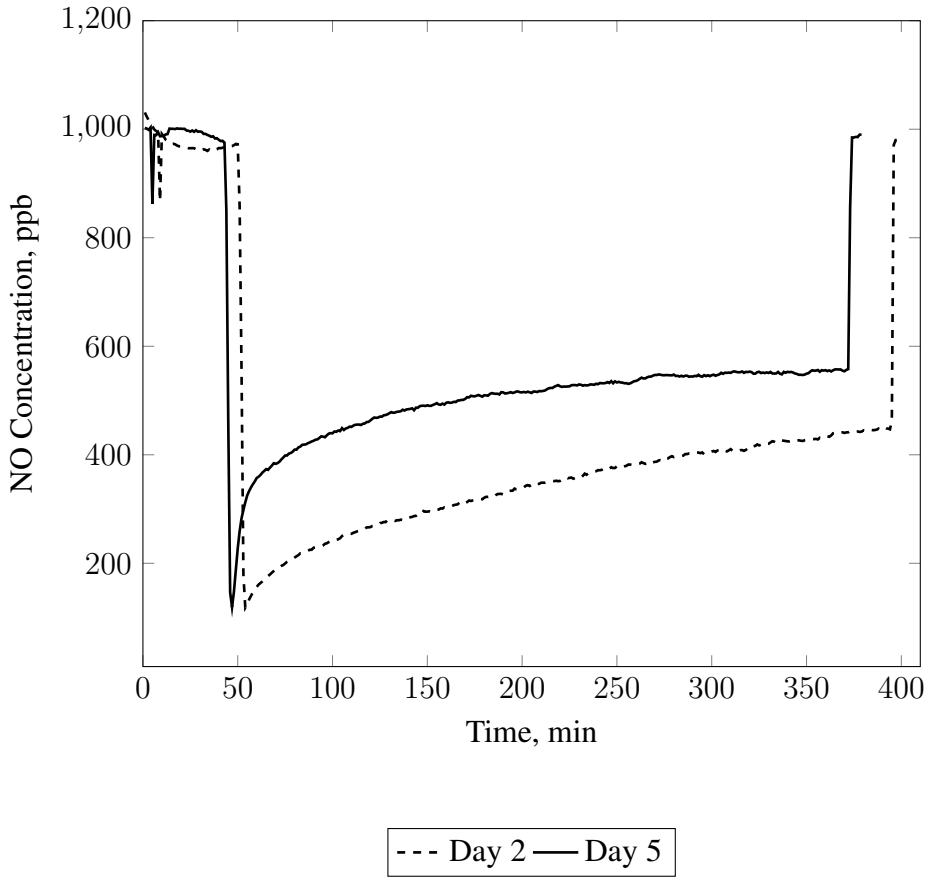

Figure 4.9: Catalyst usage effect at 15 mW/cm^2 illumination intensity. Difference between day 2 and day 5 of usage can be seen. The experiments belong to the first set of measurements discussed above.

The same effect was also observed for the second set of experiments (see Figure 4.10). The first usage performs better in terms of conversion, and takes a longer time to reach steady-state. With this set of experiments, the catalyst was stable after the first use.

The second set of experiments were done in 15 consecutive days, starting from high illumination intensity. By day 2 of usage, the catalyst was stable at 45 mW/cm^2 illumination. After day 2, the experiments were conducted until very low light intensities were reached and the experiment set was completed. To see the effects of 15 experiments on the catalyst behavior, another 45 mW/cm^2 experiment at day 16 was done. There is a slight difference in the behavior of the catalyst seen in Figure 4.10. Many factors, such as long usage, catalyst poisoning and deactivation, illumination intensity and therefore the reaction rate of the prior experiment can be in effect. Figure 4.11 shows the steady-state conversion with respect to catalyst history at 45 mW/cm^2 light intensity.

Keeping this effect in mind, further calculations and discussions will consider results from stabilized test pieces.

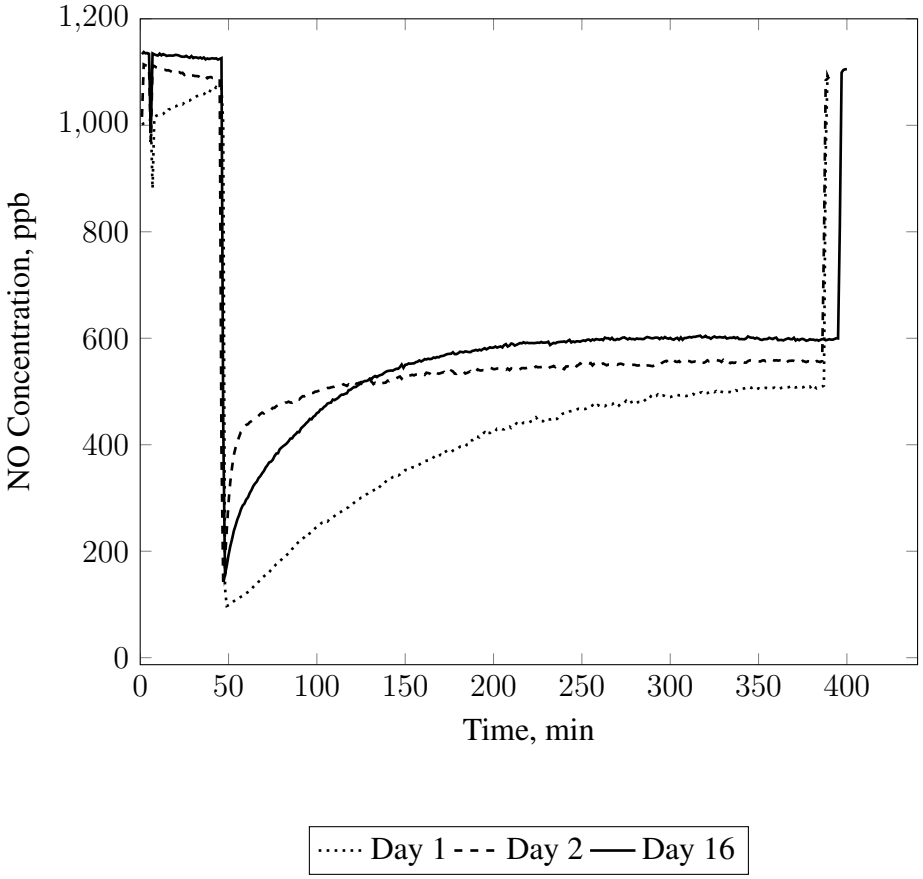

Figure 4.10: Consecutive uses of the same catalyst at 45 mW/cm^2 illumination intensity. The experiments belong to the second set of measurements discussed above.

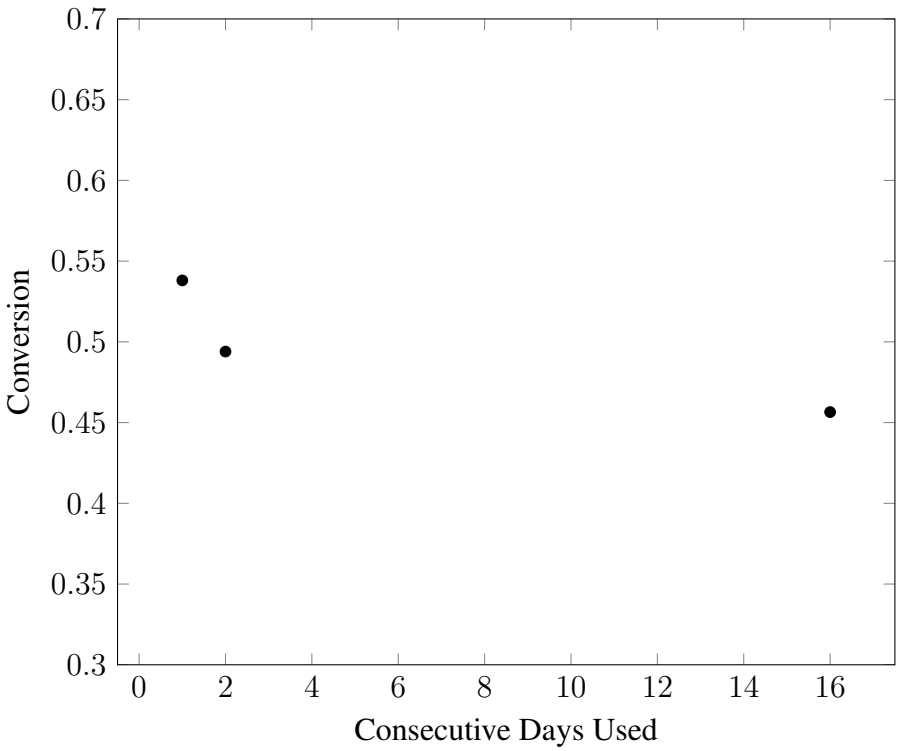

Figure 4.11: Effect of consecutive usage on catalyst performance. At 45 mW/cm^2 illumination intensity. The experiments belong to the second set of measurements discussed above.

Effect of humidity on NO oxidation was also tested (see Figure 4.12). Air is supplied to the experiment set-up from an air compressor. This limits the minimum relative humidity attainable to the humidity content of the ambient air and the compressor outlet. Therefore NO oxidation was carried out at 30%, 50% and 100% relative humidity. Best results in terms of conversion was achieved at 30% relative humidity.

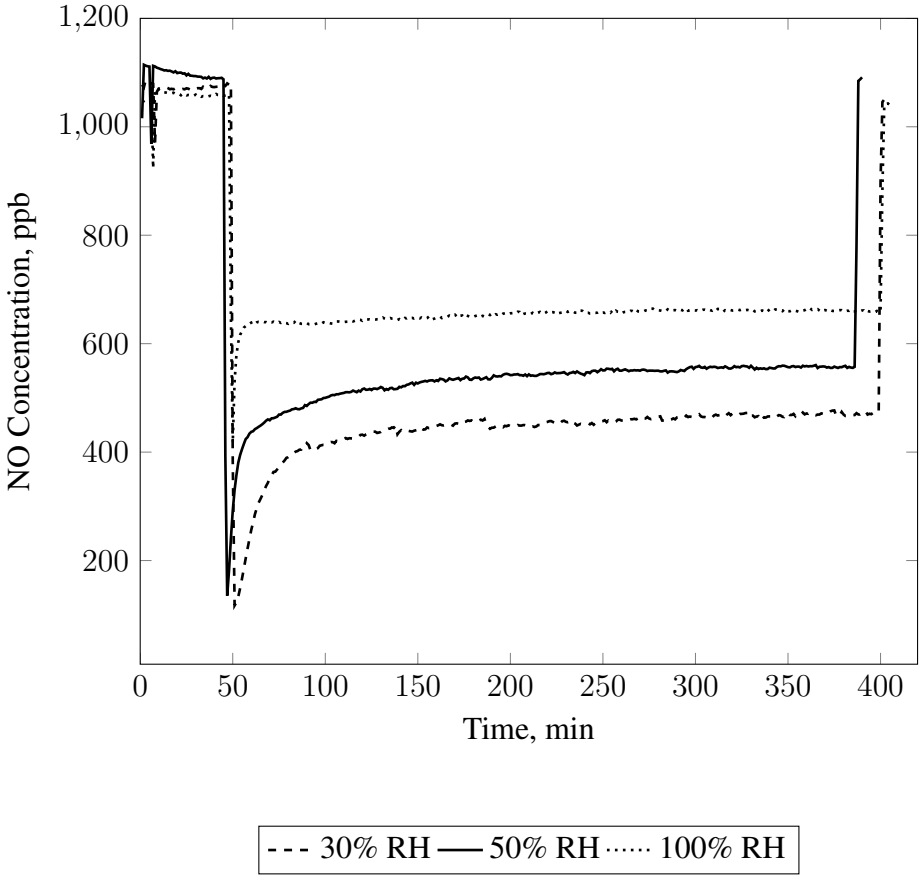

Figure 4.12: Effect of humidity at 45 mW/cm^2 illumination intensity.

In Figure 4.13 rates of changes of NO concentration of Figure 4.12 with respect to time are plotted. It can be observed that steady-state is achieved faster with higher relative humidity. The moment derivative changes signs (from less than zero to greater than zero) corresponds to the maximum conversion level after illumination is started.

In Figure 4.14, steady-state conversion with respect to relative humidity is plotted. Conversion decreases with increasing relative humidity of the gas stream.

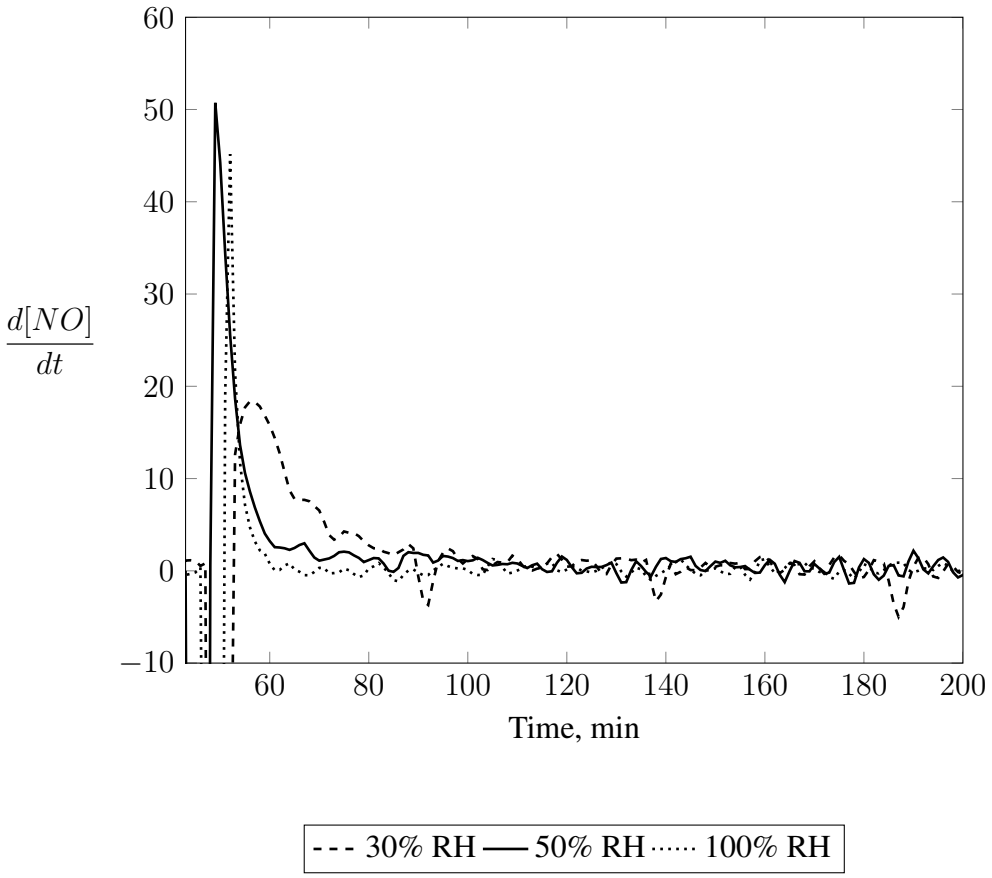

Figure 4.13: Rates of changes of NO concentration with respect to time at different relative humidities and 45 mW/cm^2 illumination intensity.

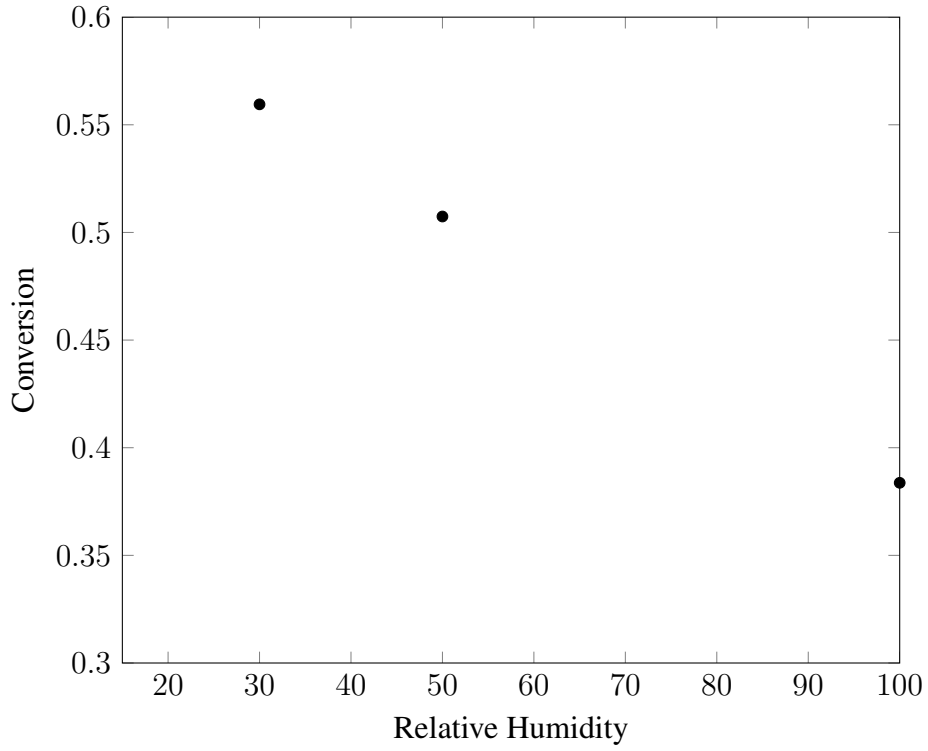

Figure 4.14: Steady-state conversion with respect to relative humidity at 45 mW/cm^2.

4.2.4 Steady State Conversion and Data Fitting

The steady state conversion with respect to light intensity was calculated and plotted in Figure 4.15. Conversion increases rapidly at low illumination but slows down as light intensity gets higher. Figure 4.16 shows a log-log plot of conversion versus light intensity.

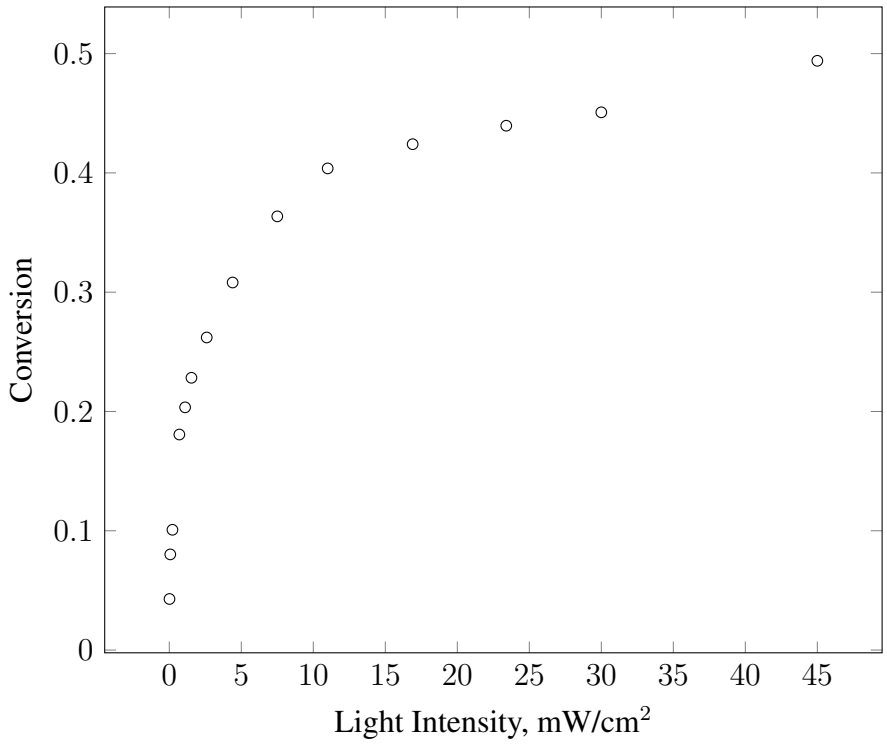

Figure 4.15: NO conversion at steady state with respect to illumination intensity.

The steady-state data was fitted using the curve fit application of MATLAB. The data can be fitted to the equation $y = \frac{ax^b}{c + ax^b}$ where a = 0.1809, b = 0.3733, c = 0.7265 with an R^2 value of 0.992. The fit can be seen in Figure 4.17.

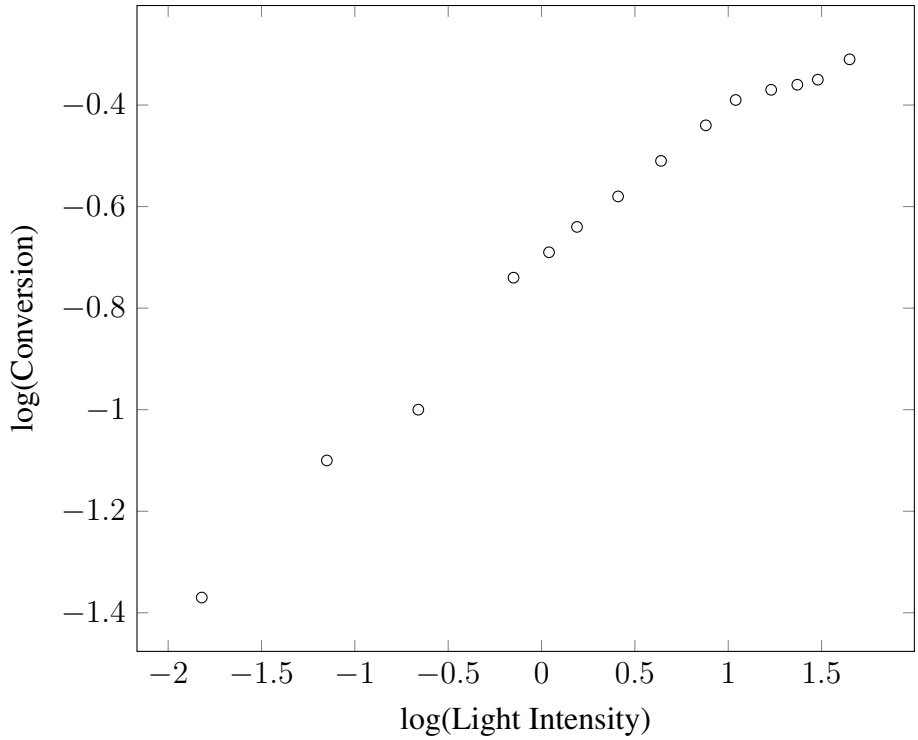

Figure 4.16: NO conversion at steady state with respect to illumination intensity on a log-log plot.

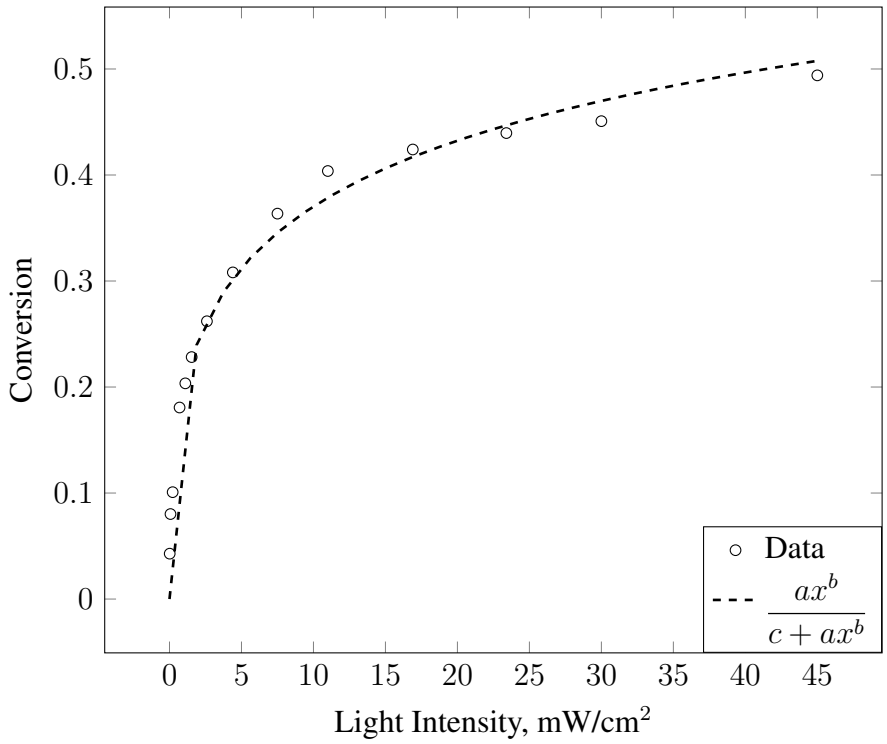

Figure 4.17: NO conversion at steady state with respect to illumination intensity and curve fit (a = 0.1809, b = 0.3733, c = 0.7265 and R^2 = 0.992).

4.3 Water Injection Experiments

4.3.1 Water Injection During NO Oxidation Experiments

Water and OH radicals are major species involved in photocatalytic reactions as discussed in Chapter 2. Furthermore, the interactions between H_2O and TiO_2 surfaces are very complex and dependent on several factors [71],[72].

Humidity content of the feed gives information about effects of water on photocatalytic NO oxidation, however, water content of the feed is relatively stable and does not change throughout the reaction. This paints an incomplete picture of the process. Therefore, the response of the system to pulses of water was investigated.

Water was periodically injected to the system through a septum at the inlet of the reactor. NO concentration data is coupled with data from the homemade humidity sensor. The results are shown in the Figures 4.18, 4.19, 4.20, 4.21. Effects of light intensity with water injections were also tested.

As water is injected to the system, there is a clear rise in the relative humidity of the stream. This rise also corresponds to the time the reaction responds to the injections. The reaction rate increases as water is injected to the reactor, however the effect subsides as the humidity content of the stream stabilizes and returns back to its initial value.

One exception was observed at 45 mW/cm^2 illumination intensity which can be seen in Figure 4.18. The first injection decreases conversion, which remains there even after the effect of water injection in the stream vanishes. The following 2 injections causes a similar effect of briefly increasing the reaction rate as seen in Figures 4.19, 4.20, 4.21. The last 3 water injections initially increase the reaction rate, but this quickly reverses which results in upward peaks. The reason for this is not known, but could be related with the water presence on the surface. When compared, the relative humidity rises up to 50% in this experiment, however it remains below 45% with the remaining water injection experiments. It is not thought to be related to illumination intensity since blank water injection experiments performed in the dark and under UV light do not show a major difference.

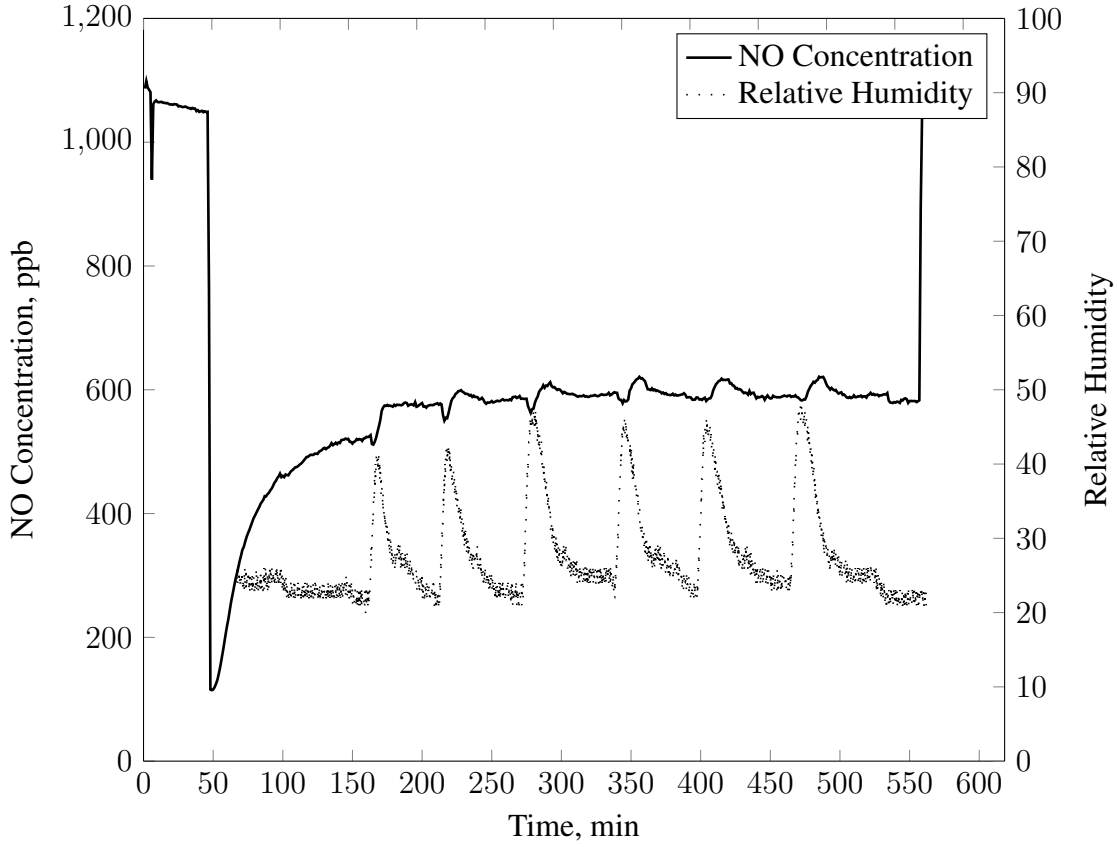

Figure 4.18: Water injections at 45 mW/cm^2 illumination intensity.

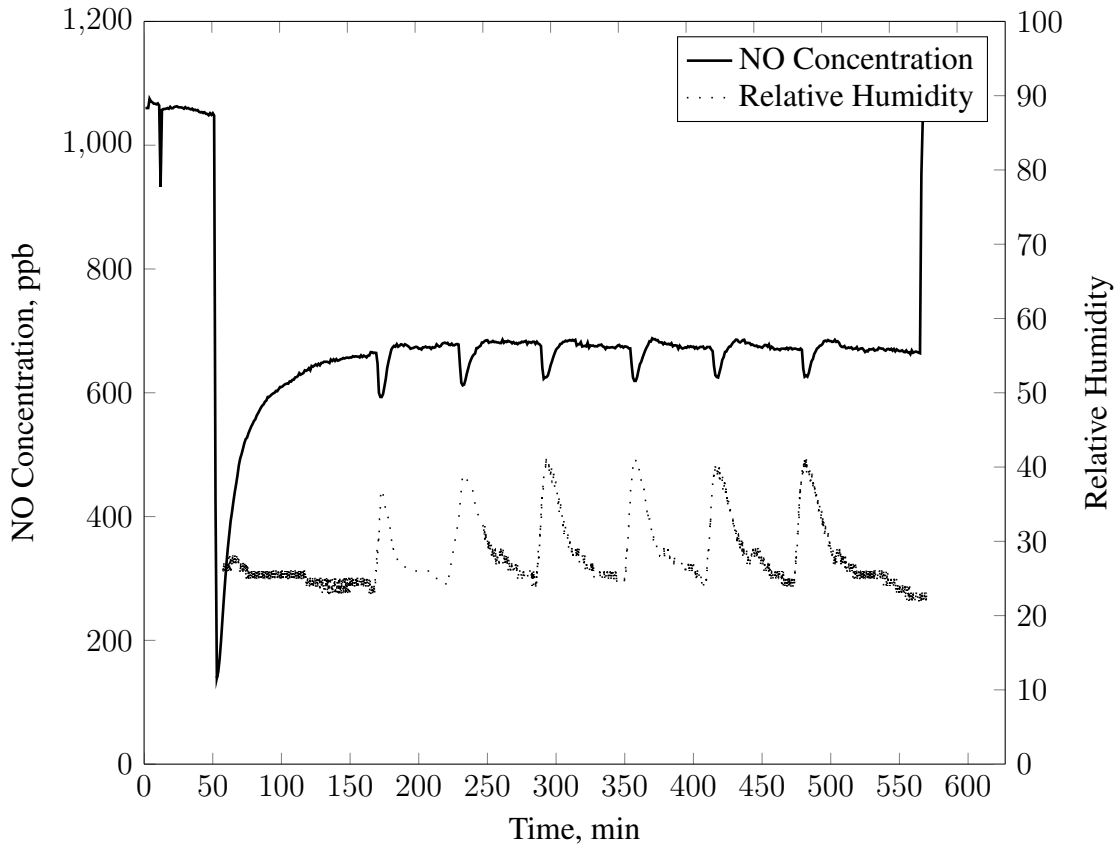

Figure 4.19: Water injections at 21.5 mW/cm^2 illumination intensity.

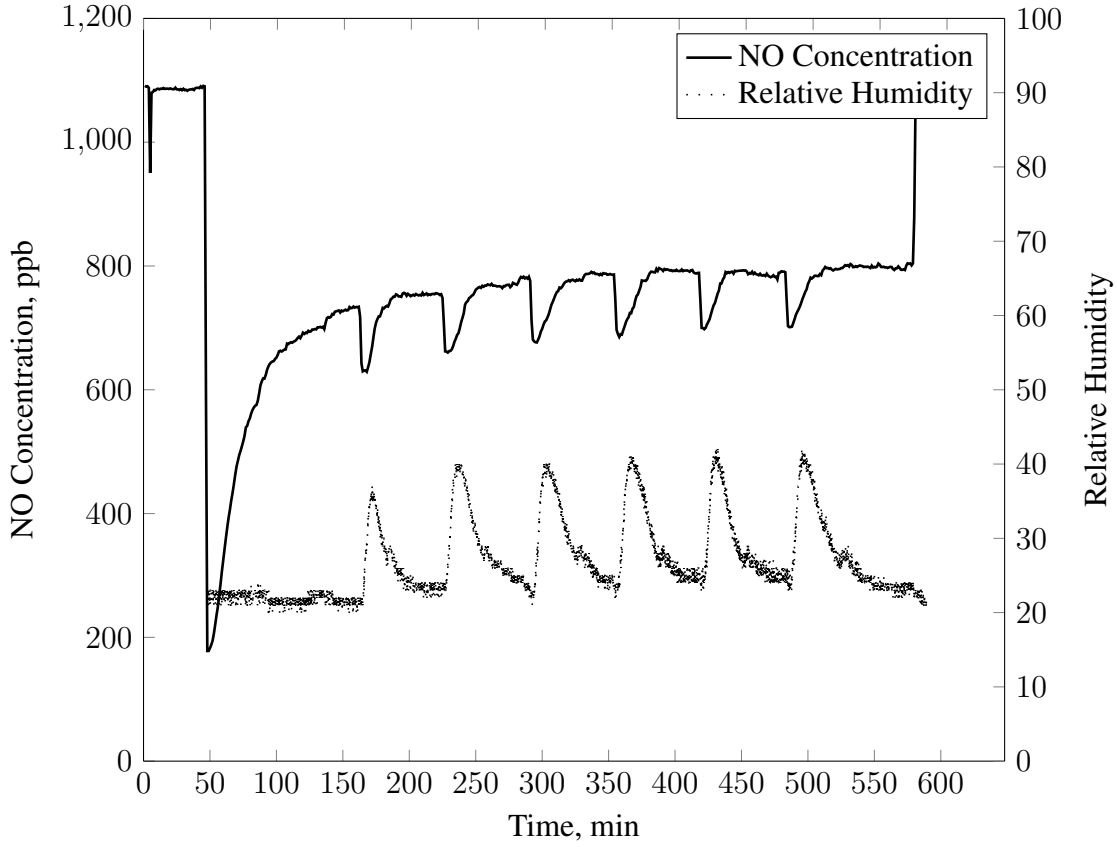

Figure 4.20: Water injections at 5.6 mW/cm^2 illumination intensity.

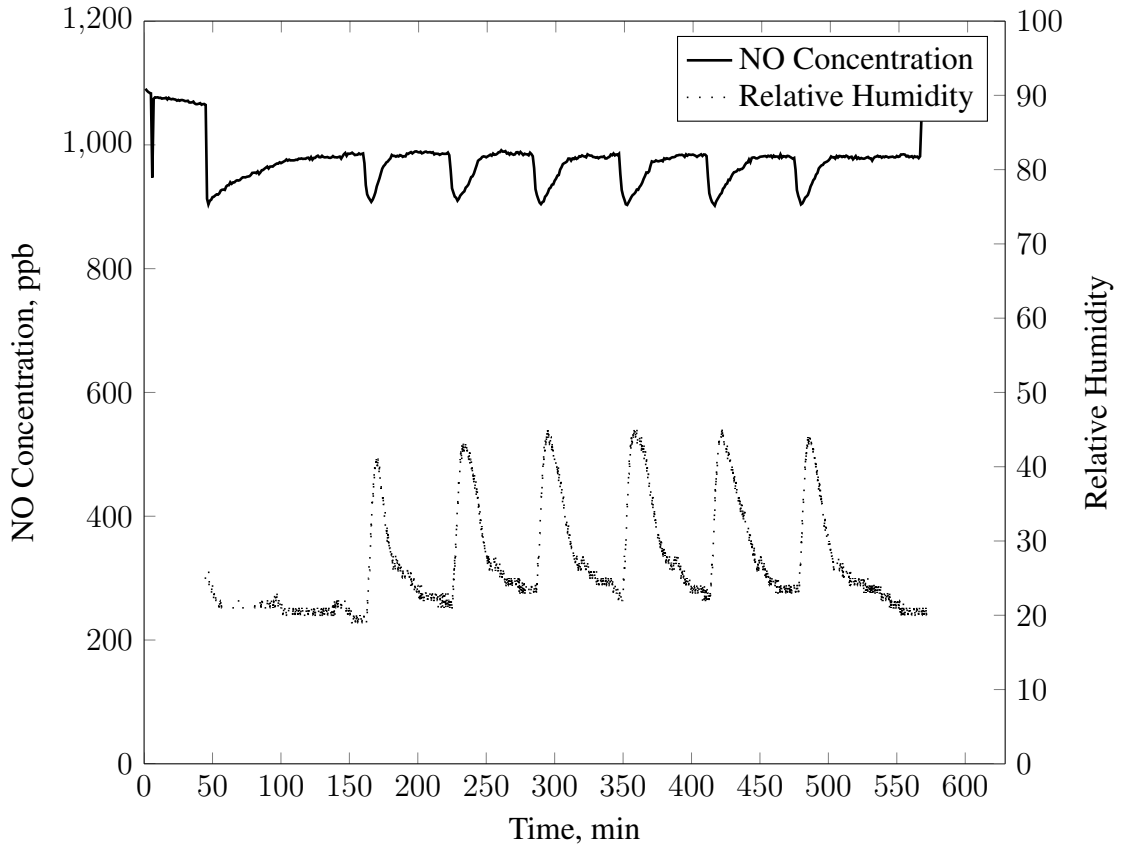

Figure 4.21: Water injections at 0.08 mW/cm^2 illumination intensity.

There is a study by Muggli et al. in 2000 which also tests water injections on photocatalytic oxidation over TiO_2 [73]. Similar results of brief rate increases were also observed by the authors. In addition, authors also tested the effect of water injections on photocatalytic decomposition, which is carried out in lack of molecular oxygen. Water injections did not increase nor decrease the rate of reaction when no oxygen was present [73].

A close up view of water injections can be seen in Figure 4.22. Water injections were done 150 minutes after UV illumination was started. This figure summarizes the effect of water injections on photocatalytic NO oxidation. The response of the system, the shape of the NO concentration curve after water injections resemble the initial transient period.

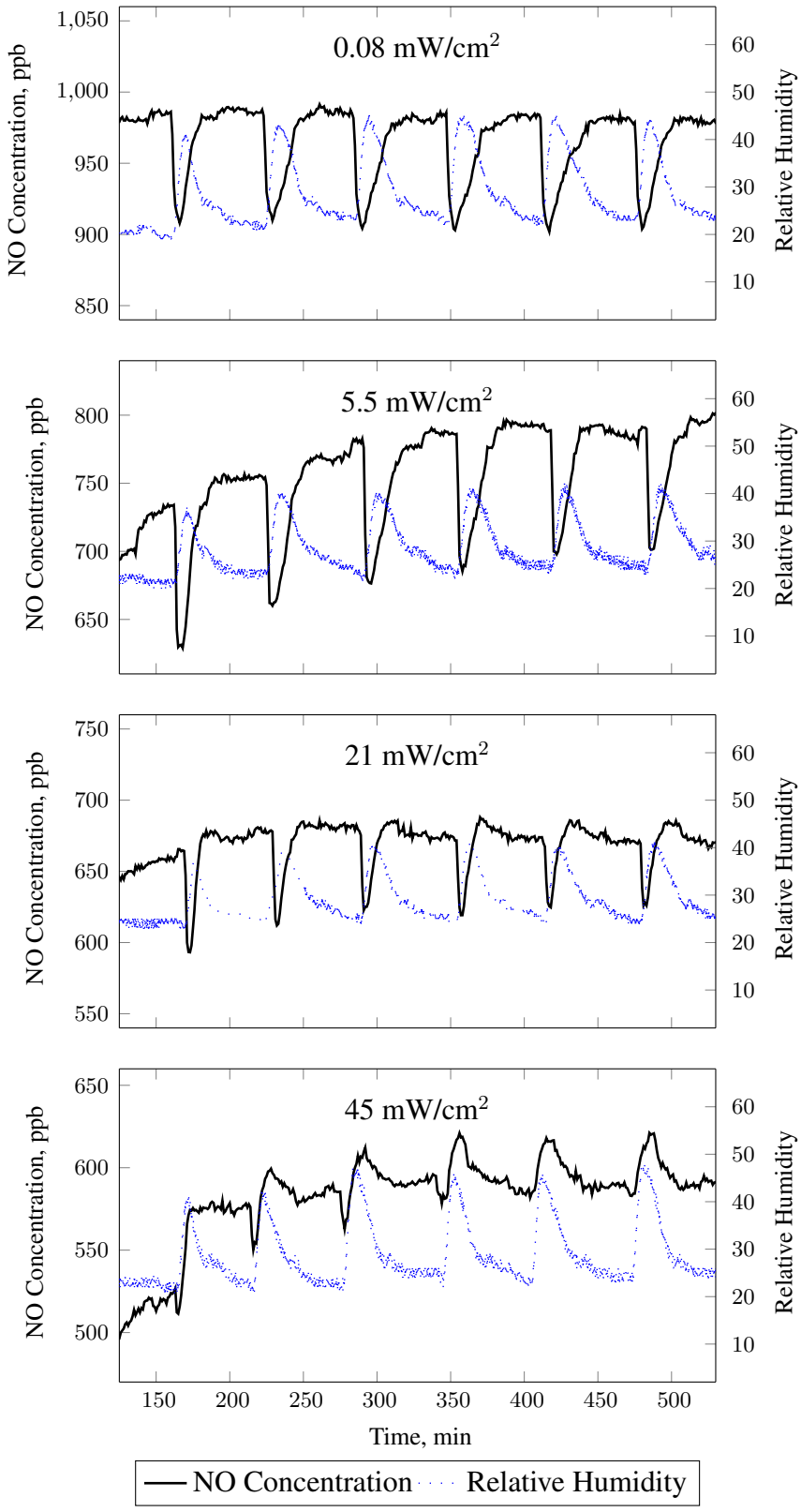

Figure 4.22: Magnified views of water injections.

4.3.2 Effect of Water Injection on Relative Humidity Without NO Oxidation

Water injection procedure was repeated at dark and 45 mW/cm^2 without nitric oxide gas flowing over the catalyst to observe the effects of water injections without NO oxidation. Tests seen in Figures 4.23 and 4.24 were performed at 20% and 50% relative humidity respectively. The small variations in heights of the peaks are well within the sensitivity range of the digital humidity sensor. It can also be observed that when the inlet humidity is at 50%, the response of the system takes longer than with 20% humidity, resulting in broader peaks.

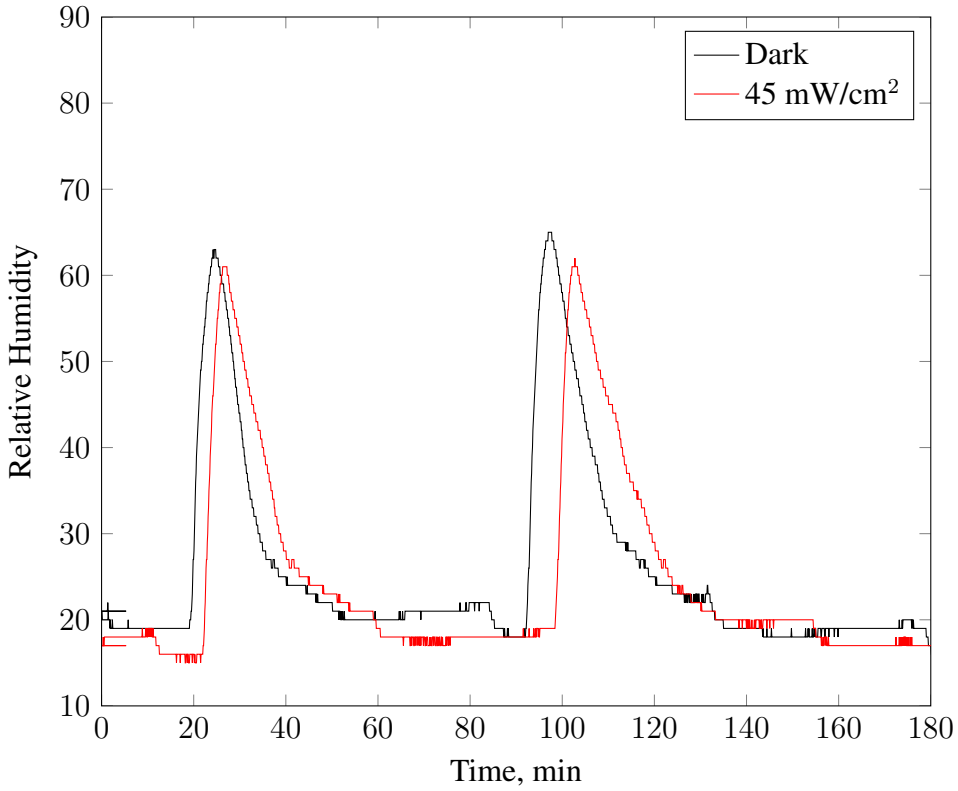

Figure 4.23: Effect of water injections at 20% RH.

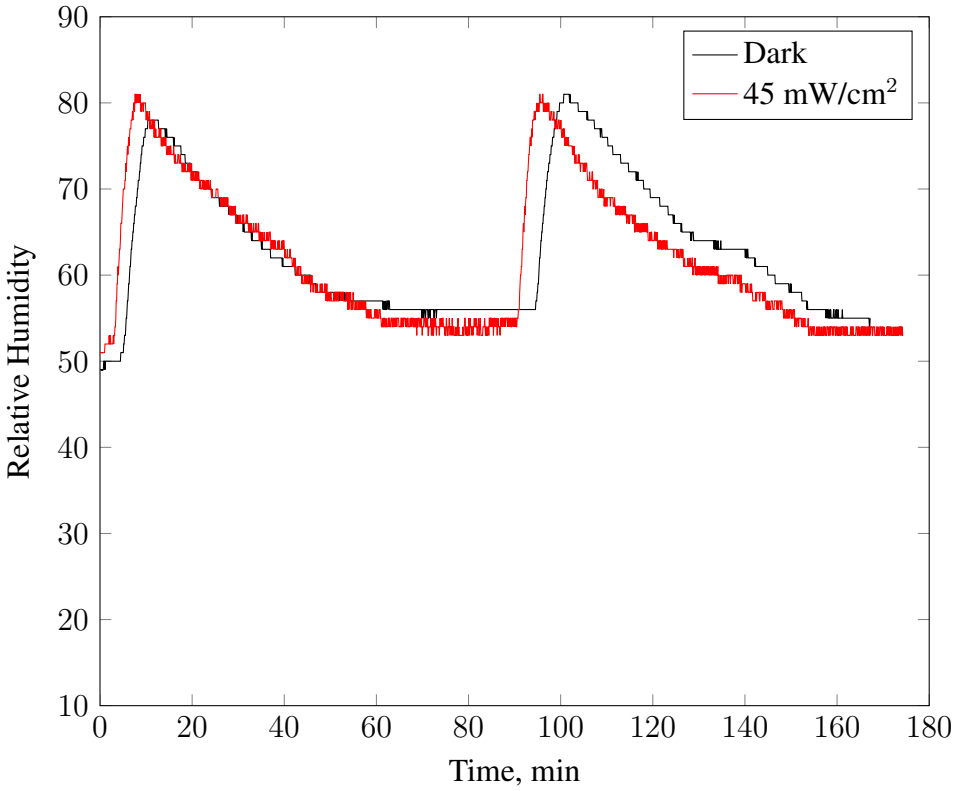

Figure 4.24: Effect of water injections at 50% RH.

4.4 Water + UV Pretreatment

Nitrate/nitrite species accumulation on the surface is the common explanation for the transient behavior of the NO oxidation reaction. However, with water injection tests, it was seen that introducing water pulses to the system can briefly increase the photocatalytic activity.

To test if water presence on the surface has any relation to the transient behavior, or if it is solely a result of nitrate species accumulating, the following experiment was conducted. Test gas composed of humid air and dry air was sent through the reactor under UV illumination for couple of hours. The difference between a standard NO oxidation experiment is that the test gas does not contain nitric oxide gas initially. After an amount of time that would lead to steady-state with a standard photocatalytic NO oxidation had passed, NO gas was introduced to the system.

Figure 4.25 shows both a standard photocatalytic NO oxidation experiment and UV + humid air pre-treated experiment. Both of the experiments were done at 45 mW/cm^2 illumination intensity. The pre-treatment was done for 230 minutes. During this time, 1 L/min air at 50% relative humidity was flowed over the reactor under UV light. After pre-treatment, the gas flow was directed to the by-pass line and NO gas flow was started. It takes 6 minutes to reach 1000 ppb NO concentration from 0 ppb. After 6 minutes, flow was again directed to the reactor. The initial large dip characteristic to a photocatalytic NO oxidation was not seen. The reaction starts with a conversion very close to its steady-state level and takes approximately 10 minutes to completely reach steady-state.

A similar experiment involving a brief dark stage was also conducted. After 3 hours of humid air flowing through the reactor under UV illumination, test gas was directed to the by pass line, NO gas was introduced to the system and UV illumination was stopped. After NO concentration reached 1000 ppb, flow was directed to the reactor. After 10 minutes of dark stage, UV illumination was started. The results are presented in Figure 4.26.

These experiments show that the transient behavior is not related to nitrate accumulation on the surface. Had the deactivation been due to excess nitrate species accumu-

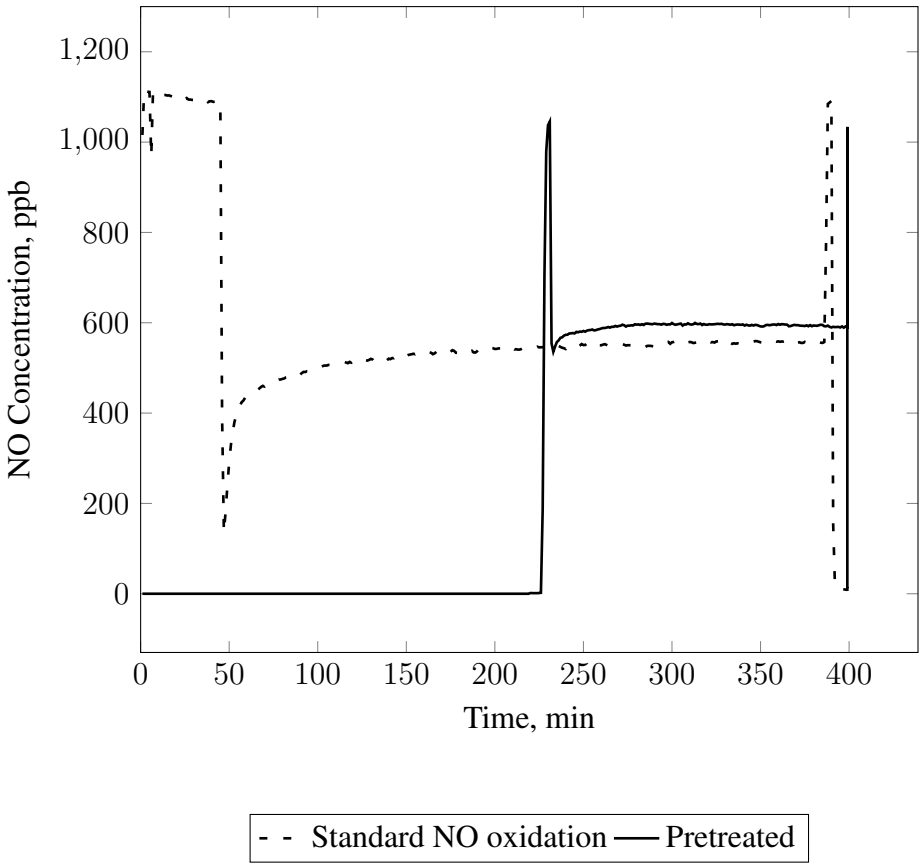

Figure 4.25: UV + water pretreatment at 45 mW/cm^2 illumination intensity and 50% RH.

lating on the surface, the prior 3-4 hours in the absence of NO gas should have had no effect. This is clearly not the case. The 3-4 hours of pre-treatment under humid air without NO gas makes NO conversion afterwards start from almost at the lower steady-state conversion.

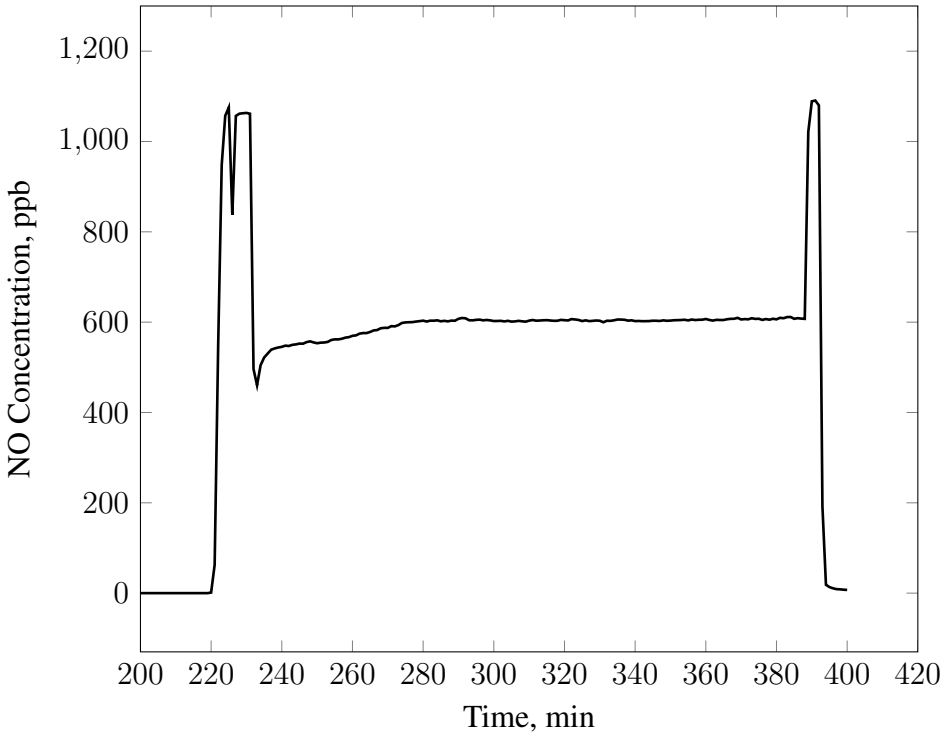

Figure 4.26: UV + water pretreatment at 45 mW/cm^2 illumination intensity and 20% RH.

4.5 Light Intensity Measurements

This study focuses on the effects of illumination intensity. The illumination intensity is adjusted by varying the height difference between the reactor and the light source. Therefore light intensities with respect to distance (source height) were measured using a commercial UV intensity sensor. The two measurement coordinates are height and base distance as explained in Chapter 3. Light intensities with respect to height and base position are shown in Table 4.2. The illumination intensity at base distance of 10 cm with respect to height is plotted in Figure 4.27.

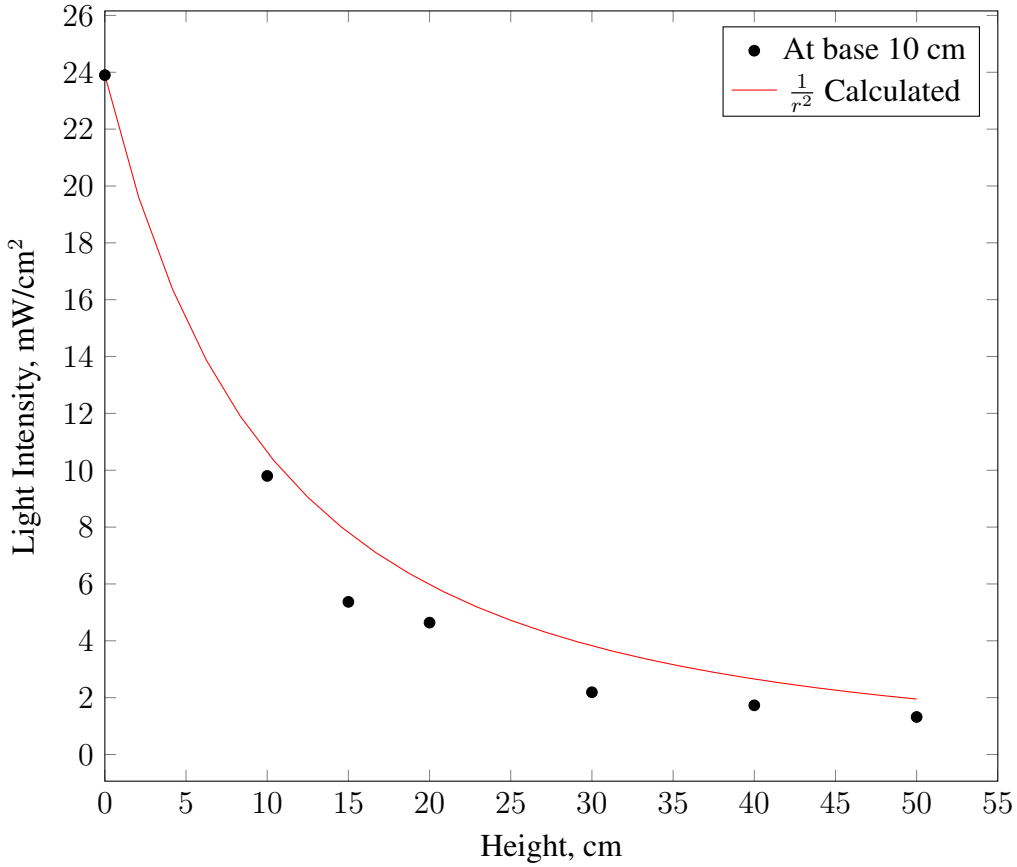

Figure 4.27: UV light intensity at base distance of 10 cm.

Table 4.2: Light intensities with respect to height and base distance.

Height (cm)	Base (cm)	Intensity (mW/cm^2)
0	0	0.18
0	5	2.95
0	10	23.9
0	15	35.4
10	0	0.84
10	5	2.63
10	10	9.8
10	15	33.5
15	0	0.76
15	5	1.47
15	10	5.37
15	15	14.23
20	0	0.4
20	5	1.46
20	10	4.64
20	15	12.16
30	0	0.63
30	5	0.8
30	10	2.19
30	15	4.31
40	0	0.57
40	5	0.87
40	10	1.73
40	15	3.478
50	0	0.51
50	5	0.77
50	10	1.32
50	15	2.56
50 cm + Filter	0	0
50 cm + Filter	5	0
50 cm + Filter	10	0
50 cm + Filter	15	0.27

4.5.1 UV Lamp Start-Up

The UV lamp has a start-up period where it exhibits a drop in illumination intensity in the first minutes it is turned on. The illumination intensity reaches steady-state after 15 minutes. The time dependent behavior of the UV lamp is presented in Figure 4.28. For reliability and repeatability of measurements, experiments involving the UV source were started after the lamp reached steady-state.

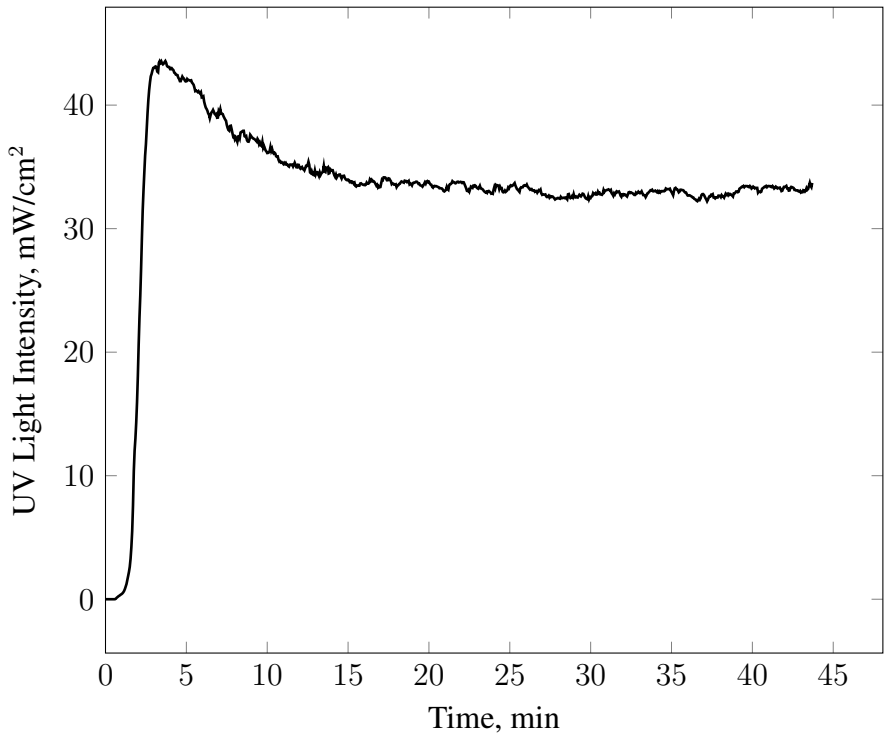

Figure 4.28: Transient behavior of the UV lamp.

4.6 UV Lamp Induced Heating

The UV lamp gets hot while in use therefore it is a heat source. Temperature increase due to the UV lamp was measured with a thermocouple inserted into the reactor. Four different measurements were made. First measurement is a blank measurement made without a catalyst present with no airflow through the reactor. The second measurement was made with a TiO_2 coated test piece without airflow. Third and fourth measurements were made under 1 L/min air flow with 20% and 50% relative humidity respectively. The results are plotted in Figure 4.29.

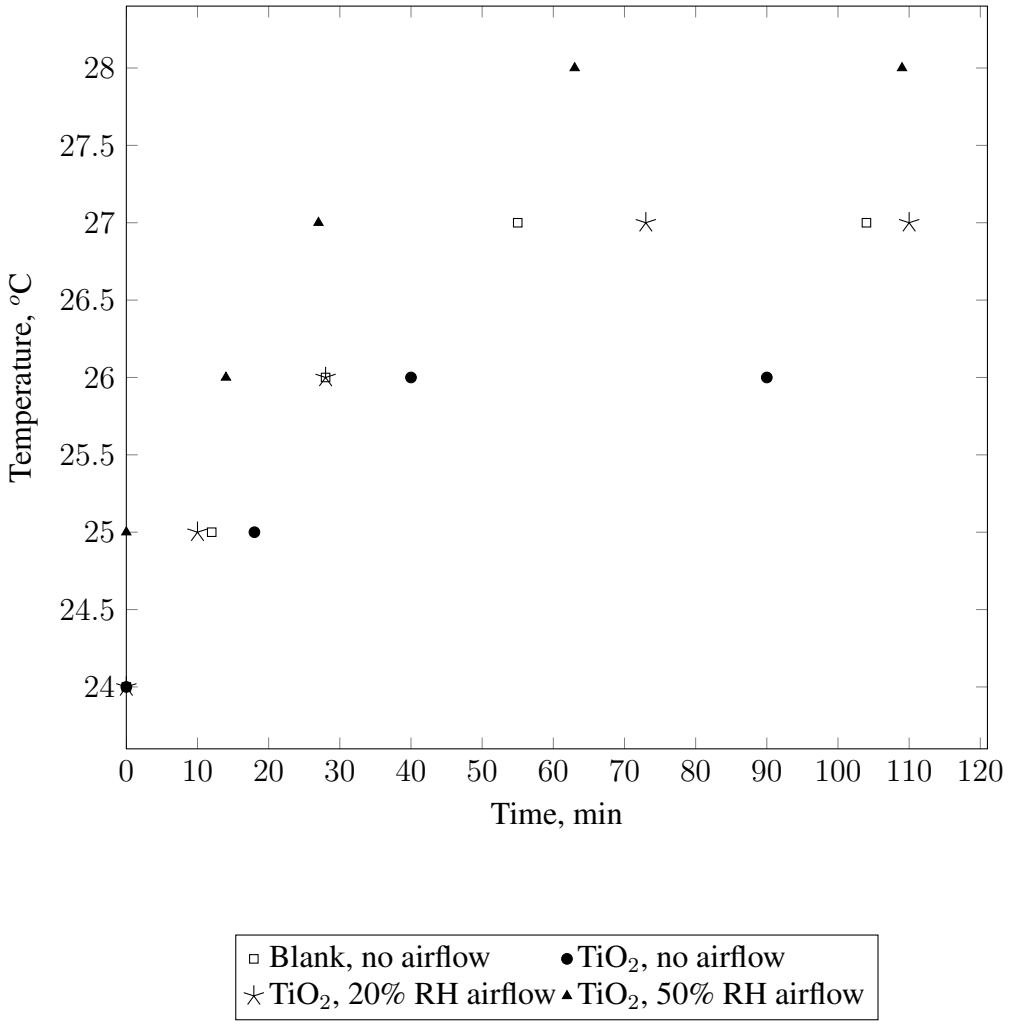

Figure 4.29: UV lamp induced heating in the reactor.

CHAPTER 5

CONCLUSIONS

To measure UV illumination intensity during experiments, a commercial UV sensor was coupled to a microcontroller to acquire serial data. Similarly, to measure the humidity content of the outlet stream, a digital temperature and humidity sensor connected to a microcontroller and the device was placed at the outlet of the system. The data was sent to a computer serially where it was logged. These devices were successfully built and used in experiments.

To test the effect of UV illumination intensity, multiple photocatalytic NO oxidation experiments were performed at varying light intensities. The illumination intensity was found to be directly related with the reaction performance and behavior. As light intensity increases conversion increases, as light intensity decreases conversion decreases. The process also has a transient behavior, conversion changes throughout the reaction. It was found that illumination intensity has an effect on the transient behavior of the reaction. At high illumination intensities, conversion is very high at the beginning of the reaction, but performance decreases with time and the system reaches a steady-state at a lower conversion value. However, with very low illumination intensities, steady state is achieved immediately after reaction starts, and there is no decaying behavior in the system. The steady state conversion was related to illumination intensity by curve fitting. The relationship between light intensity and steady state conversion was found to be $X = \frac{aI^b}{c + aI^b}$ where a = 0.1809, b = 0.3733, c = 0.7265.

Effect of water was also tested with water injection experiments. Water was injected into the system periodically in small amounts to see the effects. After water injections, conversion of NO was increased for a brief period of time but the effect did

not last very long, typically observed times were 5-10 minutes. The change in the reaction rate and the increase in the relative humidity of the stream occurred simultaneously. The change in conversion also resembles the transient behavior inherent to the reaction which is observed at the beginning of experiments.

REFERENCES

[1] Hagen, J. *Industrial Catalysis: A Practical Approach* (Wiley-VCH Verlag GmbH I& Co. KGaA, 2015), third edition edn.

[2] Administration, U. S. E. I. Monthly energy review (2021). URL `https://www.eia.gov/energyexplained/use-of-energy/`.

[3] International Organization for Standardization, Geneva, CH. *Fine ceramics (advanced ceramics, advanced technical ceramics) — Test method for air-purification performance of semiconducting photocatalytic materials* (2007).

[4] Beiser, A. *Concepts of Modern Physics* (McGraw-Hill, 2003), 6 edn.

[5] Kittel, C. *Introduction to Solid State Physics* (John Wiley I& Sons, Inc, 2005), 8 edn.

[6] Gaya, U. I. *Heterogeneous Photocatalysis Using Inorganic Semiconductor Solids* (Springer, 2014).

[7] Murphy, C. J. & Coffer, J. L. Quantum dots: A primer. *Applied Spectroscopy* **56** (2002).

[8] Simon, S. H. *The Oxford Solid State Basics* (Oxford University Press, 2013).

[9] Böer, K. W. & Pohl, U. W. *Semiconductor Physics* (Springer, 2018).

[10] Moss, T. S., Burrel, G. J. & Ellis, B. *Semiconductor Optoelectronics* (London Butterworths, 1973).

[11] Hofmann, P. *Solid State Physics: An Introduction* (Wiley-VCH, 2015).

[12] Stoneham, A. M. Non-radiative transitions in semiconductors. *Reports on Progress in Physics* **44**, 1251–1295 (1981).

[13] Emeline, A. V., Ryabchuk, V. K. & Serpone, N. Dogmas and misconcenption in heterogeneous photocatalysis. some enlightened reflections. *Journal of Physical Chemistry B* **109**, 18515–18521 (2005).

[14] Henderson, M. A. A surface science perspective on tio2 photocatalysis. *Surface Science Reports* **66**, 185–297 (2011).

[15] Fox, M. A. & Dulay, M. T. Heterogeneous photocatalysis. *Chemical Reviews* **93**, 341–357 (1992).

[16] Schneider, J. *et al.* Understanding tio2 photocatalysis: Mechanisms and materials. *Chemical Reviews* **114**, 9919–9986 (2014).

[17] Yılmaz, B. *Elucidating the role of adsorbed states of hydrogen, water and carbon dioxide over TiO2 and Pd/TiO2*. Master's thesis, Middle East Technical University (2020).

[18] Turchi, C. S. & Ollis, D. F. Photocatalytic degradation of organic water contaminants: Mechanisms involving hydroxyl radical attack. *Journal of Catalysis* **122**, 178–192 (1990).

[19] Minero, C., Mariella, G., Maurino, V. & Pelizzetti, E. Photocatalytic transformation of organic compounds in the presence of inorganic anions. 1. hydroxyl-mediated and direct electron transfer reactions of phenol on a titanium dioxide-fluoride system. *Langmuir* **16**, 2632–2641 (2000).

[20] Minero, C., Mariella, G., Maurino, V., Vione, D. & Pelizzetti, E. Photocatalytic transformation of organic compounds in the presence of inorganic ions. 2. competitive reactions of phenol and alcohols on a titanium dioxide-fluoride system. *Langmuir* **16**, 8964–8972 (2000).

[21] Choi, W., Kim, S., Cho, S., Yoo, H. I. & Kim, M. H. Photocatalytic Reactivity and Diffusing OH Radicals in the Reaction Medium Containing TiO2 Particles. *Korean Journal of Chemical Engineering* **18**, 898–902 (2001).

[22] Villarreal, T. L., Gómez, R., González, M. & Salvador, P. A kinetic model for distinguishing between direct and indirect interfacial hole transfer in the heterogeneous photooxidation of dissolved organics on TiO2 nanoparticle suspensions. *Journal of Physical Chemistry B* **108**, 20278–20290 (2004).

[23] Lana Villarreal, T., Gómez, R., Neumann-Spallart, M., Alonso-Vante, N. & Salvador, P. Semiconductor photooxidation of pollutants dissolved in water:

A kinetic model for distinguishing between direct and indirect interfacial hole transfer. I. photoelectrochemical experiments with polycrystalline anatase electrodes under current doubling and absence of recombination. *Journal of Physical Chemistry B* **108**, 15172–15181 (2004).

[24] Monllor-Satoca, D., Gómez, R., González-Hidalgo, M. & Salvador, P. The "Direct-Indirect" model: An alternative kinetic approach in heterogeneous photocatalysis based on the degree of interaction of dissolved pollutant species with the semiconductor surface. *Catalysis Today* **129**, 247–255 (2007).

[25] Murakami, Y., Kenji, E., Nosaka, A. Y. & Nosaka, Y. Direct detection of OH radicals diffused to the gas phase from the UV-irradiated photocatalytic TiO2 surfaces by means of laser-induced fluorescence spectroscopy. *Journal of Physical Chemistry B* **110**, 16808–16811 (2006).

[26] Murakami, Y., Endo, K., Ohta, I., Nosaka, A. Y. & Nosaka, Y. Can OH radicals diffuse from the UV-irradiated photocatalytic TiO 2 surfaces? Laser-induced-fluorescence study. *Journal of Physical Chemistry C* **111**, 11339–11346 (2007).

[27] Murakami, Y., Ohta, I., Hirakawa, T. & Nosaka, Y. Direct detection of oh radicals in the gas-phase diffused from the pt/tio2 and wo3/tio2 photocatalyts under the uv-light irradiation. *Chemical Physics Letters* **493**, 292–295 (2010).

[28] Vincentt, G., Aluculesei, A., Parker, A., Fittschen, C. & Marquaire, O. Z. P.-M. Direct detection of oh radicals and indirect detection of h2o2 molecules in the gas phase near a tio2 photocatalyst using lif. *Physical Chemistry Letters C* **112**, 9115–9119 (2008).

[29] Thiebaud, J., Thevenet, F. & Fittschen, C. Oh radicals and h2o2 molecules in the gas phase near to tio2 surfaces. *Journal of Physical Chemistry C* **114**, 3082–3088 (2010).

[30] Ding, L. *et al.* The vital role of surface Brönsted acid/base sites for the photocatalytic formation of free ·OH radicals. *Applied Catalysis B: Environmental* **266**, 118634 (2020).

[31] Li, W. *et al.* Evidence for the active species involved in the photodegradation

process of methyl Orange on TiO 2. *Journal of Physical Chemistry C* **116**, 3552–3560 (2012).

[32] Yang, W. *et al.* Effect of the Hydrogen Bond in Photoinduced Water Dissociation: A Double-Edged Sword. *Journal of Physical Chemistry Letters* **7**, 603–608 (2016).

[33] Sambur, J. B. & Chen, P. Distinguishing direct and indirect photoelectrocatalytic oxidation mechanisms using quantitative single-molecule reaction imaging and photocurrent measurements. *The Journal of Physical Chemistry C* **120**, 20668–20676 (2016).

[34] Jiang, G., Cao, J., Chen, M., Zhang, X. & Dong, F. Photocatalytic no oxidation on n-doped tio2/g-c3n4 heterojunction: Enhanced efficiency, mechanism and reaction pathway. *Applied Surface Science* **458**, 77 – 85 (2018).

[35] Dalton, J. S. *et al.* Photocatalytic oxidation of nox gases using tio2: a surface spectroscopic approach. *Environmental Pollution 120* **120**, 415–422 (2002).

[36] Ohko, Y., Nakamura, Y., Negishi, N., Matsuzawa, S. & Takeuchi, K. Unexpected release of hno3 and related species from uv illuminated tio2 surface into air in photocatalytic oxidation of no2. *Environmental Chemistry Letters* **8**, 289–294 (2010).

[37] Yu, Q. L., Ballari, M. M. & Brouwers, H. J. H. Indoor air purification using heterogeneous photocatalytic oxidation. part ii: Kinetic study. *Applied Catalysis B: Environmental* **99**, 58–65 (2010).

[38] Üner, D., Bayar, I. & Tabari, T. The influence of relative humidity on photocatalytic oxidation of nitric oxide (no) over tio2. *Applied Surface Science* **354**, 260–266 (2015).

[39] Ollis, D. F., Pelizetti, E. & Serpone, N. Destruction of water contaminants. *Environmental Science and Technology* **25**, 1523–1529 (1991).

[40] Lim, T., Jeong, S., Kim, S. & Gyenis, J. Photocatalytic decomposition of no by tio2 particles. *Journal of Photochemistry and Photobiology A: Chemistry* **134**, 209–217 (2000).

[41] Hüsken, G., Hunger, M. & Brouwers, H. J. H. Experimental study of photocatalytic concrete products for air purification. *Building and Environment* **44**, 2463–2474 (2009).

[42] Ballari, M. M., Hunger, M., Hüsken, G. & Brouwers, H. J. H. Modelling and experimental study of the nox photocatalytic degradation employing concrete pavement with titanium dioxide. *Catalysis Today* **151**, 71–76 (2010).

[43] Hunger, M., Hüsken, G. & Brouwers, H. J. H. Photocatalytic degradation of air pollutants - from modeling to large scale application. *Cement and Concrete Research* **40** (2010).

[44] Yu, Q. L. & Brouwers, H. J. H. Indoor air purification using heterogeneous photocatalytşic oxidation. part 1: Experimental study. *Applied catalysis B: Environmental* **92**, 454–461 (2009).

[45] Dillert, R., Stötzner, J., Engel, A. & Bahnemann, D. W. Influence of inlet concentration and light intensity on the photocatalytic oxidation of nitrogen(ii) oxide at the surface of aeroxide tio2 p25. *Journal of Hazardous Materials* 240–246 (2012).

[46] Dillert, R., Engel, A., Grosse, J., Lindner, P. & Bahnemann, D. W. Light intensity dependence of the kinetics of the photocatalytic oxidation of nitrogen(ii) oxide at the surface of tio2. *Physical Chemistry chemical Physics* **15**, 20876–20886 (2013).

[47] Sikkema, J. K., Ong, S. K. & Alleman, J. E. Photocatalytic concrete pavements: Laboratory investigation of no oxidation rate under varied environental conditions. *Construction and Building Materials* **100**, 305–314 (2015).

[48] Ballari, M. M., Yu, Q. L. & Brouwers, H. J. H. Experimental study of the no and no2 degradation by photocatalytically active concrete. *Catalysis Today* **161**, 175–180 (2011).

[49] Hadjiivanov, K., Bushev, V., Kantcheva, M. & Klissurski, D. Infrared spectroscopy study of the species arising during nitrogen dioxide adsorption on titania (anatase). *Langmuir* **10**, 464–471 (1994).

[50] Hadjiivanov, K. & Knözinger, H. Species formed after no adsorption and no+o2 co-adsorption on tio2: an ftir spectroscopic study. *Physical Chemistry Chemical Physics* **2**, 2803–2806 (2000).

[51] Sivachandiran, L., Thevenet, F., Gravejat, P. & Rousseau, A. Investigation of no and no2 adsorption mechanisms on tio2 at room temperature. *Applied Catalysis B: Environmental* **142-143**, 196 – 204 (2013).

[52] Loganathan, S., Thevenet, F., Rousseau, A. & Bianchi, D. No2 adsorption mechanism on tio2: an in-situ transmission infrared spectroscopy study. *Applied Catalysis B Environmental* **198**, 411–419 (2016).

[53] Mikhaylov, R. V. *et al.* Ftir and tpd analysis of surface species on a tio2 photocatalyst exposed to no, co, and no-co mixtures: Effect of uv-vis light irradiation. *The Journal of Physical Chemistry C* **113**, 20381–20387 (2009).

[54] Mikhaylov, R. V. *et al.* Ftir and tpd study of the room temperature interaction of a no–oxygen mixture and of no2 with titanium dioxide. *The Journal of Physical Chemistry C* **117**, 10345–10352 (2013).

[55] Pichat, P. An overview on the use of adsorption and reactions of no to probe (photocatalytic) tio2. *Catalysis Today* **340**, 26–33 (2020).

[56] Dines, T. J., Rochester, C. H. & Ward, A. M. Infrared and raman study of the adsorption of nitrogen oxides on titania-supported vanadia catalysts. *Journal of the Chemical Society, Faraday Transactions* **87**, 1617–1622 (1991).

[57] Sorescu, D. C., Rusu, C. N. & Yates, J. T. Adsorption of no on the tio2(110) surface:: An experimental and theoretical study. *The Journal of Physical Chemistry B* **104**, 4408–4417 (2000).

[58] Rodriguex, J. A. *et al.* Chemistry of no2 on oxide surfaces: Formation of no3 on tio2(110) and no2<->o vacancy interactions. *Journal of the American Chemical Society* **123**, 9597–9605 (2001).

[59] Devahasdin, S., Chiun Fan, J., Li, K. & Chen, D. H. Tio2 phototcatalytic oxidation of nitric oxide: transient behavior and reaction kinetics. *Journal of Photochemistry and Photobiology A: Chemistry* **156**, 161–170 (2003).

[60] Ohko, Y., Nakamura, Y., Negishi, N., Matsuzawa, S. & Takeuchi, K. Photocatalytic oxidation of nitrogen monoxide using tio2 thin films under continuous uv light illumination. *Journal of Photochemistry and Photobiology A: Chemistry* **205**, 28–33 (2009).

[61] Mills, A. & Elouali, S. The nitric oxide iso photocatalytic reactor system: Measurement of nox removal activity and capacity. *Journal of Photochemistry and Photobiology A: Chemistry* **305**, 29–36 (2015).

[62] Krysa, J., Baudys, M., Vislocka, X. & Neumann-Spallart, M. Composite photocatalyst based on tio2-carbon for air pollutant removal: Aspects of adsorption. *Catalysis Today* **340**, 34–39 (2020).

[63] Sofianou, M.-V. *et al.* Study of tio2 anatase nano and microstructures with dominant 001 facets for no oxidation. *Environmental Science and Pollution Research* **19**, 3719–3726 (2012).

[64] Guo, M.-Z., Chen, J., Xia, M., Wang, T. & Poon, C. S. Pathways of conversion of nitrogen oxides by nano tio2 incorporated in cement-based materials. *Building and Environment* **144**, 412–418 (2018).

[65] Wang, H., Wu, Z., Zhao, W. & Guan, B. Photocatalytic oxidation of nitrogen oxides using tio2 loading on woven glass fabric. *Chemosphere* **66**, 185–190 (2007).

[66] Bayar, I. *Photocatalytic NO Oxidation of NOx Over TiO2 Containing Cement Based Materials*. Master's thesis, Middle East Technical University (2013).

[67] Toulson, R. & Wilmshurst, T. *Fast and Effective Embedded Systems Design: Applying the ARM mbed* (Elsevier, 2017), 2 edn.

[68] Frdm-k64f | mbed. Webpage (2021). URL `https://os.mbed.com/platforms/FRDM-K64F/`.

[69] Grove base shield v2.0 for arduino. Webpage (2021). URL `https://www.seeedstudio.com/Base-Shield-V2.html`.

[70] Spurr, R. A. & Myers, H. Quantitative analysis of anatase-rutile mixtures with an x-ray diffractometer. *Analytical Chemistry* **29** (1957).

[71] Fukishima, A., Zhang, X. & Tryk, D. A. Tio2 photocatalysis and related surface phenomena. *Surface Science Reports* **63**, 515–582 (2008).

[72] Levchenko, A. A., Li, G., Boerio-Goates, J., Woodfield, B. F. & Alexandra. Tio2 stability landsacpe: Polymorphism, surface energy, and bound water energetics. *Chemistry of Materials* **18**, 6324–6332 (2006).

[73] Muggli, D. S. & Falconer, J. L. Role of lattice oxygen in photocatalytci oxidation on tio2. *Journal of Phototcatalysis* **191**, 318–325 (2000).

Appendix A

EMBEDDED SYSTEMS

A.1 Compilation

The initial step to set up the microcontroller board is to compile the source code. Several compilers including online versions are available. After compilation the resulting binary file is flashed onto the microcontroller board. Mbed Studio IDE was used for compilation and flashing in this study.

Source code for mbed microcontroller board is below. Programming language used is C/C++ for the arm mbed platform.

A.2 Source Code

Necessary libraries are imported in the beginning. Some of the libraries are written specifically for the hardware used. These hardware include a Grove RGB LCD and the digital temperature and humidity sensor. The libraries have useful functions to control the hardware.

The main() part of the code is used for initialization and for the start up message to be displayed on the LCD.

A while loop which is conditioned to execute indefinitely is used for continuous operation of the device. A timer is started at the beginning of the loop. The timer will be stopped at the end of the while loop to measure the time passed for each reading.

Analog output from the UV sensor is read with read(). A thousand of these readings

is summed within a for loop. The total sum is later divided by a thousand to get an average reading. The result is assigned to UV_int variable of float type.

Digital outputs from the temperature and humidity sensor are read with readData(), ReadTemperature() and ReadHumidity(). The readings are assigned to the temperature_C and humidity_RH variables of float type.

All the readings from the sensors are now assigned to variables of float type. These variables are added to newly created stringstreams. They are then are formatted by using setprecision(). They are then converted to string type by using str().

The string type values for sensor readings are then printed on the LCD with 1700 ms sleep time. The display is cleared using the clear() function before anything is printed. The cursor is set to the desired location using locate(). The results are also printed on a terminal if a computer is connected.

The timer is stopped at the end of the while loop. Time passed is printed while the timer is counting. This is done to evade a time delay while printing, however the first execution of the loop does not print anything for time passed.

```
// DHT11 digital humidity and temperature sensor library
#include "DHT.h"
#include "DigitalOut.h"
#include "I2C.h"
#include "MK64F12.h"
#include "PinNames.h"
#include "ThisThread.h"
#include "i2c_api.h"
#include "mbed.h"
// For timer.
#include <chrono>
#include <cstdio>
// To set the precision of string, setprecision()
#include <iomanip>
```

```
// string stream, for precision of string
#include <sstream>
#include <string>
// Grove RGB LCD library
#include "Grove_LCD_RGB_Backlight.h"

Timer timer;

// Variables defined below.
float temperature_C;
float humidity_RH;
float uv_val;

// Initialize LCD.
Grove_LCD_RGB_Backlight GroveLCD(D14, D15);

int main() {

  GroveLCD.clear(); // clears display, library function
  GroveLCD.setRGB(255, 128, 0); // set backlight color
  GroveLCD.locate(0, 0);
  GroveLCD.print((char *)"Starting up...");
  ThisThread::sleep_for(1700);

  AnalogIn sensor(A1);  // Grove UV Sensor on analog pin A1
  DHT dht11(D3, DHT11);   // DHT sensor on digital pin D3.
  DigitalOut myLed(LED1); // For testing purposes.

  while (1) {

    timer.start();

// Read UV sensor data 100 times, average the result.
```

```
    float sum = 0;
    for (int i = 0; i < 1000; i++) {
      uv_val = sensor.read();
      sum = sum + uv_val;
    }

    float meanUV_val = sum / 1000;
    float UV_int = (meanUV_val * 307); // Intensity mW/m2

// Read temperature and humidity data.
    dht11.readData();
    temperature_C = dht11.ReadTemperature(CELCIUS);
    humidity_RH = dht11.ReadHumidity();

    myLed = !myLed;

    printf("Temperature: %.2f %s %.2f %s %2.2f \n",
    temperature_C,   "- Humidity: ", humidity_RH,
     "- UV intensity: ", meanUV_val * 307);

// Create string stream named UVstrstream.
    std::ostringstream UVstrstream;
    // Set precison of stream
    // Add float UV_int_mWm2 to stream.
    UVstrstream << std::setprecision(3) << UV_int;
    std::string UV_str = UVstrstream.str();

    std::ostringstream tempStrStream;
    tempStrStream << setprecision(3) << temperature_C;
    std::string temperature_C_str = tempStrStream.str();

    std::ostringstream humStrStream;
    humStrStream << setprecision(2) << humidity_RH;
```

```
std::string humidity_str = humStrStream.str();

// Print UV Intensity on LCD.
GroveLCD.clear();
GroveLCD.setRGB(142, 112, 219);
GroveLCD.locate(0, 0);
GroveLCD.print((char *)"UV intensity: ");
GroveLCD.locate(0, 1);
GroveLCD.print((char *)UV_str.c_str());
ThisThread::sleep_for(1700);

// Print Temperature on LCD.
GroveLCD.clear();
GroveLCD.setRGB(255, 128, 0);
GroveLCD.locate(0, 0);
GroveLCD.print((char *)"Temperature: ");
GroveLCD.locate(0, 1);
GroveLCD.print((char *)temperature_C_str.c_str());
ThisThread::sleep_for(1700);

// Print Humidity on LCD.
GroveLCD.clear();
GroveLCD.setRGB(0, 204, 204);
GroveLCD.locate(0, 0);
GroveLCD.print((char *)"Humidity: ");
GroveLCD.locate(0, 1);
GroveLCD.print((char *)humidity_str.c_str());
ThisThread::sleep_for(1700);

/* Print time passed on LCD
// Code is commented out. Use when necessary.
GroveLCD.clear();
GroveLCD.setRGB(255, 104, 104);
```

```
    GroveLCD.locate(0, 0);
    GroveLCD.print((char*)"Time passed (s): ");
    std::ostringstream timeStrStream;
    GroveLCD.locate(0, 1);
    timeStrStream << setprecision(2) << timer.read();
    std::string time_str = timeStrStream.str();
    GroveLCD.print((char*)time_str.c_str());
    ThisThread::sleep_for(1700);
    */

    printf("Time: %.2f \n", timer.read());
    timer.stop();

  }
}
```

Appendix B

EXPERIMENTAL PROCEDURES

NO oxidation measurements are standardized by the ISO-22197:2007(E) standard. The experiment set-up consists of a NO gas cylinder, an air compressor, three mass flow controllers (MFCs), a humidifier, a photo-reactor, a by-pass line, and a Thermo Scientific model 42i NOx analyzer.

In addition to the NO oxidation set-up, an analog UV light intensity and a digital temperature and relative humidity sensor were integrated to the system.

Experimental procedures and how to use the sensors are explained below.

B.1 NO Oxidation Experiment Procedure

1. Start the air compressor. The compressor will work for 40-60 seconds until the air pressure reaches 8 bars.
2. Open the compressor valves.
3. Open cylinder valves.
4. Start the MFCs. Adjust the inlet concentration from the control station.
5. The water inside the humidifer will become saturated after 20 minutes. Wait for 20 minutes.
6. Direct the inlet stream from the by-pass line to the reactor. Dark stage is started, and takes 30-40 minutes.
7. Cover the reactor with an opaque sheet.

8. Turn the UV light on. The lamp requires 20-30 minutes to reach a steady-state.

9. Measure the UV light intensity with the UV sensor after the UV lamp reaches steady state. Always measure the light intensity from the same point on the reactor.

10. After 40 minutes of dark stage is over, remove the cover on the reactor to start the illumination.

11. The reaction starts immediately when illumination is started. Steady- state is achieved after a few hours depending on the state and the type of the catalyst.

12. For water injection experiments, inject water from the septum located at the inlet of the reactor using a syringe. A detailed procedure for water injections are described below.

13. When necessary steps for a planned experiment is complete, turn of the UV lamp. Wait for 4 minutes.

14. Shut off NO flow into the system for degassing. Let air flow through the reactor for 15 minutes.

15. Direct the flow to the by-pass stream from the reactor.

16. Collect data from the computer.

17. Shut off air flow into the system from the MFCs and the compressor.

B.2 Catalyst Replacement

1. Catalysts are coated on to glass substrates of suitable sizes.

2. A UV transparent glass is siliconed to the top of the reactor. The photo-reactor is sealed with gaskets and screws which attach the top and the bottom parts of the reactor.

3. To open up the reactor, the top part of the reactor must be unscrewed from he bottom part.

4. Carefully start unscrewing the screws in a symmetrical fashion. Be sure not to apply torsional stress on the glass part. Uneven screwing may cause this glass to break.

5. Once the top part can be detached, the catalyst coated glass can be removed and replaced with another test piece. Place the new test piece inside the reactor.

6. Place the top part of the reactor and tighten the screws in a symmetrical fashion to avoid stressing the glass.

7. The gaskets will be pressed on the plastic which ensures a leakproof seal. The reactor is then ready for operation.

B.3 Injection Steps for Water Injection Experiments

1. For liquid injections into the system, a septum is placed at the inlet of the reactor.

2. Using a syringe, draw 0.01 ml of distilled water.

3. Inject the water through the septum. Start a timer.

4. Wait for 30 seconds. Draw another 0.01 ml of water into the syringe during this time.

5. Repeat the injection.

6. A total of 10 injections are necessary for a set of injections. Therefore, one set of injections take five minutes to complete.

7. Check the outlet relative humidity from the humidity sensor regularly. Repeat the next set of injections when the humidity content of the outlet stream returns to pre-injection levels. Time required to stabilize depends on ambient temperature and humidity, This usually takes an hour with 1 L/min flow rate.

8. Do 4-6 sets of water injections depending on the results.

B.4 UV Intensity Measurements

1. Connect the UV sensor SiG to analog pin A1, GND to GND, Vcc to 5 volts on the microcontroller. If using a sensor shield, connect Grove connector to A1 port on the shield.
2. Connect the microcontroller board to a computer or a power source. If there is an LCD display attached, data will be displayed on the LCD and there is no need for a computer for serial data acquisition. A 5 Volt power supply is sufficient to power up the microcontroller board.
3. Place the sensor where UV intensity measurement is necessary.

B.5 Relative Humidity Measurements

1. Connect the DHT sensor SiG to digital pin D3, GND to GND, Vcc to 5 volts on the microcontroller. If using a sensor shield, connect Grove connector to D3 port on the shield.
2. The sensor is placed in a container located at the outlet of the experiment set-up. This ensures that the readings are from the system.
3. Connect the microcontroller board to a computer.
4. Open a terminal emulator application. For windows machines TeraTerm can be used.
5. Set up a new connection to the mbed board. From serial connections find the comm port mbed is attached to.
6. Sensor reading will be displayed on the screen if successful connection is made.
7. Start keeping a log from the terminal emulator for data processing later.

Appendix C

VOLUMETRIC ANALYSIS OF WATER INJECTIONS

Water injections introduce an additional volume into the system. This can cause a dilution in the gas which can lower the NO concentration. The effects seen with water injections should be discriminated from this dilution effect. A simple mathematical analysis is constructed in this section.

Water is injected with 30 second intervals within 5 minutes which adds up to 10 injections. 1 μl liquid water is injected with every water injection. Therefore, the total amount of water injected is 10 μl. Roughly, a thousandfold increase in volume is typical for a liquid-vapor transition. If all the liquid water vaporizes upon injection, the volume of vapor added within 5 minutes equals:

$$10\ \mu\text{l liquid water} * 1000 \approx 10\ \text{ml water vapor}$$

In 5 minutes, 5 liters of gas flows through the system with a 1 l/min flow rate. The percentage of added volume of water injections is therefore:

$$\frac{10\ \text{ml}}{5\ \text{l}} * 100 = 0.2\%$$

The concentration change this would account for can be calculated by the equation $C_1V_1 = C_2V_2$. For 1000 ppb NO, the concentration would drop to:

$$1000\ \text{ppb NO} * 5\ \text{l} = C_2 * 5.01\ \text{l}$$
$$C_2 = 998\ \text{ppb NO}$$

This change in concentration is negligible.

Appendix D

PREVIOUS WORK

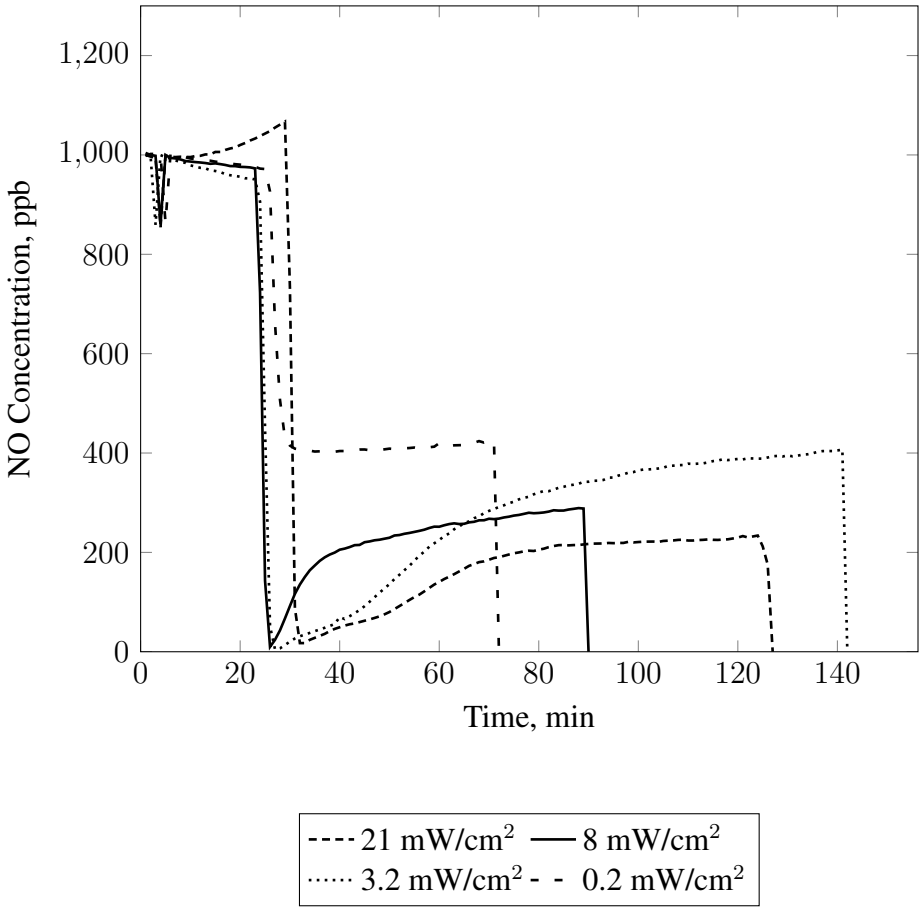

Figure D.1: Effect of UV light intensity on NO oxidation. Results of preliminary studies.

Light intensities are approximate. The measurements were done before the UV intensity measurement device was built.

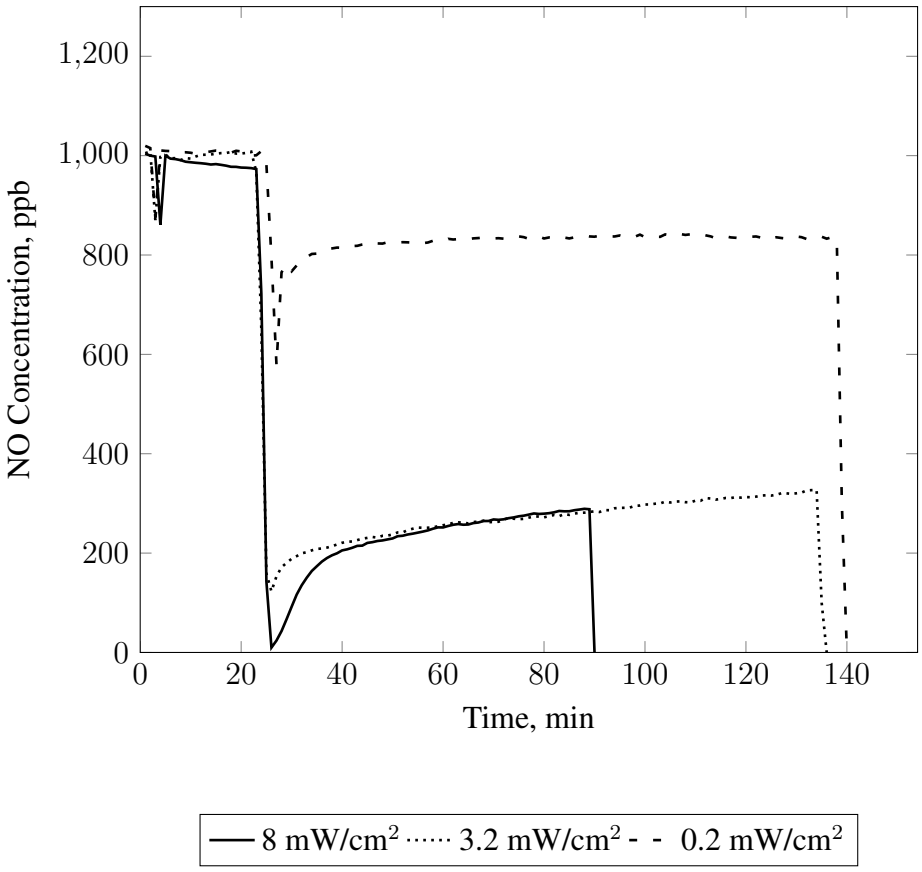

Figure D.2: Effect of UV light intensity on NO oxidation. Results of preliminary studies.

Light intensities are approximate. The measurements were done before the UV intensity measurement device was built.

Appendix E

CALIBRATION OF MASS FLOW CONTROLLERS

The mass flow controllers are calibrated using a soap bubble flow meter and a chronometer. Calibration curves for the MFCs are below.

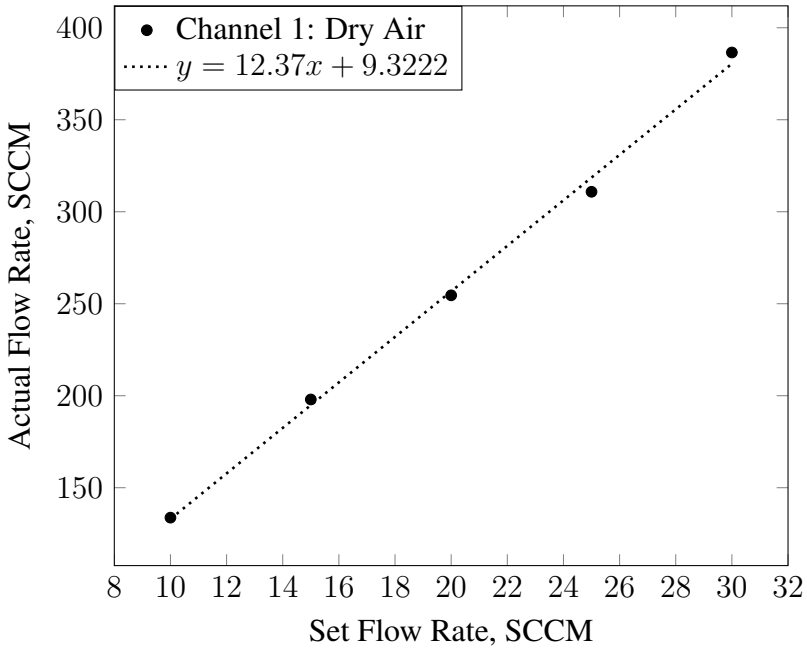

Figure E.1: Calibration curve for dry air channel (CH 1).

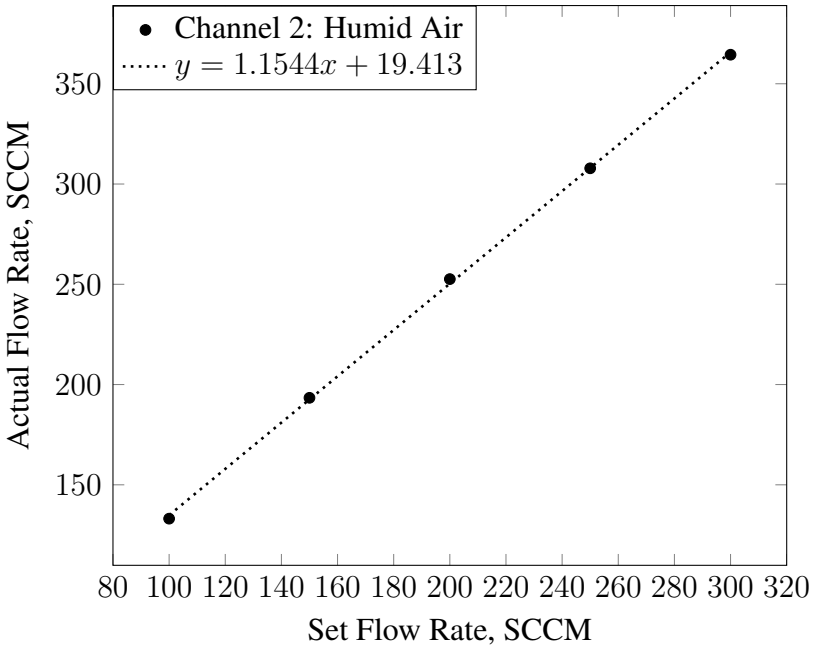

Figure E.2: Calibration curve for humid air channel (CH 2).

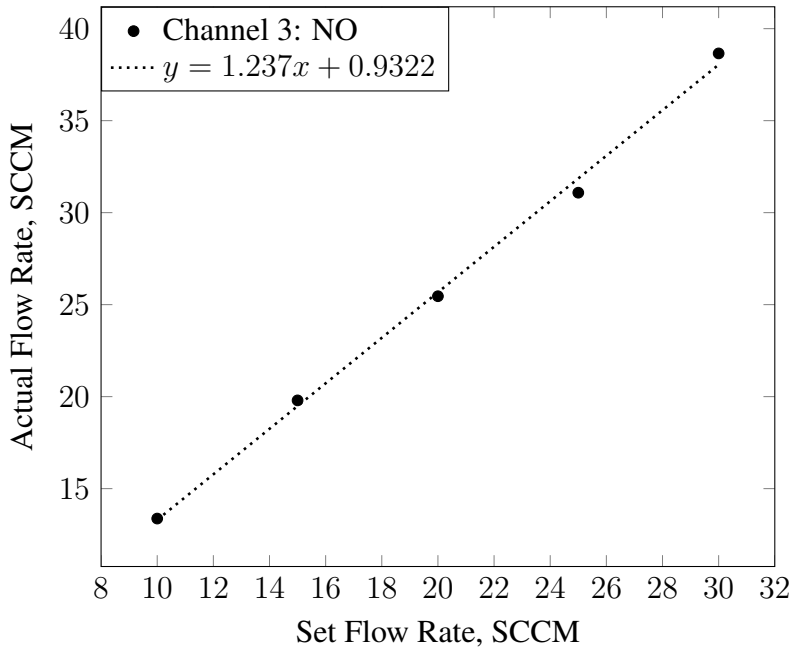

Figure E.3: Calibration curve for NO channel (CH 3).

Appendix F

MATLAB CURVE FIT

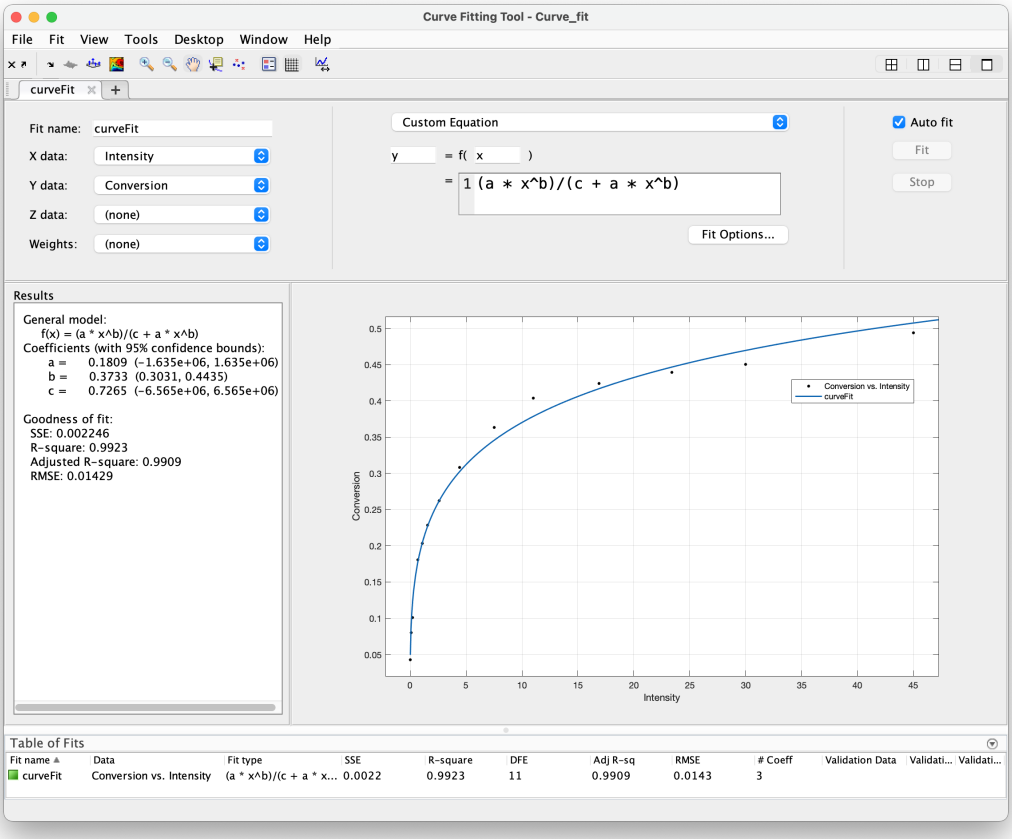

Figure F.1: Screenshot of the Matlab curve fitting tool results.

Appendix G

SENSOR SPECIFICATIONS

UV-A Sensor

GUVA-S12SD

Genuine UV Technology

GenUV

Features

Gallium Nitride Based Material
Schottky-type Photodiode
Photovoltaic Mode Operation
Good Visible Blindness
High Responsivity & Low Dark Current

Applications

UV Index Monitoring
UV-A Lamp Monitoring

Outline Diagrams and Dimensions

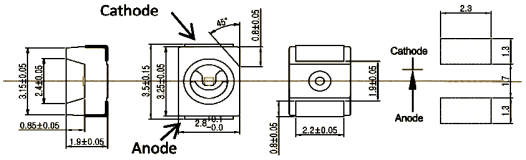

Absolute Maximum Ratings

Parameter	Symbol	Min.	Max.	Unit	Remark
Storage Temperature	T_{st}	-40	90	℃	
Operating Temperature	T_{op}	-30	85	℃	
Reverse Voltage	$V_{r,\ max.}$		5	V	
Forward Current	$I_{f,max.}$		1	mA	
Optical Source Power Range	P_{opt}	0.1μ	100m	W/㎠	UVA Lamp
Soldering Temperature	T_{sol}		260	℃	within 10 sec.

※Notice: apply to us in the case that Optical Source Power is over 100㎽/㎠

Characteristics (at 25℃)

Parameter	Symbol	Min.	Typ.	Max.	Unit	Test Conditions
Dark Current	I_d			1	nA	Vr = 0.1 V
Photo Current	I_{ph}	101	113	125	nA	UVA Lamp, 1㎽/㎠
			21		nA	1 UVI
Temperature Coefficient	I_{tc}		0.08		%/℃	UVA Lamp
Responsivity	R		0.14		A/W	λ = 350 ㎚, Vr = 0 V
Spectral Detection Range	λ	240		370	㎚	10% of R
Active area			0.076		㎟	

Responsivity Curve

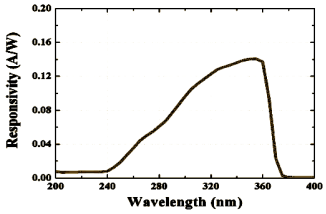

Photocurrent along UV Power

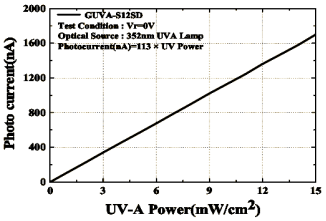

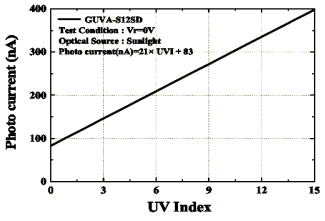

Caution

ESD can damage the device hence please avoid ESD.

Figure G.1: Technical specifications of the sensor used.